ABSTRACT

Title of Dissertation: INTEGRATED MONITORING OF DISTURBANCE AND FOREST ATTRIBUTES

Jiaming Lu, Doctor of Philosophy, 2024

Dissertation directed by: Dr. Chengquan Huang, Research Professor, Department of Geographical Sciences

Forests provide numerous ecosystem services and are shaped by historical disturbance events. The intensity of disturbance significantly influences the post-disturbance forest structure, species composition, and subsequent forest regrowth. Under the influence of anthropogenic activities and climate change, disturbance regime has undergone unprecedent changes and is subsequently affecting a suite of interrelated forest attributes that are critical in understanding forests dynamics. Historical large-scale disturbance intensity information is needed for understanding the change in disturbance regimes and create linkage to forest dynamics, but such dataset was not available. Forest attributes can be estimated from the spectral information of remote sensing imagery; however, inconsistency exists among the developed product, and the usage of the dataset is limited by accuracy. To fill the research gaps, this dissertation aims to develop a framework that integrates the historical disturbance and the inter-relationship between forest attributes to provide more consistent, and likely more accurate forest attribute estimations. Age, a key attribute that can be the determinant of many ecosystem processes and tree/forest stand develop stage, was selected as the prototype attribute to study. The dissertation started by producing the first set of annual forest disturbance intensity map products quantifying the

percentage of basal area removal (PBAR) at the 30-m resolution for the CONUS from 1986 to 2015, by integrating field plot measurements collected by the Forest Inventory and Analysis program with time series Landsat observations. Compared to other published disturbance products, the maps derived through this study can provide the unique thematic (intensity) information on forest disturbances, precise details critical for understanding forest dynamics across CONUS over multiple decades. The dissertation then proceeded to quantify individual tree age. The tree age was estimated for every tree in the FIA database (over 10 million trees) across the US from our modeling approach that had higher accuracies than existing studies. The developed tree age dataset allows better characterization of tree age distribution, which is important for understanding the disturbance history, functioning, and growth vigor of forest ecosystems. With the disturbance intensity and tree age dataset, the dissertation was able to develop an integrated modeling approach for the forest age mapping. The forest age and complexity maps were produced for 2015 and 2005. The combination of the two metrics should provide a more comprehensive characterization of the forest development condition. The maps provide valuable information for knowing forest conditions, estimating forest growth and carbon sequestration potential, understanding the relationship between age and other forest attributes, evaluating forest health, and planning sustainable forest management practices. This modeling framework developed by the dissertation will enhance the ability to retrieve forest attributes in a broader scale so that with the remote sensing observation, we can not only provide spatially explicit forest structure information, but also review forest status over the decades. Furthermore, when combined with the ecosystem models, these estimations will provide a better prediction for future vegetation and climate dynamics.

INTEGRATED MONITORING OF DISTURBANCE AND FOREST ATTRIBUTES

By

Jiaming Lu

Dissertation submitted to the Faculty of the Graduate School of the
University of Maryland, College Park, in partial fulfillment
of the requirements for the degree of
Doctor of Philosophy
2024

Dissertation Advisory Committee

Dr. Chengquan Huang, Chair
Dr. Matthew C. Hansen, Co-chair
Dr. George C. Hurtt
Dr. Zhiliang Zhu
Dr. Karen Schleeweis
Dr. Jiuzhou Song

Dedication

To my parents, Chen Lu (路臣) *and Xiujie Jiang* (姜秀杰),

for your unconditional love, and the perfect childhood you gave me.

This dissertation is for you.

Acknowledgements

First and foremost, I want to sincerely thank my amazing advisor, Dr. Chengquan Huang. Thank you for guiding me every step of the way, providing valuable insight, and always being available when I needed help. I gained my understanding of the scientific process and learned better logical thinking from observing and talking to you. You are a true role model and the best team leader I could ever ask for. None of this would have been possible without you.

I also want to express my gratitude to my distinguished committee members. Dr. Matt Hansen, thank you for your affirmation and encouragement. I am honored to have had your support on this journey from the very beginning. Dr. George Hurtt, thank you for providing valuable guidance for this dissertation from an ecological perspective. Because of you, I was fortunate to become a part of the GEL lab and the CMS team, and to make small contributions to the important topics you are working on. I also want to thank Dr. Zhiliang Zhu, Dr. Karen Schleeweis, Dr. Jiuzhou Song, and Dr. Joe Sullivan for their valuable input, which helped improve this dissertation enormously.

Many thanks to Dr. Jack Ma and the MSGIS program for the long-term funding support. Being a TA in the program has been one of the most memorable experiences I have had during these years. I would also like to thank Dr. Rachel Haber, Dr. Laixiang Sun, Dr. Leila De Floriani, Vicky Berry, Mary Mitkish, Jenny Hu, Jack O'Bannon, and Fernando Ramirez for their timely and effective responses when I needed help.

To my uncle, Dr. Zhong Lu, thank you for your guidance and for being encouraging. Thank you for being a great figure whom I looked up to while growing up. You are what inspired me to start the PhD, so you deserve credit for everything I have learned and achieved.

To my dear friends, Diyang Cui and Zheng Liu, Moying Li and David Loebman, Yiming Zhang, Aolin Jia, Lei Ma, Jing Xu, and Chunyan Tong, thank you for always being there for me. To my fellow PhD friends and colleagues in the department, Amber Liang, Zhiyue Xia, Xinyuan Li, Ruohan Li, Zhili Li, Jiaying He, Yuan Zhou, Yanjia Cao, Weishu Gong, Zhenhua Zou, Hannah Younes, Allison Bredder, Walid Ouaret, and many others, thank you for making this journey so much fun.

To Yao Li, I am so grateful to have shared all the laughter and tears in life with you. I cannot wait to see what life holds for us in the future!

To all the days and nights in Maryland, you will surely be missed.

Table of Contents

List of Figures

List of Tables

List of Abbreviations

Basal Area Weighted Mean Tree Age (BAWMT)

Day of Year (DOY)

Ecosystem Disturbance Adaptive Processing System (LEDAPS)

Environmental Protection Agency (EPA)

Forest Inventory and Analysis (FIA)

Forest Z-score (FZ)

Global Ecosystem Dynamics Investigation (GEDI)

Ice, Cloud, and land Elevation Satellite-2 (ICESat2)

Integrated Forest Z-score (IFZ)

Landsat Bands 4 (B4FZ) and 5 (B5FZ)

Landsat Terrain-corrected Level 1 (L1T)

Landsat Time Series Stacks (LTSS)

NASA-ISRO SAR (NISAR)

National Forest Inventories (NFIs)

National Land Cover Dataset (NLCD)

Normalized Burn Ratio (NBR)

Normalized Difference Moisture Index (NDMI)

Normalized Difference Vegetation Index (NDVI)

Oak Ridge National Laboratory Distribution Active Archive Center (ORNL-DAAC)

PRISM (Parameter-elevation Regressions on Independent Slopes Model)

Proportion of Stand Clearing Area (PSCA)

Root Mean Square Error (RMSE)

Shuttle Radar Topography Mission (SRTM)

Synthetic Aperture Radar (SAR)

The Conterminous United States (CONUS)

US Forest Service (USFS)

Vegetation Change Tracker (VCT)

Worldwide Reference System-2 (WRS2)

Chapter 1: Introduction

1.1 Background and Motivations

1.1.1 Forest and Global Change

Forests, covering approximately 30% of the world's land surface, are vital for numerous ecosystem services, such as climate regulation, water management, and biodiversity conservation (FAO 2018). They play critical roles in the global carbon cycle, sequestering about 20% of atmospheric carbon through photosynthesis and constituting the largest terrestrial carbon sink with an estimated 450 Gt C, a significant portion of the earth's total 550 Gt C (Bar-On et al., 2018; Houghton, 2005; Pan et al., 2011). Beyond carbon sequestration, forests influence climate through hydrological processes and cooling effects, including moisture production and temperature regulation (Ellison et al., 2017). In several regions, forests are the primary source of energy, with harvested firewood being extensively used (Hoogwijk et al., 2005; IPCC, 2014). Forests also support approximately two-thirds of terrestrial biodiversity (FAO, 2018; Giam, 2017). Over the past three centuries, forests have experienced continuous and significant transformations due to both natural and human-induced factors, impacting climate, the terrestrial carbon cycle, and biodiversity. Anthropogenic activities, such as deforestation for agriculture and timber, have significantly altered over 50% of the earth's land surface, leading to the permanent clearing of more than a quarter of the world's forests (Hurtt et al., 2011; Vitousek et al., 1997). Natural disturbances, including wind, fire, insect outbreaks, hurricanes, and disease, contribute to tree mortality and alter forest compositions (Chambers et al., 2007; Seidl et al., 2017; Sieg et al., 2017). Despite international and national efforts towards sustainable forest management, global

forest loss amounted to 2.3 million square kilometers between 2000 and 2012 (Hansen et al., 2013). Annually, this deforestation accounts for approximately 12-20% of global anthropogenic CO2 emissions (Van der Werf et al., 2009). Furthermore, forest fragmentation has left 70% of the remaining forests within 1 km of an edge (Haddad et al., 2015), with such edge effects in tropical regions causing additional carbon emissions of 0.34 Gt annually and exacerbating species loss (Broadbent et al., 2008; I. M. Turner, 1996).

1.1.2 Disturbance and Forest Attributes

Anthropogenic influences and climate change have significantly altered forest disturbance regimes. Recent decades have seen an escalation in the frequency and intensity of these disturbances (Allen et al., 2010). This trend is expected to continue, with projections indicating an increase in the frequency and severity of natural disturbances in North America, potentially leading to a reduction in forest carbon stocks (Peterson, 2014). Concurrently, the impact of human activities on terrestrial ecosystems has intensified (Millar & Stephenson, 2015; Venter et al., 2016). The nature of these changes varies: they may be fewer but more intense, more frequent but less severe, or both more frequent and more intense, each scenario having distinct implications for forest structure and carbon storage. The intensity of disturbance, whether it is clearcutting or partial removal, significantly influences the post-disturbance environmental conditions, species composition, and subsequent forest regrowth. Thus, a comprehensive understanding of historical disturbance patterns is crucial for predicting future forest dynamics.

In parallel with changes in disturbance regimes, key forest attributes that dictate forest functioning and response to disturbances have also undergone substantial transformations. Stand characteristics such as basal area, age, and biomass are critical in influencing forest recruitment,

growth, mortality, and the carbon stored in flora and soil. These attributes are also indicative of biodiversity potential, not only through direct provision of habitat resources for various species but also indirectly by sustaining essential ecological processes like leaf-litter decomposition and micro-climate stability (Gibson et al., 2011; Schall et al., 2018). Collectively, forest attributes represent the forest's overall condition and are interlinked throughout its development. The intensity of a disturbance dictates the extent to which these key attributes are altered, either completely or to a certain degree (Dale et al., 2001; Luisa, 2012). During the regrowth phase, these forest attributes, including basal area, age, and biomass, begin to accumulate, with their interrelated increases over time depicted in Figure 1-1. Among the suite of forest attributes, age holds values in several unique aspects:

(1) By providing a chronological record of a tree's or forest's life, age indicates how long a tree or stand has been growing. It is critical in understanding the developmental stage of a tree or forest. Different stages (e.g., seedling, sapling, mature, senescent) have distinct ecological characteristics and roles(Caswell & Salguero-Gómez, 2013; Gatsuk et al., 1980). Therefore, age can be the indicator for other important structural and physical attributes like height, biomass, and growth rate, etc.

(2) Age can provide insights into the historical context of a forest, such as past disturbances (fire, logging) or climatic conditions. This historical perspective is unique compared to instantaneous measurements like biomass or basal area, which provide a "current snapshot" but not the historical narrative.

(3) Age can act as the determinant of ecological processes (Whitney & Foster, 1988). The age of a forest influences various ecological processes differently than physical

attributes. For example, older forests might have more developed soil communities and greater biodiversity, influencing nutrient cycling and habitat complexity.

(4) Forest age is the basis for management and conservation decisions. Age information is often used in forest management and conservation to determine harvesting schedules, assess forest health, and implement restoration or conservation strategies. Therefore, age information is invaluable for a range of environmental, scientific, and conservation-related purposes. The dissertation will focus on disturbance intensity (using basal area change as the proxy) and tree/forest age.

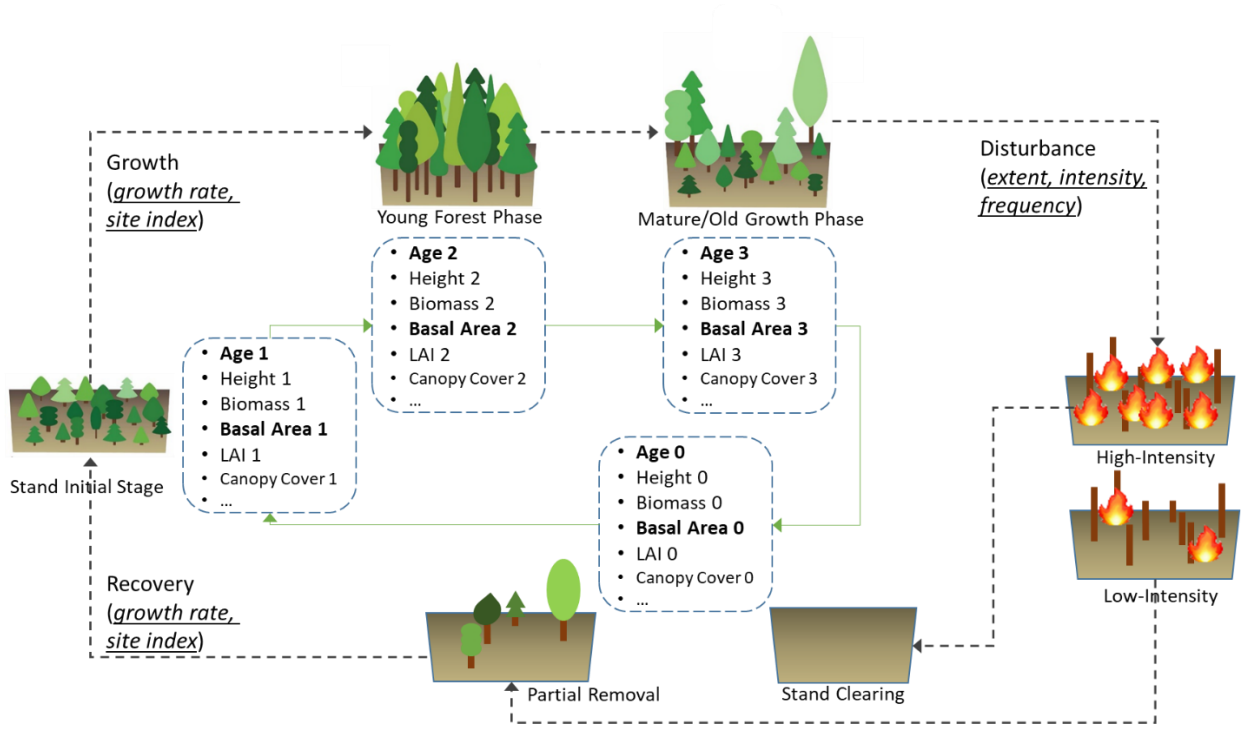

Figure 1-1 Forest attributes as a whole entity affected by disturbance and different growing stages

1.1.3 Need for Integrated Approaches for Forest Attribute Monitoring

To monitor forest changes effectively, two primary methodologies are employed: forest inventory and remote sensing. Forest inventory involves direct measurement of trees within

sample plots. These measurements, considered as the 'ground truth,' are crucial for accuracy assessment in research. However, field inventories are time-consuming and labor-intensive, leading to their limited implementation. Comprehensive ground-based inventories, like the Forest Inventory and Analysis (FIA) program by the US Forest Service or the National Forest Inventory (NFI) by the Swedish University of Agricultural Sciences, are rare and often absent in remote regions. Moreover, sample plots from national inventories are usually sparsely placed, the measurements from which cannot form spatially continuous maps as desired by lots of applications (Fassnacht et al., 2023). Field measurements record plot conditions at the time of survey, and it can take years for crews to revisit the same site. But changes to forests caused by disturbance events can be sudden and rapid; thus, important information related to these changes may not be reflected by inventories in a timely manner.

Remote sensing, the second approach, revolutionizes our ability to observe Earth's vegetation from space or air, offering broad-scale, temporal views of forests (DeFries, 2008). The Landsat data archive is unique in combining a global acquisition and provision of a multi-decade historical record. Many studies have utilized Landsat time series for monitoring, providing detailed information on forest area and canopy cover (Avitabile et al., 2012; Chrysafis et al., 2017; Cohen et al., 2001; Dube & Mutanga, 2015; Hall et al., 2006; Pflugmacher et al., 2012; Powell et al., 2010; P. Zhao et al., 2016). However, challenges exist, such as the saturation of optical signals in dense forest areas (Duncanson et al., 2010; Lu, 2006; Lu et al., 2016). LiDAR, while effective in measuring vertical structures beneath canopies, offers only one-time, sample-based height estimates and lacks temporal data. Consequently, there is a growing need to combine field and/or LiDAR measurements with continuous remotely-sensed data to generate comprehensive maps of forest structures (Coops et al., 2021).

Table 1-1 presents studies demonstrating the feasibility of integrating multiple data sources for characterizing forest attributes. These studies often correlate satellite reflectance data with field and/or LiDAR data for calibration and validation, modeling various forest structural response variables. Models typically incorporate spectral indices, disturbance variables, topography, and other site condition indicators. *However, because different attributes are often studied individually from different data sources and with different methods, inconsistencies may exist among those attributes, as the interrelationships among those attributes are often overlooked.*

For instance, in areas where regrowth has commenced, pixels may indicate a substantial age value, yet the aboveground biomass value might be nearly zero (Figure 1-2 A). Similarly, in pixels where the stand age exceeds zero, biomass values might be overlooked in carbon stock calculations because of different data coverage (Figure 1-2 B). Consequently, these maps, when used in isolation, may provide inconsistent or non-comparable data for assessing forest conditions. If employed separately for calibrating ecosystem models or aiding in strategic-level forest monitoring, such discrepancies can lead to conflicting results. Conversely, using these data sources in tandem presents challenges in reconciling these differences.

Another limitation of current methodologies is the consideration of long-term disturbance history. Many studies use time since disturbance as an indicator of forest regrowth stage. This approach, however, typically assumes a clear-cut disturbance followed by immediate reforestation (Bradford et al., 2008). Yet, natural disturbances often do not remove all trees in a stand, resulting in regenerating trees growing among surviving older trees. Additionally, regeneration can be a protracted process, with newly grown trees varying in age even after decades. Hence, alongside time since disturbance, the intensity of the disturbance - quantifying

the strength of the disruptive force - should also be factored in to more accurately estimate forest regrowth post-disturbance.

Table 1-1 Summary of selected studies mapping forest attributes

Reference	Attributes	Data	Area	Method
Chen et al., 2016	Stand Age	Landsat, MODIS, AVHRR	Siberia	Random Forest
Pan et al., 2011	Stand Age	SPOT, Landsat, Inventory	Canada, US	Dating and mapping disturbance; Voronoi polygons
Diao et al., 2020	Stand Age	Landsat time series, Inventory	Three plantations in China	Dating and mapping disturbance; Random Forest
Frazier et al., 2014	Biomass, stem volume, basal area, Lorey's height	Landsat (multi-temporal) Airborne LiDAR	Site in British Columbia/Yukon Territory, Canada	Random Forest
Zald et al., 2016	Biomass, height, basal area, volume, canopy cover	Landsat (multi-temporal), Airborne LiDAR	Saskatchewan, Canada	Random Forest
Lefsky, 2010	Height	MODIS, GLAS (Spaceborne LiDAR)	World	Decision trees, linear regression
Hansen et al., 2016	Height	Landsat (multi-temporal), GLAS (Spaceborne LiDAR)	Sub-Saharan Africa	Regression Trees
Ahmed et al., 2015	Canopy Cover, Height	Landsat (multi-temporal), Airborne LiDAR	Site in British Columbia, Canada	Random Forest, Linear Regression

Hudak et al., 2002	Height	Landsat, Airborne LiDAR	Site in Oregon, US	Linear regression, kriging
Lefsky et al., 2005	Biomass	Landsat (multi-temporal), Airborne LiDAR	Site in Oregon, US	Linear regression, unsupervised classification
Tomppo et al., 2008	Stem Volume	Landsat, SPOT, NFI plots	Sweden, Finland	k-NN Regression
Qi & Dubayah, 2016	Height	LVIS, Tandem-X InSAR	Site in New Hampshire, US	Random Volume over Ground (RVoG) model
Englhart et al., 2011	Biomass	SAR, airborne LiDAR	Tropical Forest Site	Multiple linear regression
Matasci et al., 2018	Height, Biomass, Basal Area, Stem Volume	Landsat (multi-temporal), LiDAR	Canada	Random Forest
Saatchi et al., 2011	Biomass	GLAS, field plots, MODIS, SRTM	Tropical Region	Allometric Equation, Maximum Entropy Model
Li et al., 2011	Height	GLAS, SRTM, Landsat	Mississippi	Stepwise Linear Regression, Regression Tree
Potapov et al., 2021	Height	Landsat, LiDAR	Global	Regression Tree
Rishmawi et al., 2021	Height, canopy cover, foliage height diversity, plant area index	VIIRS, LiDAR	US	Random Forest

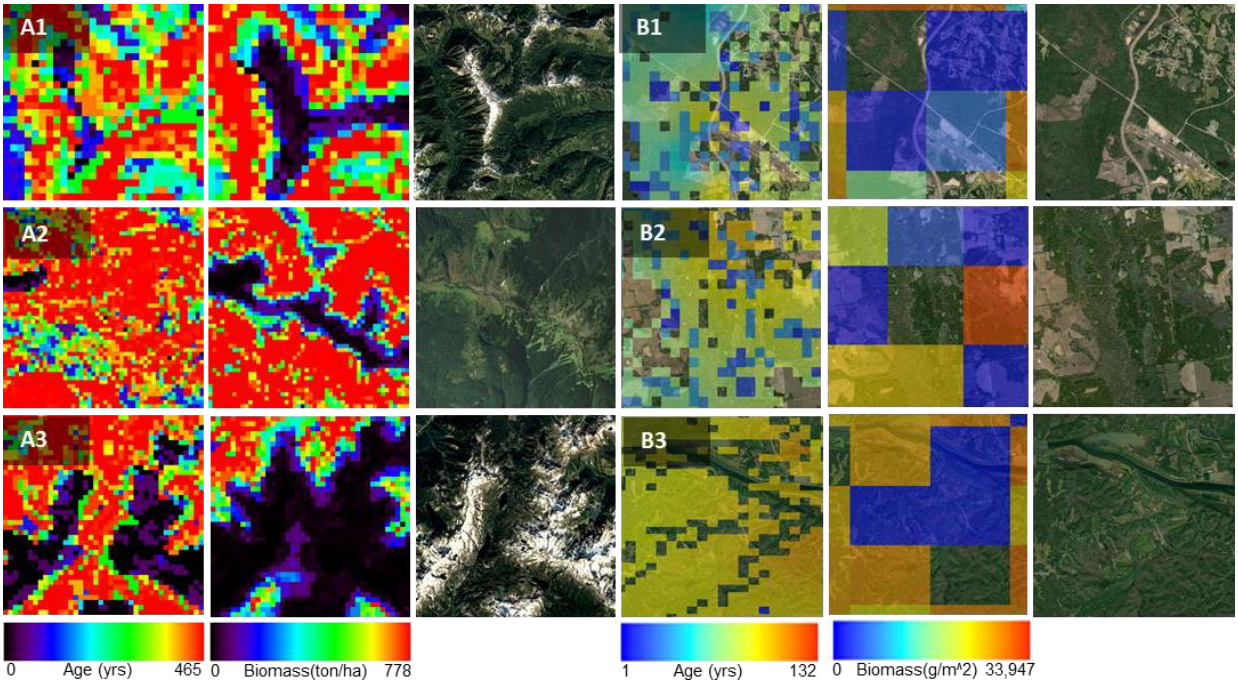

Figure 1-2 Three columns in Panel A are Canada NFI MODIS-based 250m age and biomass maps for 2011, and corresponding Google Earth high resolution image indicating true ground condition. The maps are derived from MODIS images and field plot using k-NN (Beaudoin et al., 2018).. *Three columns in Panel B are LandCarbon Landsat-based age and biomass maps for 2006* (Zhu et al., 2010), *and corresponding Google Earth imagery. Initial 30m age maps are established from disturbance records; biomass is estimated at 2km using the General Ensemble Biogeochemical Modeling System (GEMS) under future scenarios.*

1.2 Research Questions and Dissertation Structure

Remote sensing provides unique capabilities for monitoring a range of key forest attributes, but individual attribute-based approaches can result in conflicting information. Many forest attributes are interrelated as they change throughout a forest's life cycle (disturbance/recovery); considering such inter-relationships through integrated modeling of a suite of forest attributes should result in more consistent and likely more accurate products than mapping each individual attribute separately. The overarching question of this study is how to explore such inter-

relationships for integrated and improved monitoring of important forest attributes over large areas. Building on recent progress in monitoring forest disturbances using time series Landsat observations, this research seeks to advance remote sensing-based monitoring of forest disturbance intensity and forest age. Forest age is especially difficult to map, because forest age is inherently difficult to define in the first place, especially for natural forests that are typically uneven aged. For such forests, the age of all individual trees may be needed in order to determine a meaningful age value for a forest. However, conventional ground-based methods for estimating tree age are time consuming, making it impractical to measure the age of all trees within a forest stand. To address these challenges, this study is designed to answer the following specific questions:

(1) How well can forest disturbance intensity can be mapped across the United States?
(2) How to define forest age for uneven-aged forests? How to obtain age values for adequate tree samples needed to define forest age?
(3) How to integrate remote sensing-based forest disturbance information to improve forest age mapping?

The methods developed through this study will be applied across the conterminous United States (CONUS). The derived products will then be analyzed to answer the follow questions:

(4) What are the spatial-temporal patterns of forest disturbance intensity across the country?
(5) How are tree age and forest age distributed over CONUS?

This dissertation presents five chapters. Chapter 1 introduces the background and motivation of the research, as well as the research questions and dissertation structure.

Chapter 2 presents the first set of annual forest disturbance intensity map products quantifying the percentage of basal area removal (PBAR) at the 30-m resolution for the conterminous United States from 1986 to 2015 by integrating field plot measurements collected by the FIA program and time series Landsat observations. The chapter describes in detail the methods to calculate disturbance intensity, derive reference data, link field measurements to remote sensing imagery, and assess the model accuracy.

Chapter 3 developed a modeling framework which factors in tree size, species and environmental variables to estimate tree age. Age was quantified for every tree in the FIA database (over 10 million trees) across the US, which was previously unavailable. From individual tree age, the population distribution of tree age was estimated for 2015. The chapter describes the modeling design, bias correction process, and the distribution of tree age across the conterminous United States (CONUS). This chapter also discusses the implication of a more complete tree age dataset.

Chapter 4 produced the first set of 30-m forest age and complexity maps for US forest in 2015 and 2005 considering historical disturbance intensity, time series spectral trajectory, and environmental variables. Forest age was calculated using the tree age estimates from Chapter 3. Detailed methods and discussion on the model accuracies are also included in this chapter.

Chapter 6 concludes with a summary of the major findings from all chapters and explores potential directions for future research.

Chapter 2: Annual forest disturbance intensity mapped using Landsat Time Series and field inventory data for the Conterminous United States (1986-2015)[1]

2.1 Abstract

Forest disturbances can have broad impact on the climate, local environment, and the regeneration of the forest ecosystem. The nature and magnitude of such impact is largely driven by disturbance intensity. In this study, by integrating field plot measurements collected by the Forest Inventory and Analysis program with time series Landsat observations, we produced the first set of annual forest disturbance intensity map products quantifying the percentage of basal area removal (PBAR) at the 30-m resolution for the CONUS from 1986 to 2015. The derived map products revealed that during the 30-year study period, the annual average PBAR values of all disturbed pixels across CONUS ranged from 66% to 70%, and the proportion of those pixels having stand-clearing disturbances ranged from 40% to 58%. High disturbance intensities were concentrated in the Southeastern states from Texas to Virginia and along the Pacific coast and the Cascades in the West. At the national scale, the annual mean PBAR and proportion of stand clearing area (PSCA) values both appeared to follow second order trajectories, with increasing trends at the beginning, decreasing trends towards the end, and turning points around 2003. Overall, there is a net increase of 2% in PBAR and 3% in PSCA from 1986 to 2015. The

[1] This chapter has been published on the Remote Sensing of the Environment. The citation for the published version is: Lu, J., Huang, C., Tao, X., Gong, W., & Schleeweis, K. (2022). Annual forest disturbance intensity mapped using Landsat time series and field inventory data for the conterminous United States (1986–2015). Remote Sensing of Environment, 275, 113003.

temporal trends of PBAR and PSCA were also investigated at state and ecoregion levels, with substantial differences found among many states and ecoregions. While states and ecoregions generally follow second order trajectories, the majority had increasing trends throughout much of the study period, reflecting higher disturbance intensities during the later years compared to earlier years. Large increase (>10%) in PBAR was seen in several states (e.g., Virginia, Arkansas, and Minnesota) and ecoregions (e.g., Northern Minnesota Wetlands); however, large decreases (>10%) in PBAR were not observed in any states, but seen in only one ecoregion, the Blue Mountains in the southeast.

2.2 Introduction

Disturbance regimes (i.e., extent, severity, and frequency of disturbance) have intensified in recent decades as a result of both climatic changes (e.g., in temperature and precipitation) and changing human activities (e.g., in timber production) (Seidl et al., 2011, 2017; M. G. Turner, 2010). Reported changes include the increasing frequency of wildfires in the western US (Abatzoglou & Kolden, 2011; Westerling et al., 2006), intensifying windthrow and insect outbreaks in Europe (Kautz et al., 2017; Paritsis & Veblen, 2011), increasing occurrence and severity of drought (Allen et al., 2010; Diffenbaugh et al., 2015) and so on. In North America, this trend is expected to continue in the future as climate changes (Wuebbles et al., 2017). The changes in disturbance regimes alter the mortality and regrowth pattern of forest ecosystems, potentially affecting the resilience of forest ecosystems to future disturbances and the capacity of forests to provide various ecosystem services (Dale et al., 2001; Johnstone et al., 2016). As an important component in disturbance regimes measuring the strength of the disturbance force, disturbance intensity immediately affects the changes of forest structure, composition (Panfil &

Gullison, 1998; Parrotta et al., 2002), subsequent forest productions (Egnell, 2017), and plant litter input. The changes caused by disturbances, dictated by their intensities lead to long-term impacts on forest carbon storage (Scheller et al., 2011), soil carbon and nutrient stocks (Akselsson et al., 2007; Mushinski et al., 2017; Olsson et al., 1996; Yanai et al., 2003), and microbial communities in adjacent water environment (Reid et al., 2010). Knowing how disturbance intensity changes over time and how forests respond to historical disturbances will help in evaluating disturbance risk, preparing for future disturbances, and minimizing their negative effects (Buma & Schultz, 2020; Thom & Seidl, 2016).

To empirically quantify forest changes, efforts have been focused on two approaches: field inventory and remote sensing. National Forest Inventories (NFIs) are mandated by many countries' governments, with the USFS FIA program being one of the oldest and largest (Bechtold & Patterson, 2005; Gelfand et al., 2013; McRoberts et al., 2005). For NFIs to be useful in monitoring the state and trends of forests standardized plot designs, definitions, and protocols are paramount. NFI datasets with repeated field measurements allow for the estimation of attribute changes over time (Bechtold & Patterson, 2005; Fridman et al., 2014). The spatial distribution of FIA plot designs cannot always provide the spatial resolution necessary for all applications (McRoberts & Tomppo, 2007; Tomppo et al., 2008). Tracking annual forest disturbances with strategic national field inventories alone is challenging given the highly localized and clustered nature of many natural disturbance processes in space and time (Bradford et al., 2010). Tree regrowth rates after disturbance can be very rapid in areas with high productivity or management, confounding field data collected at longer intervals. Image-based remote sensing can provide spatially contiguous and frequent observations useful to detect disturbance location, extent, and severity over large areas. Since the 1970s, Landsat has been

providing multi-decades observations over the Earth's surface (Cohen & Goward, 2004). In 2008, all Landsat data were made available for free (Woodcock et al., 2008) marking a new era for utilizing Earth observation data; thereby allowing researchers to better document changes to terrestrial ecosystems at large space scales, including developing novel methods in forest disturbance mapping (Hansen & Loveland, 2012). Many algorithms have been developed to estimate the occurrence location, extent, time and duration of disturbances by detecting changes in spectral trajectory from Landsat time series (DeVries et al., 2015; He et al., 2011; Hermosilla et al., 2015; Huang et al., 2010; Zhu, Zhang, et al., 2019). Yet deriving forest change from optical remote sensing data alone is restricted by the spectral saturation of optical signals in highly productive forests (Lu, 2006; Lu et al., 2016), and limited usable data availability due to cloud contamination (Asner, 2001). Further, many remote sensing-based disturbances products can have high uncertainties (Cohen et al., 2016). Field data are necessary in order to further model meaningful variations in biophysical variable of interest, such as basal area. Both field inventory and remote sensing have strengths and weaknesses, and with either one alone, the spatial and temporal pattern of disturbance intensity would not be well understood.

In previous studies, disturbance magnitude has been calculated as the difference of spectral reflectance ratio-based indices between pre- and post-disturbance observations (Huang et al., 2010; Kennedy et al., 2010). While the calculated disturbance magnitude can be used as the approximation to the disturbance severity or intensity (Senf & Seidl, 2021), this spectral change cannot be directly used to measure the biophysical consequences of a disturbance event. The quantification of a disturbance's impact on biophysical variables such as changes in biomass, basal area, and height would require accurate reference data from pre- and post-disturbance events. Following the concept that harvest intensity can be estimated as changes in basal area and

canopy cover (Healey et al., 2006; Hill et al., 2015), Tao et al., 2019 demonstrated the feasibility of combining Landsat time series and multi-temporal field measurements to quantify disturbance intensity in North and South Carolina for over 30 years. Here disturbance intensity, measured by changes in basal area, is a combination of both natural disturbance severity and anthropogenic activity intensity (e.g., logging intensity). Building on that study, the objective of this research was to test the applicability of the approach over larger geographies, then use it to generate yearly maps of forest disturbance intensity in the conterminous United States (CONUS) from 1986 to 2015. The resultant maps provided quantitative estimates of changes in basal area following each disturbance event. We examined the spatial patterns and temporal trends of disturbance intensity across CONUS at both the state and the level-3 ecoregion (U.S. Environmental Protection Agency, 2010) level. The derived map products will not only provide a more precise quantification of forest disturbances across the US, but they can also be used to derive a more accurate assessment of the impacts of those disturbances on ecological functions.

2.3 Data

2.3.1 Landsat Time Series Stacks

Landsat time series stacks (LTSS) (Huang et al., 2009) were used to detect disturbance occurrence in this study. LTSS are formed by ready-to-use Landsat 5 TM, Landsat 7 ETM+ and Landsat 8 OLI images that were acquired from leaf-on season with minimum cloud cover (<5%) and shadows, and they have been geometrically and radiometrically corrected by the Landsat Ecosystem Disturbance Adaptive Processing System (LEDAPS) (Huang et al., 2009; Masek et al., 2006). When no cloud-free image could be found for a specific year, multiple partially cloudy (<50%) images from that leaf-on season were used to create compositions that met the

threshold of less than 5% cloud cover (F. Zhao et al., 2018). More details on the selection of images can be found in (K. Schleeweis et al., 2016). Thus, an annual LTSS was constructed for each Landsat WRS2 tile and should contain one optimal image for each year. To achieve the complete coverage of CONUS, a total of 434 annual LTSS were used, and each was comprised of about 30 annual cloud-free or near cloud-free images from 1986 to 2015.

2.3.2 FIA Plot Data

Reference disturbance intensity data was derived from the FIA database. FIA has over 377,000 plots, with roughly 1/3 forest sample plots, distributed across the Nation (Smith, 2002). Starting in 2000, FIA plots were divided into 5 panels in the eastern states (see Northern Region and Southern Region states in Table 2) and 10 panels in the western states (see Interior West Region and Pacific Northwest Region states in Table 2) with the intention to measure one panel per year (Gillespie, 1999). The panel design samples 14-20% of eastern plots and 10% of western plots each year with the full state remeasured inventories completed roughly every 5 years for eastern states and 10 years for western states. A panel corresponds to a measurement year of the 5-year or 10-year cycle. After the last panel is measured, the cycle is repeated. For example, for most eastern states, if the plots from panel one was measured in 2010, each of the remaining four panels (2-5) would be assigned to the four succeeding years (2011-2014) and plots from panel one will be measured again in 2015 (Brand et al., 1981). Additionally, each panel's design ensures a statistically balanced sample of plots that can estimate forest inventory variables annually for the entire state. During each field visit, the FIA crew measures the diameter at breast height (d.b.h) for timber species, the diameter at the stem root collar (d.r.c) for woodland species. Trees ≥ 12.7 cm d.b.h./d.r.c located within subplots and trees < 12.7 cm d.b.h./d.r.c located

within microplots are measured for other attributes. See (Forest Service Forest Inventory, 2023) for explanation of variables and the plot design. Repeat measurements at the same plot on different dates can be used to calculate changes in volume or basal area resulting from disturbances that occurred between those two dates.

Not all FIA plots were used to calculate reference disturbance intensity. Several criteria were applied to identify plots to be used as reference for this study. First, we excluded plots established in the periodic FIA phase prior to 1998, to ensure plot data was collected with the national standardized plot design and data collection procedures. Second, a plot was used if it had experienced disturbance between two consecutive annual inventories. This was determined by collocating exact locations of FIA plots with the 30 m vegetation change tracker (VCT) annual disturbance products. This ensures the measurements of sample trees pre- and post-disturbance are available for estimating the change. Third, a plot was used if it was not located on a forest patch edge, for the following reasons: (1) if a plot is located across disturbed patch edges, impact of disturbance on the trees within and outside the patch will be distinct, which can lead to underestimation of plot disturbance intensity (Tao et al., 2019); (2) when plots are linked to pixels, geolocation mismatch could introduce large uncertainties, given the up to ±30-m positional accuracy of Landsat terrain-corrected Level 1 (L1T) images (Storey et al., 2014, 2016). If four subplots are highly heterogeneous, both forest attribute change and its corresponding spectral change should be different across subplots. Due to the offset of pixel location, the forest attribute change of a plot could be associated with deviated spectral characteristics. The mismatch has been demonstrated to have a strong impact on the prediction accuracy of forest attributes, such as biomass (Frazer et al., 2011) and forest area (McRoberts et al., 2010). The calculation of reference disturbance intensity will be described in section 2.4.3.

2.4 Methodology

The mapping algorithm used in this study generally follows the approach developed by (Tao et al., 2019), which was used to generate forest disturbance intensity maps for North and South Carolina. In this study, we tested the approach over seven states in the Southeast region and then over four FIA regions (Table 2) of the United States before applying it to the entire CONUS. Below we provide a brief summary of this algorithm, as more details have been provided by (Tao et al., 2019). Here we focus more on the handling of reference data across CONUS, the development of disturbance products for CONUS, evaluation of the mapping approach at different scales (state, regional, and national), and assessment of the quality of the resultant CONUS-wide disturbance intensity products and the spatial-temporal patterns revealed by those products.

2.4.1 Overview of Mapping Method

The mapping approach consists of four steps (Figure 2-1). The first was to determine the disturbance year and calculate change of spectral indices from Landsat time series. The second was to derive reference disturbance intensity from repeat measurements on field inventory plots. The reference data were then used to train the Random Forest algorithm (Breiman, 2001) to establish the relationship between the spectral changes and basal area change. The random forest algorithm has been widely used to extrapolate plot measurements of biophysical variables or classification schemes of training samples to large areas with remote sensing data (Belgiu & Drăguţ, 2016). Finally, the model was applied to Landsat images covering the entire CONUS to produce annual wall-to-wall maps. The following sections describe the details in each step.

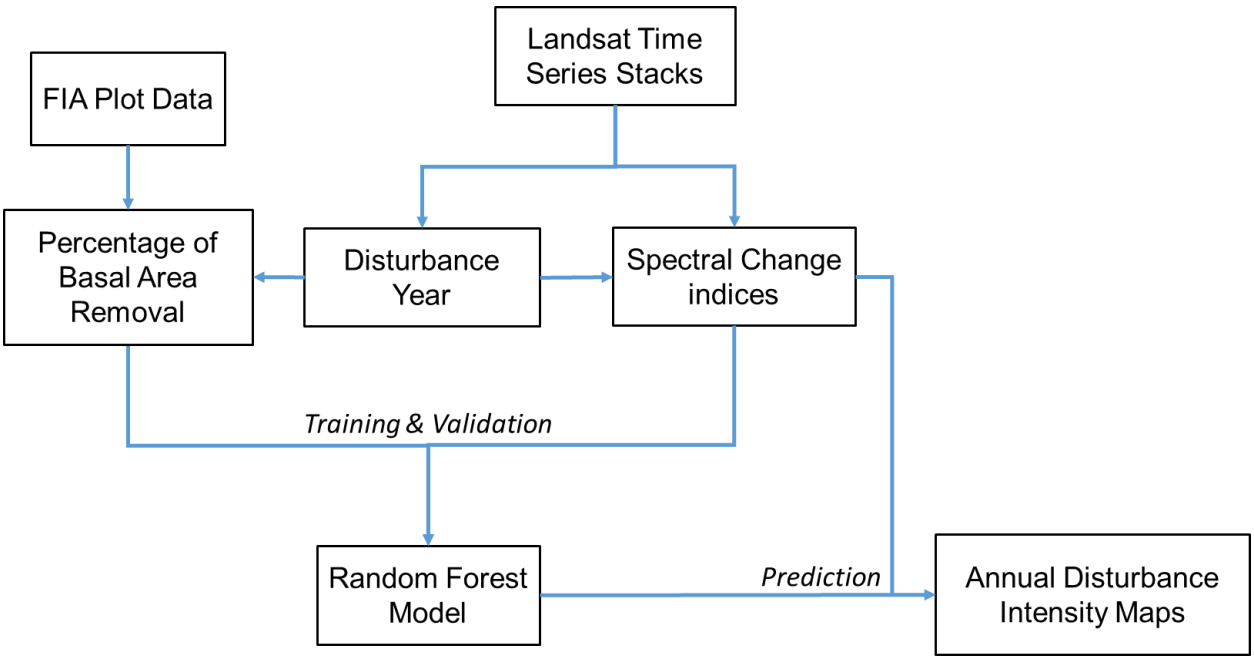

Figure 2-1Key steps of the disturbance intensity mapping framework

2.4.2 Disturbance Product and Spectral Change Metrics from Landsat

Disturbance maps used in this study were derived from Landsat time series stacks (LTSS) (Huang et al., 2009) using the VCT algorithm (Huang et al., 2010). For each image in the LTSS, the VCT algorithm determined the forest likelihood of each pixel by thresholding two spectral indices, integrated forest z-score (IFZ) (Eq. 1) and normalized difference vegetation index (NDVI) (Eq. 2).

$$IFZ = \sqrt{\frac{1}{3}\sum_{band\ red,swir1,swir2}\left(\frac{B_i-\overline{B_i}}{SD_i}\right)^2} \qquad (1)$$

$$NDVI = \frac{B_{nir}-B_{red}}{B_{nir}+B_{red}} \qquad (2)$$

For each disturbance detected, 10 magnitude measures, including 5 delta variables and 5 normalized ratio variables, were calculated using several spectral bands and indices (Table 2-1) to represent the spectral change of the pre- and post-disturbance events as described in (Tao et al., 2019). The indices include NDVI, normalized burn ratio (NBR), normalized difference moisture index (NDMI), IFZ, and forest z-score (FZ) calculated using Landsat bands 4 (B4FZ) and 5 (B5FZ) (Huang et al., 2010). These were calculated as (Eqs. 1-6), where B_i is the reflectance value of Landsat band i, and $\overline{B_i}$ and SD_i are the mean and standard deviation of band i reflectance for all forest samples identified within an image. Previous study (Tao et al., 2019) indicates that the use of all 10 magnitudes of both types would achieve better model accuracy, and thus all the 10 magnitude variables were calculated in this study.

$$NBR = \frac{B_{nir} - B_{swir2}}{B_{nir} + B_{swir2}} \quad (3)$$

$$NDMI = \frac{B_{nir} - B_{swir1}}{B_{nir} + B_{swir1}} \quad (4)$$

$$B4FZ = \frac{B_{nir} - \overline{B_{nir}}}{SD_{nir}} \quad (5)$$

$$B5FZ = \frac{B_{swir1} - \overline{B_{swir1}}}{SD_{swir1}} \quad (6)$$

Table 2-1 Spectral change indices used in disturbance intensity mapping

Category	**Equation**	**Index**
Delta	$magnitude_{\Delta} = Index_{post} - Index_{pre}$	IFZ, NDVI, NBR, B4FZ, B5FZ
Normalized Ratio (NR)	$magnitude_{NR} = 1 - Index_{pre}/Index_{post}$	IFZ, B5FZ
	$magnitude_{NR} = 1 - Index_{post}/Index_{pre}$	NDVI, NBR, NDMI

2.4.3 Reference Disturbance Intensity Derivation

Reference disturbance intensity data was derived from repeat measurements at the same FIA plots on different dates. Given the 5- to 10-year intervals between FIA remeasurements, however, changes in total basal area between two dates cannot be attributed solely to disturbance events. Growth of surviving trees and new trees between the two dates also contributes to an increase in basal area of a plot. Therefore, a simple difference of total basal area between two measures would include the growth, often resulting in an underestimation of the basal area change caused by disturbance events (Figure 2-2).

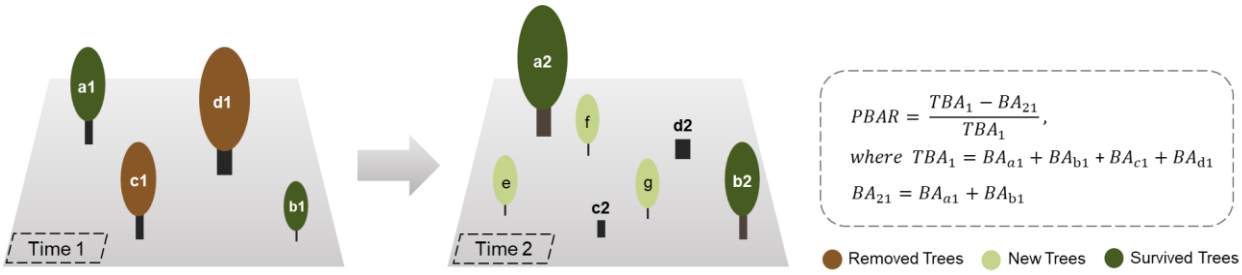

Figure 2-2 An illustration of forest change between two inventory times showing basal area loss due to disturbance (trees c and d), gain from growth (trees a and b), and establishment of new trees (trees e, f, and g). In tree labels, the letter denotes which tree it is, and the number denotes the time of inventory (e.g., a1 means tree a measured at time 1). The basal area change caused by the disturbance event would be underestimated by a simple difference between the two inventories. Instead, it should be calculated using the equation Eq. 7.

To eliminate the effect of tree growth, each tree record was tracked by its sequence number through time. Only trees recorded in the prior inventory and absent from the next inventory are assumed to be affected or removed by disturbances between the two inventories. The difference between basal areas of these trees were then used to calculate PBAR as a measure of disturbance intensity following Eq. 7:

$$PBAR = \frac{TBA_1 - BA_{21}}{TBA_1} \qquad (7)$$

where TBA_1 is the total basal area of all live trees at the first time of inventory, and BA_{21} is the total basal area measured at the prior inventory of trees alive at both inventories (Figure 2-2). Note that the diameter measured at the second inventory was not used in the calculation. If we replace BA_{21} with TBA_2, the total basal area of all live trees at the second time of inventory, which is larger than BA_{21} because it includes the growth of existing trees (trees a and b in Figure 2-2) and new trees (trees e,f and g in Figure 2-2), this will lead to an underestimation of PBAR. PBAR ranges from zero to one, with zero indicating no basal area removed, and one indicating one-hundred percent basal area removed by disturbance. Note in this study PBAR measures the loss of basal area from all possible causes, not differentiating disturbance types. After the calculation of PBAR for each disturbed plot, calculated PBAR was visually compared against available high-resolution imagery, to eliminate any discrepancies. Plots with large discrepancies (e.g. calculated PBAR is less than 20 percent while imagery saw a stand-clearing event had occurred to the same plot between the two dates and vice versa) were removed from the reference dataset. During the comparison process, all security precautions were taken per the FIA agreement, including no exact coordinates were used to search for locations on imagery in Google Earth.

After the screening process (discussed in section 2.3.2 and the previous paragraph), 3554 qualified plot records over CONUS were available for use, with 2575 in the south, 483 in the north, 220 in the Interior West, and 276 in the Pacific Northwest (Table 2-2). Seven states in the southeast (NC, SC, GA, TN, MS, AL, FL) contribute 1573 records (about 44%) to all reference plots. The high density of available reference plots in the region is due to both the frequent and

intensive timber harvesting activities in this part of the country, and the frequency of FIA full panels in the east compared to the west. The measurement years of reference plots range from 1999 to 2017 and the coverage varies by state, depending on the beginning year of transition to the annual inventory system of each state. For all the plots that passed the screening, percentage of PBAR is calculated from pre- and post-disturbance plot measurements in the FIA database, to characterize the impact of disturbance on the forest's biophysical properties, thus providing reference data to disturbance intensity modeling (Healey et al., 2006; Tao et al., 2019).

Table 2-2 Distributions and year range of FIA plots used in this study by state and FIA regions

FIA Region	State	Abbreviations	Plot Counts	Area (km^2)	Measurement Year Range
Southern Region (2575 plots)	Alabama	AL	326	135,765	1999 - 2017
	Arkansas	AR	253	137,732	1999 - 2017
	Florida	FL	120	170,312	2001 - 2016
	Georgia	GA	319	153,910	1999 - 2017
	Kentucky	KY	41	104,656	1999 - 2017
	Louisiana	LA	212	135,659	2000 - 2017
	Mississippi	MS	171	125,438	2006 - 2017
	North Carolina	NC	246	139,391	1999 - 2017
	Oklahoma	OK	34	181,037	2007 - 2015
	South Carolina	SC	293	82,933	1999 - 2016
	Tennessee	TN	98	109,153	1999 - 2017
	Texas	TX	232	695,662	2002 - 2017
	Virginia	VA	230	110,787	1999 - 2017
Northern Region (483 plots)	Connecticut	CT	1	14,357	2009 - 2015
	Delaware	DE	4	6,446	2007 - 2017
	Illinois	IL	2	149,995	2008 - 2017
	Indiana	IN	5	94,326	2002 - 2016
	Iowa	IA	1	145,746	2007 - 2012
	Kansas	KS	1	213,100	2004 - 2009

	Maine	ME	102	91,633	2001 - 2017
	Maryland	MD	4	32,131	2006 - 2013
	Massachusetts	MA	1	27,336	2011 - 2015
	Michigan	MI	88	250,487	2001 - 2017
	Minnesota	MN	122	225,163	2000 - 2017
	Missouri	MO	57	180,540	2002 - 2017
	Nebraska	NE	2	200,330	2008 - 2016
	New Hampshire	NH	7	24,214	2004 - 2016
	New Jersey	NJ	1	22,591	2005 - 2009
	New York	NY	8	141,297	2003 - 2017
	North Dakota	ND	0	183,108	N/A
	Ohio	OH	21	116,098	2002 - 2017
	Pennsylvania	PA	26	119,280	2002 - 2017
	Rhode Island	RI	0	4,001	N/A
	South Dakota	SD	22	199,729	2001 - 2017
	Vermont	VT	2	24,906	2008 - 2016
	Wisconsin	WI	0	169,635	N/A
	West Virginia	WV	6	62,756	2004 - 2014
Interior West Region (220 plots)	Arizona	AZ	31	295,234	2001 - 2017
	Colorado	CO	9	269,601	2003 - 2016
	Idaho	ID	72	216,443	2004 - 2017
	Montana	MT	89	380,831	2003 - 2017
	New Mexico	NM	11	314,917	2010 - 2017
	Nevada	NV	1	286,380	2004 - 2014
	Utah	UT	7	219,882	2000 - 2017
	Wyoming	WY	0	253,335	N/A
Pacific Northwest Region (276 plots)	California	CA	61	423,967	2001 - 2017
	Oregon	OR	129	254,799	2001 - 2017
	Washington	WA	86	184,661	2002 - 2016

2.4.4 Algorithm Assessment and National Mapping

The effectiveness of the disturbance mapping approach had been previously demonstrated in only two states (Tao et al., 2019). To evaluate its robustness more comprehensively, we first

tested it in each of the seven southeastern states (NC, SC, GA, TN, MS, AL, FL). We then tested this approach with a model for each of the FIA regions (Table 2-2) as well as a single model for the entire CONUS. Our goal was to demonstrate the feasibility of using a single model to map disturbance intensity across CONUS to avoid issues that could arise from using multiple models: 1) some states or regions did not have enough reference plots for model development (Table 2-2), and 2) discontinuities could exist between adjacent states or regions if they were mapped using different models.

To evaluate the model for each geographic area, 10-fold cross validations were performed which randomly partitioned the reference plot samples into 10 subsets. Ten different models were built, each trained with 9 of the 10 subsets and tested with the remaining subset such that each of the 10 subsets was used once as a validation set. All 10 sets of validation results were then averaged to produce a single estimation of model performance, measured by the coefficient of determination (R^2, Eq. 8) and Root Mean Square Error (RMSE, Eq. 9),

$$R^2 = 1 - \frac{\sum_{i=1}^{n}(y_i - \hat{y}_i)^2}{\sum_{i=1}^{n}(y_i - \bar{y})^2} \qquad (8)$$

$$RMSE = \sqrt{\sum_{i=1}^{n}\frac{(y_i - \hat{y}_i)^2}{n}} \qquad (9)$$

where n is number of samples, y_i is the PBAR of the ith reference plot, $\hat{y}_i$ is the predicted PBAR of the ith plot, and $\bar{y}$ is the mean PBAR for all the n sample plots.

All models developed in this study were evaluated using this approach. Because the FIA plots used in this study were selected to address the issues described in section 2.4.3, the resultant validation results likely will be different from those derived using a design-based approach

(Olofsson et al., 2014), especially in regions where the number of reference plots is less than optimal. However, because the validation plots were not used in training and had little or no spatial autocorrelation with the training plots (FIA plots are located at least 5 kilometers apart from each other), those validation results should provide a reasonably realistic assessment of the models and derived data products. After the model accuracy assessment, the national model was used to produce wall-to-wall annual disturbance intensity maps for CONUS from 1986 to 2015, where each annual map shows the PBAR values for disturbances from a specific year. In addition to the cross validation described in section 2.4.4, the derived national maps were also evaluated by examining these annual maps over many locations across CONUS where pre- and post-disturbance Google Earth images are available. The high spatial resolution of Google Earth imagery made it possible to determine disturbance intensity qualitatively by examining the pre- and post-disturbance images visually (see Figure 2-5). In total 320 random locations were examined, with 80 in each of the four FIA regions. In each region, points were drawn from two categories, 40 from pixels mapped as low-medium intensity class (0~70%), and 40 from pixels mapped as high intensity class (>70%). The mapped class at each location was compared to the Google Earth imagery pre- and post-disturbance conditions to identify obvious errors (actual low-medium estimated as high, actual high estimated as low-medium).

2.4.5 Spatial/Temporal Analysis of the Disturbance Intensity Products

The annual disturbance intensity maps derived above provided an opportunity to examine the spatial-temporal patterns of disturbance intensity across CONUS over multiple decades. To evaluate the spatial patterns, we aggregated the 30 annual maps into a time-integrated map that records the PBAR of the largest disturbance. This time-integrated map provides a picture of the

spatial variability of PBAR at the 30 m spatial resolution. From the annual maps, we also calculated the mean PBAR values at both the state scale and the Environmental Protection Agency (EPA) level 3 ecoregion scale. EPA ecoregions are defined as areas that share regional similarities in the mosaic of biotic, abiotic, terrestrial, and aquatic ecosystem components (Omernik, 1987, 2004), and therefore natural forests within an ecoregion are expected to develop and grow in similar environments. The level 3 ecoregions (U.S. Environmental Protection Agency, 2010) were used in this study because they appeared to be more appropriate than those at other levels for illustrating the spatial-temporal patterns of forest disturbance intensity mapped in this study. Since the proportion of clear-cut areas to all harvested areas is often used as an indicator of harvest intensity at the regional scale (Mikoláš et al., 2015; K. G. Schleeweis et al., 2020; Soutiere, 1979), we also examined the spatial variability of stand-clearing disturbances across states and ecoregions. Stand clearing is defined as no less than 80% basal area removal (Birdsey & Lewis, 2003).

To examine the temporal variability of disturbance intensity, we used the annual disturbance intensity maps to calculate the mean PBAR as well as the proportion of stand clearing area (PSCA) per each of the 30 years for each state, each ecoregion, and CONUS. PSCA is calculated as proportion of stand-clearing area to total disturbance area. The produced time series allow for investigations into the temporal trend of disturbance intensity. Preliminary analysis indicated there could be three types of temporal changes: trends with a turning point in the middle and similar levels of PBAR at the two ends of the study period (i.e., increase followed by decrease or decrease followed by increase), near monotonic increasing or decreasing trends, and no obvious trend.

A two-step process was used to determine the change type of a time series. First a second-order polynomial regression model ($ax^2 + bx + c$) was used to test if there were trends with a turning point. If the p-value of t-test indicates the polynomial regression was statistically significant ($p<0.01$), a positive quadratic term (coefficient a) would indicate initial decrease followed by increase in PBAR and/or PSCA, while the opposite (initial increase followed by decrease) would have a negative coefficient. Given the relatively short record (30 years) of the disturbance intensity time series, higher order polynomial models were not considered in this study. Therefore, a time series would have no obvious trend if it failed the t-tests of both the linear and 2nd order polynomial fitting. Then the turning point of the polynomial regression model was calculated to determine if the trend had a turning point in the middle and similar levels of PBAR at the two ends of the study period, or if the trend had near monotonic increasing or decreasing with a turning point outside the study period.

2.5 Results

2.5.1 Model performance at different scales

The disturbance intensity mapping algorithm appeared to be robust for most of the seven southeastern states. The cross-validation results (comparison of predicted values against reference data for samples not used in model calibration) resulted in R^2 values ranging from 0.55 to 0.80 and RMSE from 13% to 18% (Figure 2-3). Model results derived over the four US regions and CONUS were not as good as those derived over AL and other 4 southeastern states, but they were comparable to those derived over MS and TN (Figure 2-4). These regional and national models made it possible to map PBAR across CONUS despite the difficulty in developing separate mapping models for individual states due to the lack of adequate sample

plots for model development in many states. In particular, the accuracy of the national model appeared to be similar to those derived over the Southern Region (SR) and Pacific Northwest (PNW) regions and better than those over the Interior West (IW) and Northern Region (NR), suggesting that the national model could be robust enough for mapping PBAR across CONUS. Therefore, the national model was used to produce the final wall-to-wall PBAR maps annually across the country.

Since the accuracy values of the national model shown in Figure 2-4 were derived using set-aside plots that had essentially no spatial autocorrelation with those used in model calibration (FIA plots are located at least 5 kilometers apart from each other), they should provide a reasonably realistic representation of the accuracies of the derived annual PBAR maps at the national scale. While the accuracy of the national model might be driven by plots in the SR region, which contributed 44% of the plots used in this study, no obvious regional biases were found during our comprehensive visual assessments of the resultant maps against available high-resolution Google Earth images. The mapped PBAR values appeared reasonable in most of the areas we checked. Figure 2-5 provides a few visual assessment examples for different disturbance types in different regions.

In the examination against Google Earth Imagery, of the total 160 locations with estimated low-medium intensity over the four FIA regions, 90% in PNW, 85% in IW, 82.5% in NR and 97.5% in SR appeared to have experienced low-medium intensity disturbances; for the 160 locations with estimated high intensity, 92.5% in PNW, 87.5% in IW, 95% in NR and 95% in SR appeared to have experienced high intensity disturbances (Table 2-3).

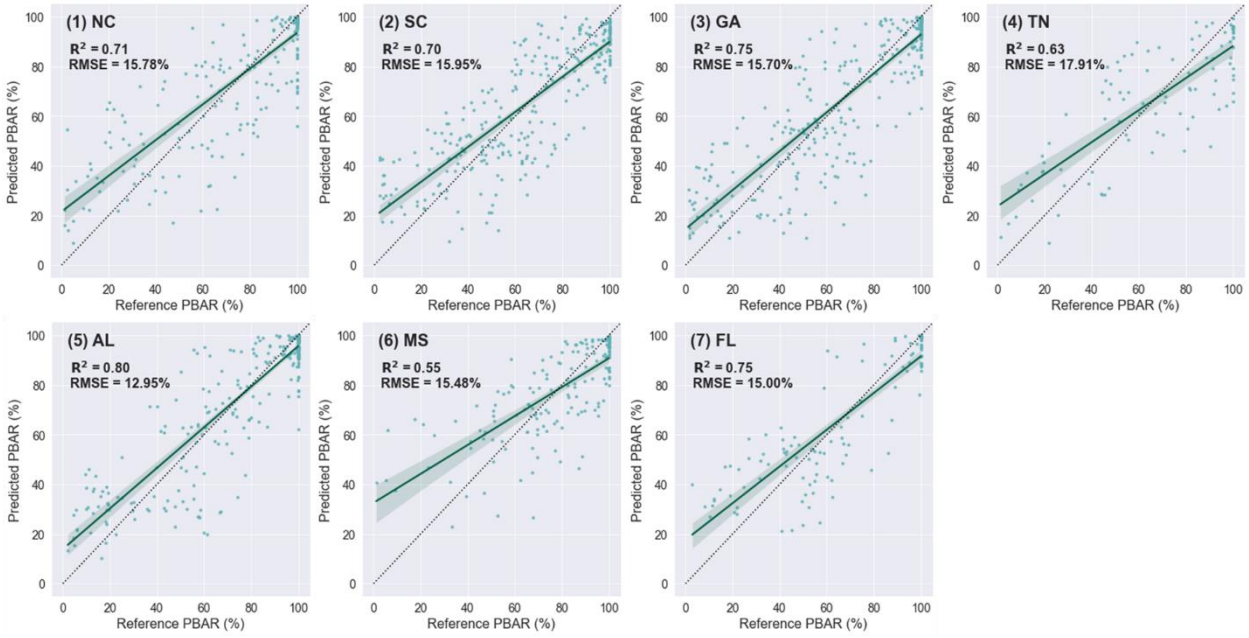

Figure 2-3 Validation of disturbance intensity mapping models developed for seven southern states using set aside reference plots not used in model calibration (notes: unit of histograms on the side is the count of plots; green solid line is the fitted line; black dashed line is the 1:1 line).

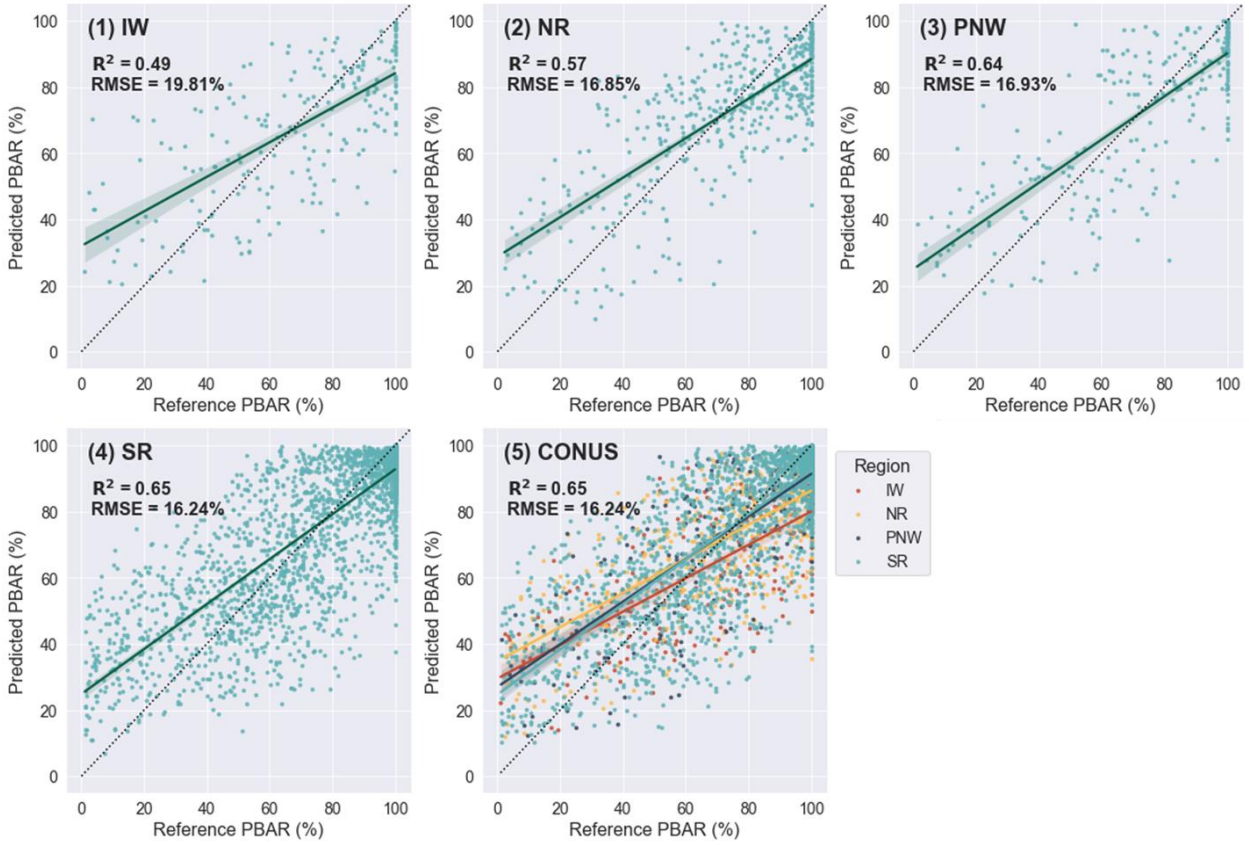

Figure 2-4 Validation of disturbance intensity mapping models developed for (1) Interior West (IW) Region; (2) Northern Region (NR); (3) Pacific Northwest (PNW) Region; (4) Southern Region (SR); and (5) CONUS using set aside reference plots not used in model calibration (notes: unit of histograms on the side is the count of plots; green solid line is the fitted line; black dashed line is the 1:1 line).

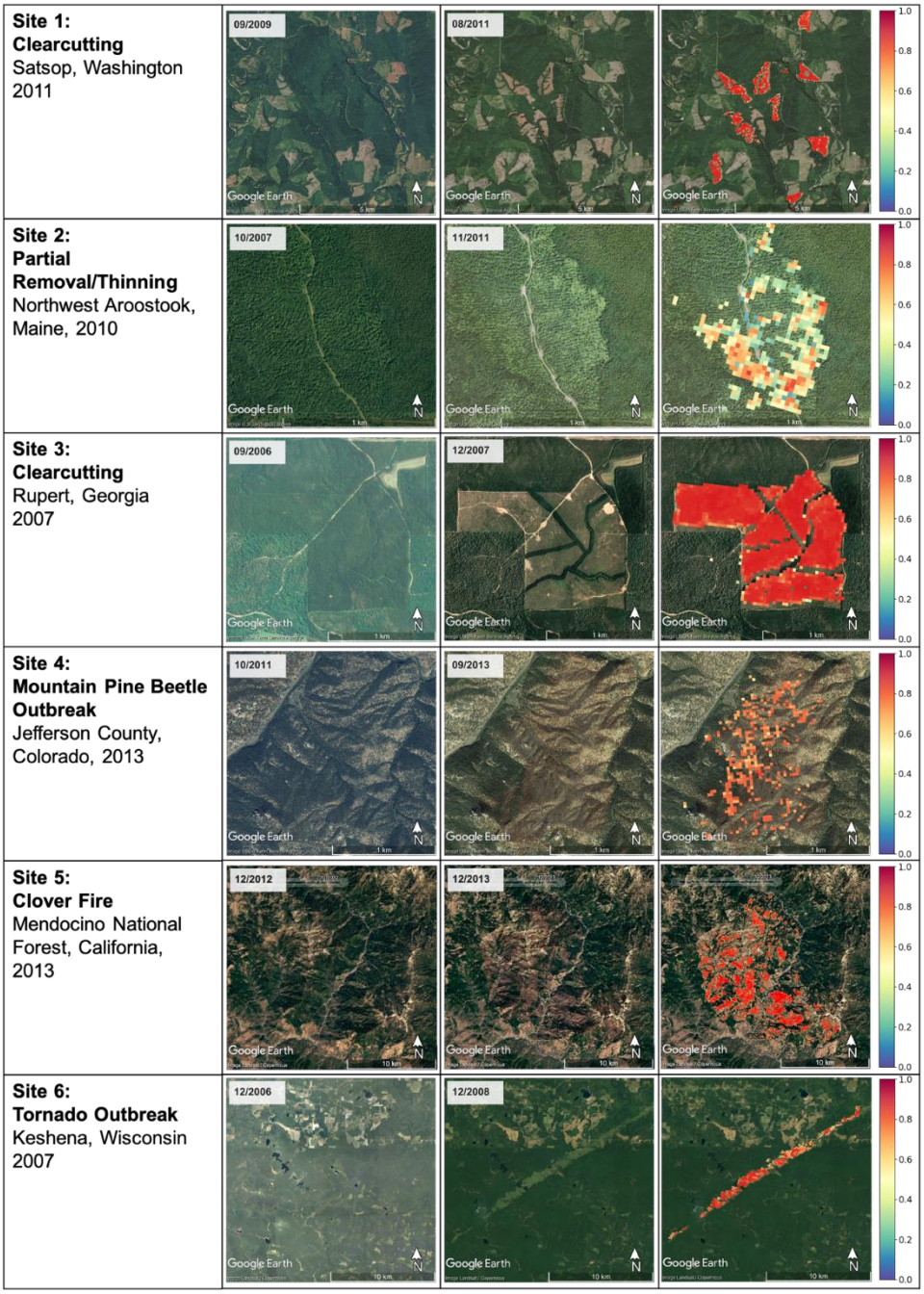

Figure 2-5 Qualitative assessment of the derived disturbance intensity maps overlaid on Google Earth images (4th column) by visually examining high resolution Google Earth images acquired before (2nd column) and after (3rd column) the mapped disturbances for different disturbance types selected from across the country. See Figure 2-6 6 for the locations of the selected examples.

Table 2-3 Visual examination results of mapped intensity over 320 random locations across CONUS with 80 locations in each of 4 FIA regions (Low-medium: PBAR < 80%; high: PBAR>=80%)

FIA Region	Prediction / Reference	Low-medium (n=40 for each region)	High (n=40 for each region)
PNW	Low-medium	36 *(90%)*	3
	High	4	37 *(92.5%)*
IW	Low-medium	34 *(85%)*	5
	High	6	35 *(87.5%)*
NR	Low-medium	33 *(82.5%)*	2
	High	7	38 *(95%)*
SR	Low-medium	39 *(97.5%)*	2
	High	1	38 *(95%)*

2.5.2 Spatial patterns of disturbance intensity in CONUS

The derived disturbance intensity maps revealed that 513,177 km^2 (19.8%) of the forested lands in CONUS were disturbed at least once. About 284,265 km^2 (55%) of the mapped disturbance areas had stand-clearing disturbance events (defined as >=80% PBAR). The time-integrated map created from the annual maps, which represents the PBAR value of largest disturbance, shows how well the spatial patterns of PBAR match the boundaries of many ecoregions (Figure 2-6). As expected, the highest disturbance intensities were found in several ecoregions in the Southeast, Lower South, and Pacific Northwest, where industrial forests with heavy timber harvests are located. Fire intensity in the West was highly variable.

At the state level, 30-year mean PBAR ranged from 52% to 81% (Figure 2-7A). The southeastern states, two states on the pacific northwestern coast (WA and OR), as well as VA and DE have the highest mean PBAR. Nebraska is one of the states that had moderately high mean PBAR, but the state has a very small forest land area. Several states in the West, including

CA, ID, MT, and NV, and two in the east (ME and MD) had moderate disturbance intensities, while values in the remaining states were relatively low.

The ecoregion-based mean PBAR map shows that the disturbance intensity had large within-state variations (Figure 2-7 B). In both WA and OR, for example, high PBAR is seen in the western ecoregions including Coast Range, Willamette Valley, and Cascades, while forestlands to the east of Cascade Range experience low- to medium-intensity disturbances. In California, the Coast Range and Central California Valley ecoregions have much higher mean PBAR (i.e., 82% and 76%) than other regions within the state. Such spatial variability also exists in Texas, where high values only exist in the two ecoregions in the east and west of the state, South-Central Plains and High Plains. For the southeastern US, where the state-level mean PBAR was high, exceptions can be seen in ecoregions such as the Mississippi Alluvial Plain, Southern Florida Coastal Plain, and Western Gulf Coastal Plain. These ecoregions are primarily dominated by land cover types other than forest land, such as crops and pastureland, grassland, and wetland (Homer et al., 2020). Mid- to low- intensity disturbances are also seen in the Blue Ridge region, where national forests and national parks occupy about 50% of the total land area. As expected, the mean PSCA had roughly the same spatial patterns as the mean PBAR but varied in wider value ranges (Figure 2-7 C, D). PSCA was lowest in NY (16%) but was over 60% in several southeastern states (e.g., AL, GA, LA) (Figure 2-7 C). The value range was slightly larger at the ecoregion level, ranging from 13% to 70% (Figure 2-7 D). Ecoregions with high PSCA values include Coast Range and Central California Valley along the Pacific coast and Southeastern Plaines, Piedmont, Middle Atlantic Coastal Plain, and Southern Coastal Plain in the southeast (Figure 2-7 D), where clearcutting has been a common practice (Siry, 2002; Smith & Darr, 2004).

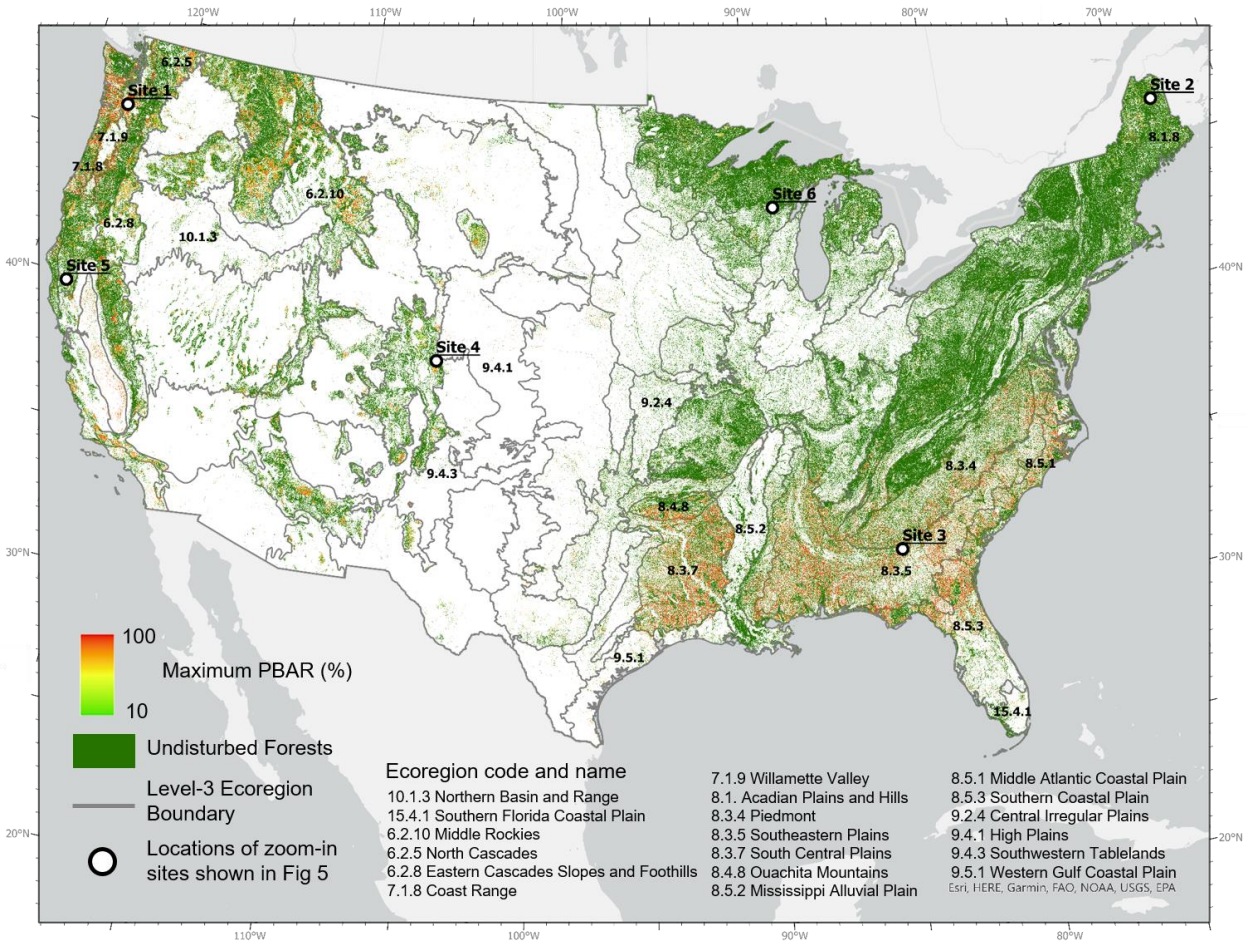

Figure 2-6 A time-integrated map representing the percentage of basal area removal (PBAR) value regardless of the disturbance year for pixel locations where only one disturbance event was detected and the maximum PBAR for locations that were disturbed multiple times overlaid with EPA Level 3 ecoregions shows that the spatial patterns of mapped disturbance intensities match the boundaries of many ecoregions

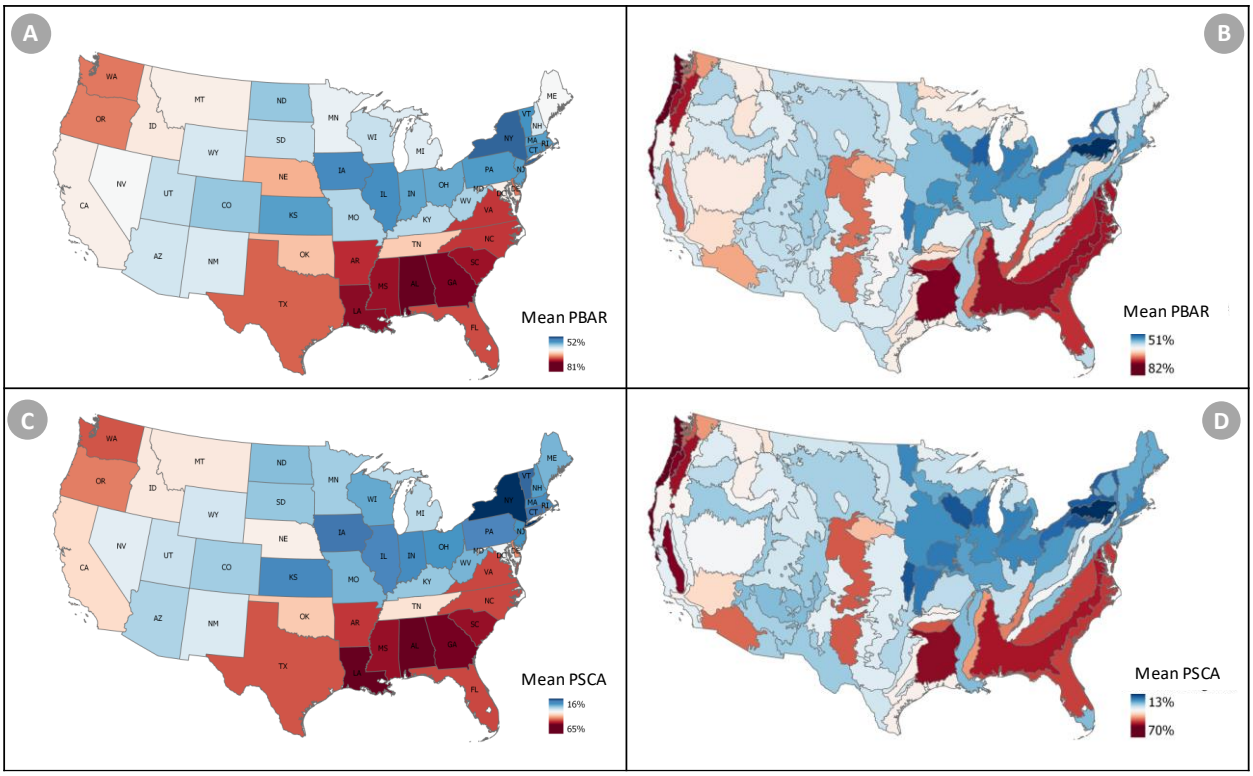

Figure 2-7 Spatial pattern of 30-year average percentage of basal area removal (PBAR) (A: by state, B: by EPA level 3 ecoregion) and average proportion of stand-clearing area (PSCA) (C: by state, D: by EPA level 3 ecoregion)

2.5.3 Temporal Trends of Disturbance Intensity

The mapped disturbance intensities had considerable temporal variations. During the 30-year study period, the annual mean PBAR values over CONUS varied between 66% and 77% while the annual mean PSCA ranged from ~40% to 58%. The result reveals that of all disturbed forest area, only around half are stand-cleared, indicating the importance of considering disturbance intensity when calculating disturbance area or disturbance rate. Both the mean PBAR and PSCA had increasing trends during the first half of the study period followed by decreasing trends in the 2nd half after they peaked at around 2003 (Figure 2-8). Overall, there is a net increase of 2%

in PBAR and 3% in PSCA from 1986 to 2015. It's worth noting that the annual total disturbance area over CONUS did not seem to have any obvious trend and varied over a much wider relative range, from below 20,000 km^2 to above 30,000 km^2 (a range of about 50% of the mean). The temporal range of state level mean annual PBAR, calculated as the difference between the annual mean PBAR values at the 90th and 10th percentiles of each state, varied from 5% to 21% among the 48 states and from 5% to 23% among the 85 ecoregions. Additionally, the range of mean PSCA varied from 10% to 37% among states and 6% to 50% among ecoregions (Figure 2-9). Likely due to large interannual variability in disturbances driven by fire and insect outbreaks (Meigs et al., 2015; Singleton et al., 2019), states and forested ecoregions located in the semiarid west had some of the highest temporal ranges. Most of the remaining states and ecoregions in the country, including those located in the eastern U.S. and along the Pacific coast, had lower temporal variations with their mean PBAR and mean PSCA values.

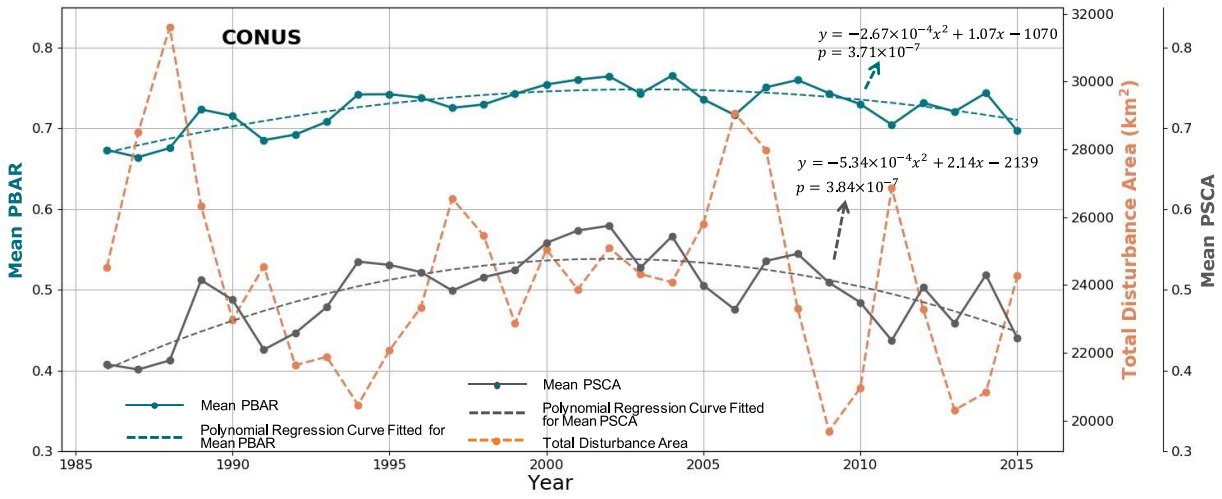

Figure 2-8 Temporal profile of annual mean PBAR (green solid line), annual mean PSCA (grey solid line), and total disturbance area (orange dashed line) along with second order polynomial trends fitted for annual mean PBAR (green dashed line) and annual mean PSCA (grey dashed line).

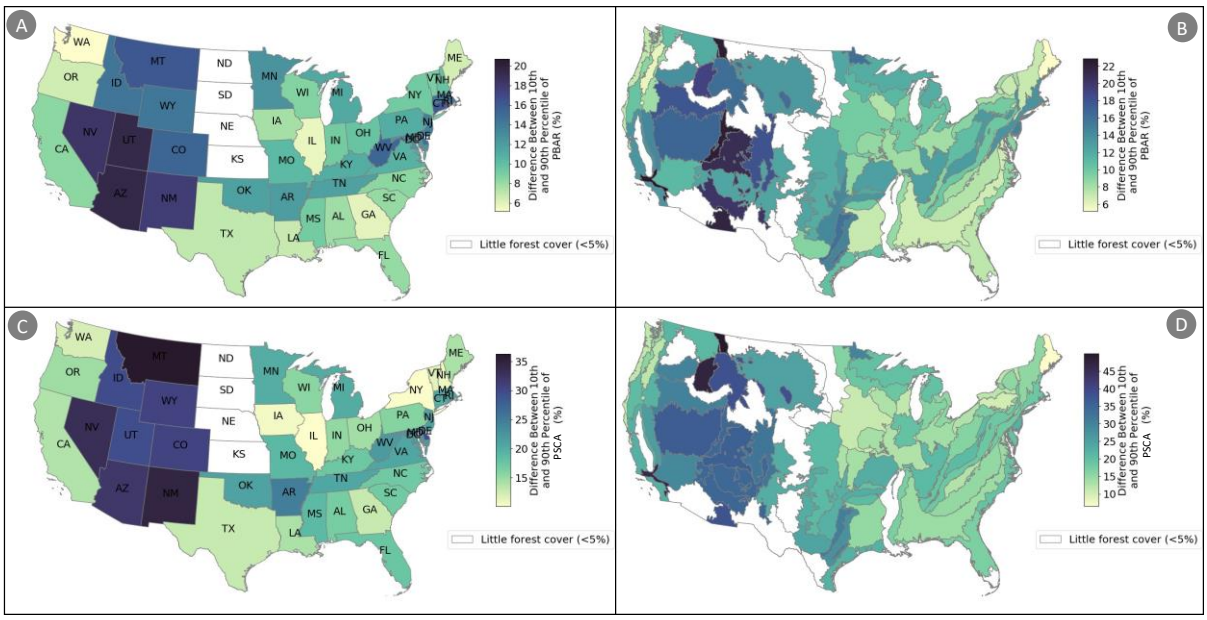

Figure 2-9 Temporal range of state level mean annual PBAR calculated as the difference between the annual mean PBAR values (A: of each state; B: of each ecoregion) and PSCA values (C: of each state; D: of each ecoregion) at the 90th and 10th percentiles.

At the state level (Figure 2-10 A), about two thirds (33 out of 48) of the states had annual mean PBAR values that seemed to follow 2nd order polynomial trajectories with negative 2nd coefficients (initial decreasing trends followed by increasing trends towards the end). The remaining 15 states either did not have statistically significant trends or had extremely low forest cover (< 5%) and hence these trends would not be that meaningful. 11 of 33 states that had statistically significant 2nd order trends (AZ, CO, CT, FL, IL, IN, KY, MD, NJ, NM, TN, TX, UT) had a relatively balanced inverse "U" shape with similar levels of PBAR at the two ends of the study period and a turning point around the middle (2000 ± 3 years). The majority (20 out of 33) had increasing trends throughout much of the study period that resulted in substantially higher disturbance intensities during the later years than the earlier years of the study period (Figure 2-11). Large increase (>10%) in PBAR was seen in several states (e.g., VA, AR, and

MN). Two states (VA, VT) had turning points beyond 2015, meaning they had near monotonic increasing trends over the 30-year study period. With a turning point in 1996, only MT had lower mean PBAR values in the 2010s than in the 1980s.

While the PBAR temporal trends of many ecoregions were similar to those of the states that intersect or overlap with them, there were a few anomalies (Figure 2-10 B). For example, although the state level mean PBAR over WA, OR, CA, and ME did not have any obvious trends, some ecoregions that were completely located within these states, including Coast Range and Acadian Plains and Hills, had near monotonic increasing trends. While none of the states had a trend with a positive 2nd coefficient, three ecoregions, including Eastern Cascades Slopes and Foothills, Ouachita Mountains, and Southwestern Tablelands had positive 2nd coefficients. Large increase (>10%) in PBAR was seen in Northern Minnesota Wetlands, and large decrease (>10%) was observed in Blue Mountains (Figure 2-12). Locations of ecoregions mentioned are marked in Figure 2-6.

Overall, the temporal trends of mean PSCA followed those of mean PBAR at both state and ecoregion levels. However, there were a few states that did not have statistically significant trends with their mean PBAR values, but their mean PSCA values showed 2nd order trends, including ID and WY having negative 2nd coefficients and OR and ME having positive coefficients (Figure 2-10 C). On the other hand, NV and NH had significant trends with their mean BPAR, but not with the mean PSCA. Similarly, several ecoregions, including Northern Basin and Range, Middle Rockies, North Cascades, and Central Irregular Plains did not have obvious trends with their mean PBAR values, but their mean PSCA showed statistically

significant trends (Figure 2-10 D). The ecoregion that had significant trends with their mean PBAR but not with their mean PSCA values was Acadian Plains and Hills.

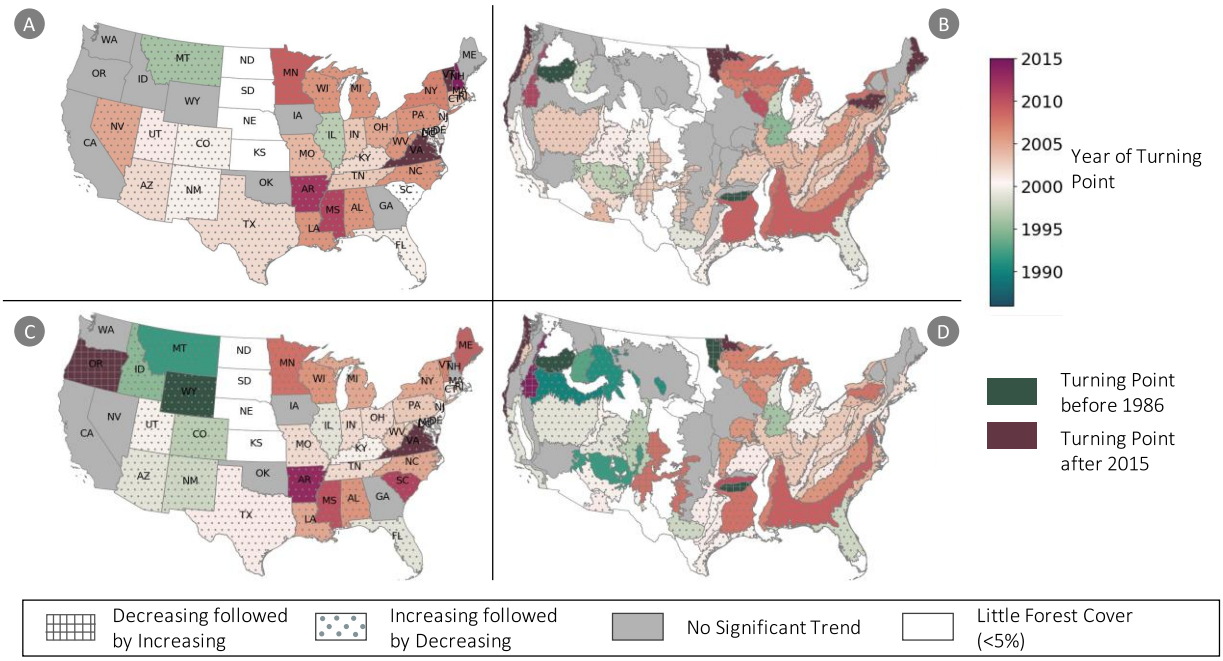

Figure 2-10 Temporal trends fitted for PBAR (A: by state, B: by ecoregion) and PSCA (C: by state, D: by ecoregion). Year of turning point is mapped for states/ecoregions with significant polynomial fitting. Point-hatched polygons are states/ecoregions with decreasing followed by increasing trends ("U" shape), while grid-hatched polygons are states/ecoregions with increasing followed by increasing trends (inverse "U" shape). Grey-colored states/ecoregions are where no significant trend is fitted, and white indicates where forest cover is low (less than 5%).

2.6 Discussion

Forest disturbances can have broad impact on the climate, local environment, and the regeneration of the forest ecosystem. The nature and magnitude of such impact, however, is largely driven by disturbance intensity. Previously, we developed an approach for mapping forest disturbance intensity by integrating time series Landsat observations and FIA field inventory measurements in a Random-Forest-based machine learning framework and demonstrated its

effectiveness in North and South Carolina (Tao et al., 2019). In this study, we evaluated this approach in seven individual states located in the Southeast, over the four FIA regions that constitute the CONUS, and for the entire CONUS. The feasibility of using a single national model to produce CONUS-wide products was evidenced by the fact that the RF model developed over CONUS was comparable to or even better than the individual models developed for four US regions when evaluated over set-aside samples. With this national model we produced the first set of disturbance intensity maps with a 30-m spatial resolution over the entire CONUS that characterize forest disturbance intensity on an annual basis for a 30-year period.

By quantifying the percentage of basal area removed by disturbance events, these products can provide a much more precise characterization of the full continuum of severity in basal area loss events. This represents an improvement over categorical maps only flagging whether or not a loss has occurred, and allows for a better understanding of the impact not only on the forests being disturbed, but also on local hydrology, energy balance, habitat, and a suite of other related environmental issues (Banks et al., 2013; Hanson & Lorimer, 2007; Reid et al., 2010; Senf & Seidl, 2021). The annual time step over three decades and the CONUS 30-m spatial resolution coverage, also represent improvements that can provide finer details for up to 30 years over any area within CONUS. The spatial-temporal PBAR patterns in the derived products were in general agreement with Forest Service reports on areas and trends of stand clearing harvest (Siry, 2002; Smith & Darr, 2004). Compared to areas affected by logging events , PBAR mapped over areas affected by natural disturbances, such as fire and insect outbreaks, were more likely to be driven by both the severity of those events and post-disturbance management practices, such as salvage logging (Leverkus et al., 2018; Lindenmayer et al., 2012), A CONUS-wide disturbance attribution map has been developed (K. G. Schleeweis et al., 2020). It is possible to combine the

PBAR and attribution maps to calculate the loss of basal area from different disturbance types. Further analyses of the temporal trends of the PBAR of different disturbance types may reveal how the drivers of different disturbance types have changed over time. For example, trends in harvesting intensity may reflect changes in forest management practices (Legaard et al., 2015), while trends in natural disturbance events are more likely due to climate change or interdecadal climate variability (Abatzoglou & Williams, 2016; Harris et al., 2018).

Our modeling approach requires both remote sensing time series observations and repeat field measurements provided by the FIA data. Optical systems such as the Landsat satellite series can provide near contiguous observations at national to global scales on near annual or even sub-annual bases (Wulder et al., 2019; Zhu, Wulder, et al., 2019). While in the past data gaps could arise from constant cloudy conditions in certain regions and/or acquisition limitations due to many practical reasons (Asner, 2001; Ju & Roy, 2008), such gaps should be greatly reduced when global observations acquired by the Sentinel-2 satellites launched in 2015 and 2017 become available. Such observations make it possible to time and map locations of disturbance events as well as spectral changes caused by those events over large areas. Further, the successful launch of the Sentinel-1 satellites in 2014 and 2016 ushered a new era where global systematic acquisitions of Synthetic Aperture Radar (SAR) data have become publicly available (Torres et al., 2012). With a planned launch date in 2023, the NASA-ISRO SAR (NISAR) mission is expected to provide L-band SAR data across the globe (Rosen et al., 2015). In general, SAR data are more sensitive to vegetation structure than optical data (Lu et al., 2016; Treuhaft et al., 2004). Methods for mapping forest disturbances using time series SAR observations have been developed and will continue to evolve (Bouvet et al., 2018; Hirschmugl et al., 2020; Rüetschi et al., 2019).

While optical and SAR data could be used to detect forest disturbances and calculate the change signals caused by those disturbances in satellite observations, field measurements are needed to convert the satellite observations to changes in physical quantities like basal area or biomass. The FIA field inventory database is an invaluable dataset for quantifying forest disturbance intensity across CONUS. The database provides field-based measurements for many basic biophysical quantities such as height, diameter, and age at tree and plot levels (Bechtold & Patterson, 2005; McRoberts et al., 2005). From these measurements other derived quantities such as basal area, volume, and biomass were also calculated. Net changes in these biophysical quantities can be derived by comparing these data through time. However, because FIA plots are revisited at 5- to 10-year intervals, these net changes in general are not the sole results of changes caused by disturbance events that occurred between two field measurements. Fortunately, the FIA database provides adequate information for tracking the same trees measured in different inventory cycles. This information made it possible to calculate the basal area loss caused by disturbances that had occurred between two consecutive field visits (Tao et al., 2019). As discussed in section 2.3.2, however, the FIA data needs to be filtered carefully in order to select the plots that could be used to derive reliable PBAR values and minimize the impact of potential misregistration errors between field measurements and satellite observations. As shown in Table 2-2, this resulted in an extremely limited quantity of useable plots, with valid reference PBAR information, for a few states in the Northern and Interior West regions, which could be a reason why the models developed for these two regions had lower R^2 values than those developed for the other two regions and across CONUS.

One way to mitigate this problem is to intensify field sampling over areas where certain disturbances (e.g., planned harvest) are known to happen ahead of time and collect field

measurements before and after those disturbances. For natural disturbances that are often unpredictable, rapidly remeasuring established field plots in and around disturbance affected areas provides useful information (Sheffield, 1992; Woodall & Leutscher, 2005). Ideally, remote sensing mapping algorithms need to be calibrated using reference data with spatial and temporal characteristics matching those of remote sensing data. As discussed in many previous studies (Hoppus et al., 2000; Nelson et al., 2009; Tao et al., 2019), there are considerable spatial-temporal mismatches between FIA measurements and Landsat observations, which likely contributed to some of the mapping uncertainties reported in this study.

Given the fact that lidar has become a locally viable alternative to field methods for measuring many forest attributes (e.g., canopy, height, etc.) (Lefsky et al., 2002; Matasci et al., 2018; Wulder et al., 2012), it may be possible to use lidar data to derive reference data required for disturbance intensity mapping. Depending on how fast trees can grow or regenerate in a study region, however, multi-temporal lidar data acquired within a short period (e.g., 1-2 years) would be needed to derive reliable reference disturbance intensity data. Such data could be obtained by acquiring new lidar data over areas that were disturbed recently and had old lidar or ground measurements acquired shortly before disturbance. Finding such areas may have been difficult in the past. Now that the GEDI (Global Ecosystem Dynamics Investigation) (Dubayah et al., 2020) and ICESat2 (Ice, Cloud, and land Elevation Satellite-2) (Neuenschwander & Pitts, 2019) are acquiring lidar samples across the globe, and airborne lidar data are acquired for increasingly more areas (Sugarbaker et al., 2014), there are more opportunities to obtain repeat lidar measurements within a year or two of disturbance events. As discussed in section 2.3.2, due to potential tree growth and/or regeneration between those measurements, the difference between two lidar measurements acquired many years apart cannot be attributed solely to changes caused

by disturbances that had occurred between the two measurements. The method we developed for calculating PBAR by tracking individual trees over time with FIA plot data, likely cannot be adapted for use with lidar data, because it is not possible to identify individual trees using large footprint waveform lidar data, and tree delineation using very dense lidar cloud point data remains a challenge (Aubry-Kientz et al., 2019; C. Zhang et al., 2015).

Despite the simplicity and convenience as well as some of the advantages of using a single national model to map disturbance intensity across CONUS, the fact that mapping models developed for 5 of the 7 southeast states performed better than the national model (Figure 2-3) demonstrated that should geographically representative reference data be available for all states or ecoregions, improved disturbance mapping could be achieved by using a collection of state- or ecoregion-based mapping models instead of a single national model. Of course, ample overlap should be provided between adjacent states or ecoregions to reduce potential discontinuities between them. Use of a set of locally calibrated models distributed over a large area has become an increasingly more common practice to improve mapping results at national to global scales (Potapov et al., 2021)

2.7 Conclusions

By integrating field plot measurements collected by the FIA program and time series Landsat observations, we have produced the first set of annual forest disturbance intensity map products quantifying the percentage of basal area removal (PBAR) at the 30-m resolution for the conterminous United States from 1986 to 2015. These products were generated using a Random Forest model that had an R^2 of 0.65 and RMSE of 16.2% when evaluated using plots not used in model calibration. Comprehensive qualitative visual assessments of annual disturbance intensity

maps appeared reasonable when compared to high temporal and spatial resolution Google Earth imagery. The derived map products revealed that during the 30-year study period, the annual average PBAR values of all disturbed pixels across CONUS ranged from 66% to 70%, and the proportion of those pixels having stand-clearing disturbances ranged from 40% to 58%. High disturbance intensity values were concentrated in the Southeastern states from TX to VA and along the Pacific coast and the Cascades in the West. At the national scale, the annual mean disturbance intensity values appeared to follow 2nd order trajectories starting with increasing trends at the beginning and decreasing trends towards the end, along with turning points around 2003. The temporal trends of disturbance intensity differed substantially among many states and ecoregions. While the mean disturbance intensity values for some states and ecoregions did not show obvious trends, most of the states' and ecoregions' disturbance intensity values presented statistically significant 2nd order trends. In particular, several states and ecoregions had near monotonic increasing trends that peaked near the end of the study period or did not reach peak value during the study period. Compared to other published disturbance products, the maps derived through this study can provide the unique thematic (intensity) information on forest disturbances, precise details critical for understanding forest dynamics across CONUS over multiple decades. The temporal dynamics of disturbance intensity revealed by these map products may shed light on different practices and processes causing basal area loss across different regions. The map product is available from Oak Ridge National Laboratory Distribution Active Archive Center (ORNL-DAAC).

2.8 Supplementary Materials

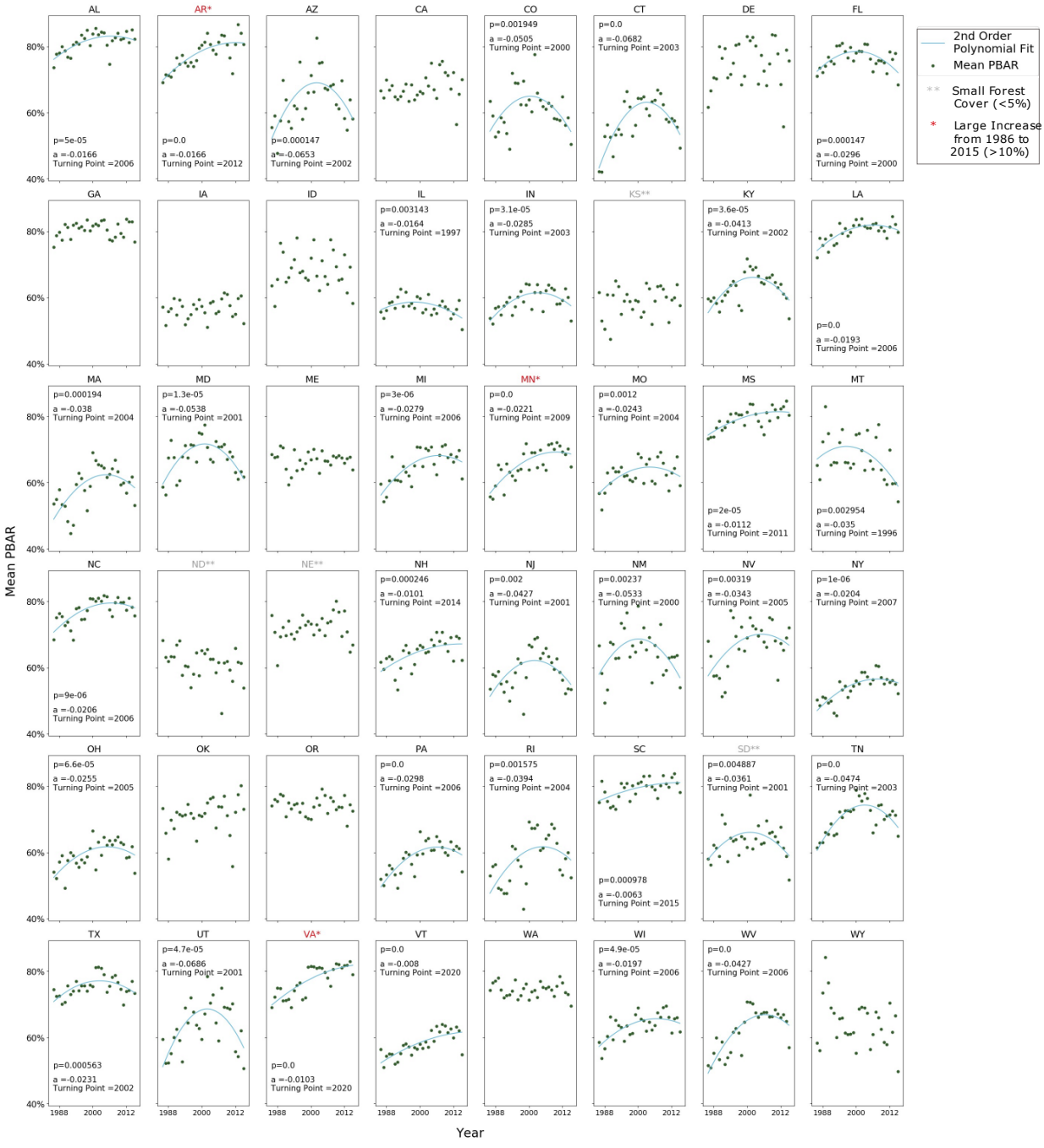

Figure 2-11 Temporal profiles of average PBAR in CONUS states. Second order polynomial trendlines (blue curve) are plotted where significant trend is fitted.

Figure 2-12 Temporal profiles of mean PBAR in level-3 ecoregions. Second order polynomial trendlines (blue curve) are plotted where significant trend is fitted. Plots are titled by North America level 3 ecoregion codes (see Table 2-4 for a list of codes and names

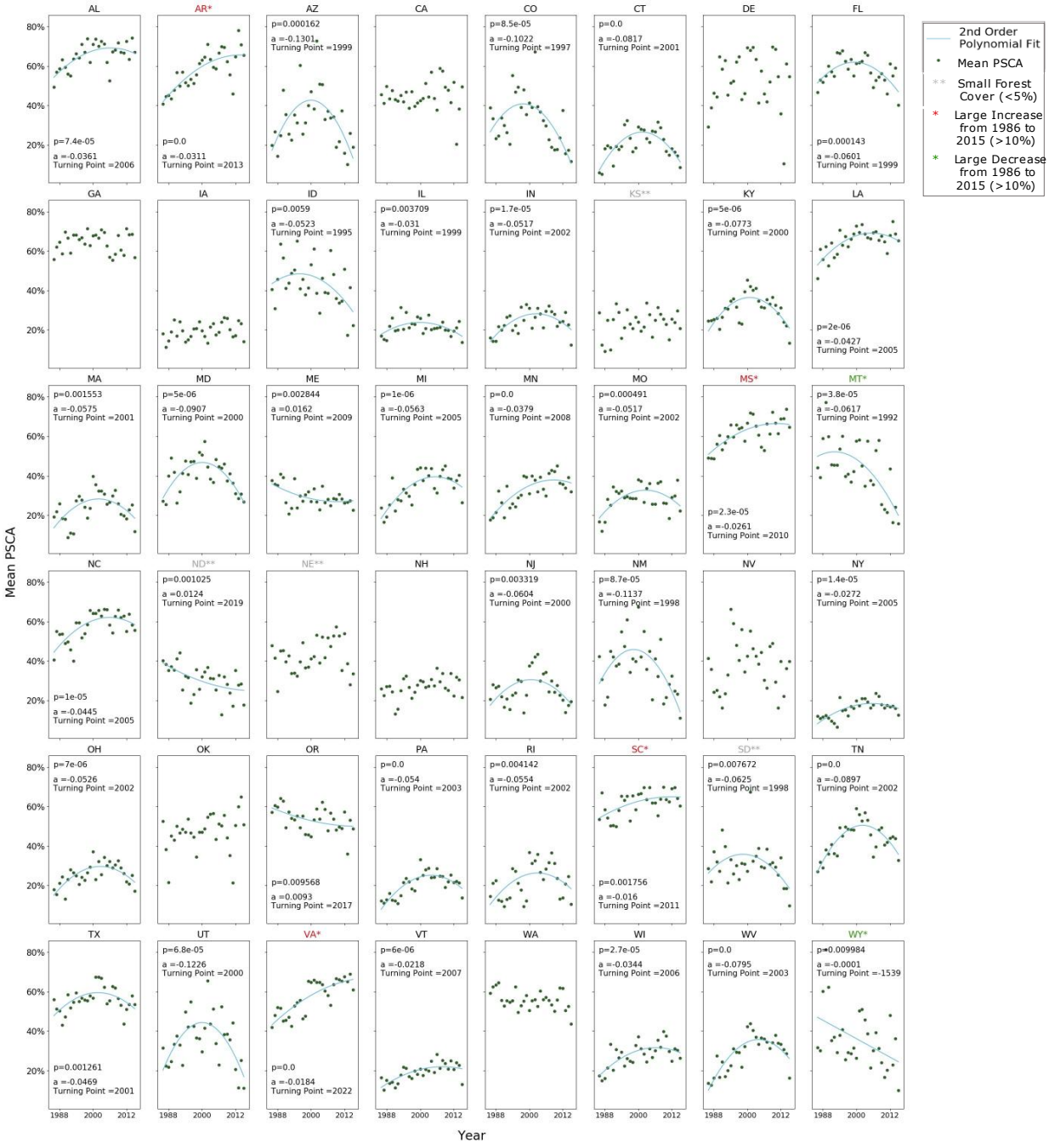

Figure 2-13 Temporal profiles of average PSCA in CONUS states. Second order polynomial trendlines (blue curve) are plotted where significant trend is fitted.

Figure 2-14 Temporal profiles of mean PSCA in level-3 ecoregions. Second order polynomial trendlines (blue curve) are plotted where significant trend is fitted. Plots are titled by North America level 3 ecoregion codes (see Table 2-4 for the list of codes and names)

Table 2-4 North American Level 3 Ecoregion Codes and Names (see the link for the full ecoregion map: https://gaftp.epa.gov/EPADataCommons/ORD/Ecoregions/cec_na/NA_LEVEL_III.pdf)

CODE	NA_L3NAME	CODE	NA_L3NAME
10.1.2	Columbia Plateau	8.1.8	Acadian Plains and Hills
10.1.3	Northern Basin and Range	8.2.1	Southeastern Wisconsin Till Plains
10.1.4	Wyoming Basin	8.2.2	Huron/Erie Lake Plains
10.1.5	Central Basin and Range	8.2.3	Central Corn Belt Plains
10.1.6	Colorado Plateaus	8.2.4	Eastern Corn Belt Plains
10.1.7	Arizona/New Mexico Plateau	8.3.1	Northern Piedmont
10.1.8	Snake River Plain	8.3.2	Interior River Valleys and Hills
10.2.1	Mojave Basin and Range	8.3.3	Interior Plateau
10.2.2	Sonoran Desert	8.3.4	Piedmont
10.2.4	Chihuahuan Desert	8.3.5	Southeastern Plains
11.1.1	California Coastal Sage, Chaparral, and Oak Woodlands	8.3.6	Mississippi Valley Loess Plain
11.1.2	Central California Valley	8.3.7	South Central Plains
11.1.3	Southern and Baja California Pine-Oak Mountains	8.3.8	East Central Texas Plains
12.1.1	Madrean Archipelago	8.4.1	Ridge and Valley
13.1.1	Arizona/New Mexico Mountains	8.4.2	Central Appalachians
15.4.1	Southern Florida Coastal Plain	8.4.3	Western Allegheny Plateau
5.2.1	Northern Lakes and Forests	8.4.4	Blue Ridge
5.2.2	Northern Minnesota Wetlands	8.4.5	Ozark Highlands
5.3.1	Northern Appalachian and Atlantic Maritime Highlands	8.4.6	Boston Mountains
5.3.3	North Central Appalachians	8.4.7	Arkansas Valley
6.2.10	Middle Rockies	8.4.8	Ouachita Mountains
6.2.11	Klamath Mountains	8.4.9	Southwestern Appalachians
6.2.12	Sierra Nevada	8.5.1	Middle Atlantic Coastal Plain
6.2.13	Wasatch and Uinta Mountains	8.5.2	Mississippi Alluvial Plain
6.2.14	Southern Rockies	8.5.3	Southern Coastal Plain
6.2.15	Idaho Batholith	8.5.4	Atlantic Coastal Pine Barrens

6.2.3	Columbia Mountains/Northern Rockies	9.2.1	Aspen Parkland/Northern Glaciated Plains
6.2.4	Canadian Rockies	9.2.2	Lake Manitoba and Lake Agassiz Plain
6.2.5	North Cascades	9.2.3	Western Corn Belt Plains
6.2.7	Cascades	9.2.4	Central Irregular Plains
6.2.8	Eastern Cascades Slopes and Foothills	9.3.1	Northwestern Glaciated Plains
6.2.9	Blue Mountains	9.3.3	Northwestern Great Plains
7.1.7	Strait of Georgia/Puget Lowland	9.3.4	Nebraska Sand Hills
7.1.8	Coast Range	9.4.1	High Plains
7.1.9	Willamette Valley	9.4.2	Central Great Plains
8.1.1	Eastern Great Lakes Lowlands	9.4.3	Southwestern Tablelands
8.1.10	Erie Drift Plain	9.4.4	Flint Hills
8.1.3	Northern Allegheny Plateau	9.4.5	Cross Timbers
8.1.4	North Central Hardwood Forests	9.4.6	Edwards Plateau
8.1.5	Driftless Area	9.4.7	Texas Blackland Prairies
8.1.6	Southern Michigan/Northern Indiana Drift Plains	9.5.1	Western Gulf Coastal Plain
8.1.7	Northeastern Coastal Zone	9.6.1	Southern Texas Plains/Interior Plains and Hills with Xerophytic Shrub and Oak Forest

Chapter 3: Quantification of Tree Age Distribution in US Forests

3.1 Abstract

Tree age information is crucial for a range of environmental, scientific, and conservation-related purposes. It helps in understanding and managing forest resources more effectively and sustainably. This study presents an approach to estimate tree age across diverse U.S. forest ecoregions using field inventory and climate datasets. The age-size relationship modeling framework incorporates species-specific and environmental variables, enabling its application across various regions. The models have higher accuracies than existing studies focusing on smaller areas, with R^2 values ranging from 0.51 to 0.87 and relative RMSEs (using the mean as the denominator) ranging from 0.14 to 0.49. The developed tree age dataset reveals marked differences in tree age distribution between Eastern and Western U.S. forests, attributed to historical land use, climatic variations, and forest management practices. In the East, forests exhibit a younger age structure due to historical deforestation and subsequent reforestation, while Western forests show an older age structure, influenced by diverse environmental conditions and less human disturbance. The study also examines the ages of most trees and age of oldest trees, uncovering regional variability. Furthermore, the research explores the relationship between tree age and above-ground biomass (AGB) growth rate, implying the importance of old-growth forests in carbon sequestration.

3.2 Introduction

Tree age is key information for several scientific and practical reasons. Trees act as natural carbon sinks, absorbing carbon dioxide from the atmosphere. Due to variations in growth rates and biomass accumulation over a tree's life cycle, knowing the age of trees improves the estimation of growth rate and the amount of carbon stored in a forest, which is vital for climate change models and carbon management strategies (Köhl et al., 2017; Repo et al., 2021). In a forest setting, understanding the age of trees within a forest stand helps in comprehending its structural complexity, thus contributing to the evaluation of resilience to disturbances (Sousa, 1980), the ability to support biodiversity and habitat diversity (Gilhen-Baker et al., 2022; Tullus et al., 2022), among other factors. Knowing the age of trees is also crucial for sustainable management and harvesting practices. In addition to inferring growth rates, tree age also serves as the basis for estimating stand age, which helps evaluate the productivity of the forest and identify optimal harvesting times (Nakajima et al., 2017; Peng, 2000).

To determine the age of a tree, several methods are currently being used, each with its own advantages and limitations. Dendrochronology requires a core sample from the tree, taken with an increment borer, then counting the growth rings from the core (Phipps, 1985). For tree species in tropical areas that do not follow the regular tree ring increment growth pattern, bud scars or branch whorls are counted instead. The method was proved to be accurate and the “gold standard” for aging most tree species, but it can be destructive, and only suitable for aging a limited number of sample trees because of the cost. Radiocarbon dating is used for very old trees where dendrochronology might not be feasible, but can be expensive and requires laboratory analysis. Non-destructive modeling approaches have also been developed to estimate age, which

consider the empirical relationship between age and other tree structural attributes that can be more readily and accurately assessed in the field, such as diameter and height. The general patterns of such relationships are that in early years, trees usually grow more in height than in diameter (King, 2011; Niklas, 1995). This rapid vertical growth is typically to outcompete other vegetation for sunlight. As trees mature, diameter growth becomes more prominent. Height growth slows down once a tree reaches a certain age, which varies by species. The relationship could be influenced by factors such as tree species, environmental conditions, and management practices, so compared to tree ring analysis, the modeling approach is less accurate. For the purpose of estimating ages for a large number of trees, however, modeling is the only feasible method. The existing studies explored the use of linear regression (Diallo et al., 2013; Kalliovirta & Tokola, 2005; Rozas, 2003; Silva et al., 2017), polynomial regression (Baker, 2003; Trotsiuk et al., 2012), and other nonlinear functions (Rohner et al., 2013; Y. Zhang et al., 2022) to fit the empirical age-diameter, age-height, age-growth relations for certain species in individual sites. And because of the scale of these studies, many of them did not consider the impact of environmental variables (i.e., climate, topography) on tree age-size relationships, therefore the modeled relationships may not be easily transferred to other species and regions.

One of the most comprehensive tree age datasets for CONUS is the tree age measurements provided by the FIA program of the US Forest Service. This dataset provides field-based age estimates for selected trees over plot locations distributed across the country. Although one of the goals of the FIA sampling design is to provide unbiased estimates of timber volume and other key forest attributes (Smith, 2002; Tinkham et al., 2018), the tree age measurements of the FIA data likely cannot represent the age distribution of all trees. This is because only small fractions of all trees surveyed by the FIA program are populated with age values. While the methods for

selecting trees within a plot to take age measurements vary by FIA regions, in general those methods are not designed to create samples that can represent the age distribution of all trees.

Accurate representation of tree age distribution is important for understanding the disturbance history, functioning, and growth vigor of forest ecosystems. The age distribution of trees in a given region is largely shaped by past disturbances and/or human management activities, and therefore may shed light on those historical events (Vlam et al., 2017). While middle-aged trees typically absorb more carbon than young and old trees, regions dominated by young trees have higher future carbon sequestration potential than those dominated by mature and old trees. Among trees of all age classes, older trees store more carbon overall and contribute significantly to biodiversity conservation and water regulation. The endangered spotted owl, for example, prefers old-growth trees as its habitat (North et al., 2017). Old-growth forests often require protection due to the unique roles they play in terrestrial ecosystems. Identifying ancient or old-growth trees and knowing their age can also provide insights into past climatic conditions, disturbance history, and the possibility of revisiting and updating classic ecological theories (Piovesan & Biondi, 2021). It should be noted that current classifications of trees into young, mature, and old-growth are mostly qualitative. Large quantities of tree age data are needed to derive more quantitative age classifications that may need to be region and species specific in order for such classifications to be ecologically meaningful.

The first purpose of this study is to develop an approach for estimating tree age based on diameter and/or other individual tree-level attributes that are measured by many forest inventory programs. This approach considers the species and environmental factors in age estimation, and hence may have the generality to be applied to different regions. In this study, the developed

approach is used to derive age estimates for all trees in the FIA database that had diameter measurements collected in recent decades. The FIA program provides crucial data on a nation's forest resources, including sample tree- and plot-level measurements. In the FIA database, diameter is reported for each sample tree, but age information is only measured for certain sample trees. The selection of the sample trees depends on the regional units. In this study, we will take the advantages of the plentiful diameter data from FIA, and use the developed modeling approach to estimate the age for all the trees in the FIA database from all the surveys over years, and generate age estimation for the tree population in 2015. Finally, the derived tree age dataset is used to characterize tree age distribution, estimate the age of average trees, and examine the oldest trees across the CONUS.

3.3 Methods

3.3.1 Data

FIA Tree and Plot Data

The FIA program, a comprehensive forest monitoring initiative administered by the USFS, has been playing a crucial role in collecting, analyzing, and reporting forest-related data for decades. In the annualized sampling design, permanent plots are established across the country, and are revisited periodically (i.e., every 5 years for eastern states and 10 years for western states) to collect data on a wide range of tree attributes, including diameter, age, species, and biomass, etc., which allows for tracking changes over time and assessing the health and productivity of forests. A standard FIA plot consists of four 7.32-m radius subplots, on which trees >= 12.7 cm d.b.h./d.r.c. are measured. Within each of the subplots is nested a 2.07-m radius microplot on

which trees < 12.7 cm d.b.h./d.r.c. are measured. Among the forest attributes, tree diameter (i.e., diameter at breast height for timber species, diameter at the stem root collar for woodland species) and species group is commonly measured or reported for all the sample trees. In the FIA database, there are 24 softwood species groups and 24 hardwood species groups, where each group is assigned with a unique code (see FIA database user guide for group codes and their associated names). Tree age on the other hand, is collected for a subset of sample trees from counting tree rings from an increment core sample, and the selection of these trees varies in four FIA regions. In the Pacific Northwest region (PNW), one tree is sampled for counting tree rings for each species, within each crown class, and for each condition class present on a plot. In Rocky Mountains (RM, also referred as Interior West) region, one tree is sampled for age for each species and broad diameter class present on a plot (Burrill et al., 2023). In Southern and Northern Region (SR and NR), age is only measured for site trees, which are selected from trees that have remained in a dominant or codominant crown position throughout their entire life span. If possible, the site trees should be at least 12.7 cm in diameter, and at least 20 years old (SRS Field Guide, 2022). For this study, we used all tree data in the west and site tree data in the east with available age measurement for model training and testing. See Figure 3-1 for data availability in each mapping zone. Similarly, tree height, another parameter relevant to age, is reported for a subset of sample trees. For trees or site trees that have age records, the percentage with reported height is 75-100%, varying across mapping zones.

On plot level, topographic variables including slope, elevation, and aspect, and geographic variables such as the approximate plot coordinates are also reported. Elevation, slope, and aspect were read from GPS, a clinometer, and a hand compass. See field guide for details of measurements. The slope and aspect were reported for each condition class in the plot. Values

from the dominant condition class (i.e., condition class with highest proportion of the plot) were used in the modeling. Plot location coordinates used were the approximate latitudes and longitudes in decimal degrees using NAD83 datum. The publicly available coordinates are within +/- 804.67- 1609.34 meters (0.5-1 mile) from the actual location. Private plot locations have additional uncertainties caused by swapping plot coordinates for up to 20 percent of the plots with another similar private plot within the same county (Lister et al., 2005).

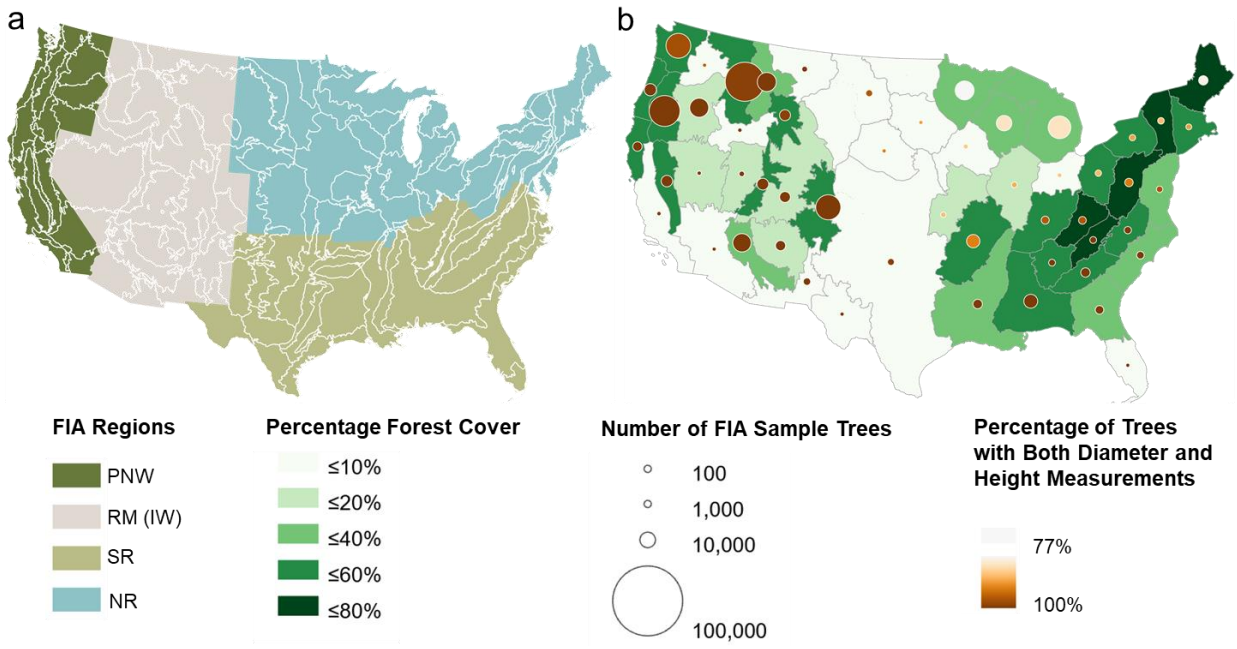

Figure 3-1 Map of EPA level 3 ecoregion boundaries (white lines in a), and mapping zones boundaries (gray lines in b). The colors denote the FIA region, forest cover calculated from NLCD, and percentage of trees with both diameter and height measurements. The size of circles maps available FIA sample tree data counts in each mapping zone.

Climate Data

The PRISM (Parameter-elevation Regressions on Independent Slopes Model) climate dataset developed by the PRISM Climate Group at Oregon State University, is designed to provide

detailed high-resolution spatial climate data (Daly et al., 2000). PRISM used known climatological gradients and patterns in conjunction with geographical and topographical information to interpolate climate data from weather stations to other locations. The 800m 30-year (1981-2010) normals dataset used in this study describes average annual conditions for seven climate element variables that can affect the tree growth: precipitation (ppt), minimum temperature (tmin), maximum temperature (tmax), mean temperature (tmean), mean dew point (tdmean), minimum vapor pressure deficit (vpdmin), and maximum vapor pressure deficit (vpdmax). Temperature could determine the length of growing season and the rate of photosynthesis (Yamori et al., 2014); precipitation decides the water availability and nutrient uptakes of plants (Kreuzwieser & Gessler, 2010); while dew point, which is the temperature at which air becomes saturated with moisture and dew forms, does not directly influence tree growth itself, the atmospheric moisture conditions it reflects can have various indirect effects, including impacts on transpiration efficiency, temperature regulation, frost risk, disease and pest incidence, and overall soil moisture availability, all of which can influence tree health and growth (Ben-Asher et al., 2010); vapor pressure deficit is defined as the difference between the amount of moisture in the air and how much moisture the air can hold when it is saturated, and is a critical factor in determining the rate of transpiration and photosynthesis in trees, impacting their growth, health, and water use efficiency (Grossiord et al., 2020). The climate variables will be extracted at the approximate plot locations to determine the climate conditions.

3.3.2 Tree Age Modeling

Modeling Framework

The modeling unit followed the mapping zones partitioned for the National Land Cover Dataset (NLCD) 2000, which segmented the United States into 66 areas that are relatively homogenous in terms of ecological and climatic characteristics. The mapping zones were initially based on ecoregions defined by (Omernik, 1987), then the boundaries were modified to ensure homogeneity in land cover types, ecological conditions, and climatic features within each zone (e.g., large ecoregions that have wide latitude or longitude ranges were divided into smaller units, small ecoregions with similar land cover types and climatic features were combined into larger units, etc.). For age modeling, the mapping zones that have too few reference data to train an individual model were combined with nearby mapping zones (Figure 3-1).

The modeling approach used in this study was built upon the ideas developed by previous researchers that tree age can be estimated by linking age to its size, species variables and site characteristics (i.e., topographic, geographic, and climate variables).

$$age = f(size, species, topographic, geographic, climate\ variables) \quad (10)$$

See Table 3-1 for the complete list of variables included in each group.

To apply the approach in Eq. 10 to national scale, the model was slightly modified depending on the variations of reference data availability collected by FIA regional units. For most mapping zones in the PNW and RM regions, most trees (>99%) have both diameter and height measurements, only less than 1% of trees have only diameter but no height recorded from the field. Zones where there are 1-10% trees without height measurements are near Columbia Plateau, Northern Rockies, Idaho Batholith, and Middle Rockies. In these PNW and RM zones, for trees with height measurements, Random Forest (RF) models were developed using all the

variables in Table 3-1 as the predictor variables. For trees without height measurements, all variable groups except height were used to build the RF model.

In SR and NR regions, only site trees were bored for their age. Site trees are selected to measure site productivity expressed by the height to age relationship of dominant and codominant trees. In these two regions, at least one site tree was selected off subplots for each forest condition class from a species that is common to the condition class. The site tree should have remained a dominant or codominant crown class throughout their lifespan, and they should be at least 12.7 cm (5 inches) in diameter, or at least 20 years old. All site trees have age, diameter, and height measurements. But this is not always true for all other trees surveyed by FIA – up to 25% of those trees in the two regions do not have height measurements. Therefore, for the mapping zones in SR and NR regions, separate sets of models are needed for trees with and without height as well. And because only large trees (> 12.7 cm in dbh) were selected as site trees, and RF models were not able to extrapolate beyond the range of training data, another set of Ordinary least squares (OLS) regression models were also trained, one for trees with height, one for trees without height. The OLS models were used to estimate the age of trees with dbh smaller than 12.7 cm through extrapolation. While the predictions derived this way typically had larger uncertainties than OLS predictions within the value range of training data, this extrapolation method provided a viable approach for estimating the age of trees with dbh less than 12.7 cm. A summary of the various models developed for each of the four FIA regions is provided in

Table 3-2.

Table 3-1 List of tree and site variables used in age modeling

Variable Groups	Data Source	Variable List

Tree Size	FIA TREE	Diameter at Breast Height (dbh), Height
Tree Species	FIA TREE	Species Group
Topographic	FIA PLOT	Elevation, Slope, Aspect
Geographic	FIA PLOT	Latitude, Longitude
Climate	PRISM	Precipitation, Minimum/Maximum/Mean Temperature, Mean Dew Point, Minimum/Maximum Vapor Pressure Deficit

Table 3-2 Tree age modeling framework. In the west, RF models were trained for both trees w/o height measurements. For the mapping zones in the east in SR and NR regions, OLS regression models were developed to extrapolate the age prediction for small trees outside the range of training data.

	With Height		Without Height	
PNW/RM	RF		RF	
(Regular Sample Trees)	age = ***f*** (diameter, height, species group, topographic, geographic, and climatic variables)		age = ***f*** (diameter, species group, topographic, geographic, and climatic variables)	
SR/NR	RF	OLS	RF	OLS
(Site Trees)	age = ***f*** (diameter, height, species group, topographic, geographic, and climatic variables)	age = ***f*** (diameter, height, species group, topographic, geographic, and climatic variables)	age = ***f*** (diameter, species group, topographic, geographic, and climatic variables)	age = ***f*** (diameter, species group, topographic, geographic, and climatic variables)

Accuracy Assessment

In assessing the model's performance across various mapping zones, a 10-fold cross-validation approach was employed. This entailed randomly dividing the reference plot samples into ten distinct subsets. Subsequently, ten separate models were constructed, each trained on nine subsets and validated against the one remaining subset. This process ensured that each subset was utilized exactly once as a validation set. The validation outcomes from all ten sets were then aggregated to yield an overall estimate of the model's efficacy. Cross-validation helps in

identifying models that may perform well on the training data but poorly on unseen data, a phenomenon known as overfitting. By using multiple training and testing sets, it ensures that the model's performance is tested across different subsets of data. Model performance was quantified using the coefficient of determination (R^2, as per Eq. 8) and the Root Mean Square Error (rRMSE, as delineated in Eq. 9). Mean R^2 and mean RMSE were calculated from all the 10 folds to provide an overall performance metric for the model. The mean values represent the average explanatory power of the model across different subsets of data. The evaluation was performed for all RF and OLS model sets in Table 3-2.

In addition to the assessment for the zone-based models, we also assessed the performance of a single set of national models (cross-validated by all available data), and regional based models (cross-validated results pulled from four FIA regional based models), and mapping zone-based models (cross-validated results pulled from individual zone-based models), to evaluate the efficiency difference of a large generic model and more locally calibrated models in tree age estimation.

Bias Correction

As will be discussed in the Results section, the RF and OLS models tend to slightly overestimate the tree age on the low end and substantially underestimate on the high end. To correct such bias, a median adjustment approach was adopted and updated from (Huang et al., 2014), where the medians of reference ages were binned with 3-year intervals, then the medians of the predicted ages in the bins sliced by reference data were also calculated. If the tree count within a bin was less than 0.1% of all data, the current bin was combined with the bin before. After getting the bin medians of both reference and predicted age, 2nd order polynomial functions were fitted through

the medians, then the fitted functions were applied to the original model predictions to get the bias corrected age. The corrected age for the low-end small ages may be corrected to below zero, these negative values were forced to 1 year old. While on the high end, because the tree count is small in the last few bins, they were combined to the younger bins. The actual tree age in the last bin could be much higher than the median value. The polynomial increase may bring the corrected values of old trees to extremely high. So, to mitigate the high values, the corrected value's high end was capped to 85th percentile of the last bin. To keep the distributions of corrected values consistent with the reference ages, the average of prediction and bias corrected value was used as the final corrected value.

The bias of the initial model predictions and averaged estimates were calculated to test the effectiveness of bias correction. The bias was compared separately for the young trees that were overestimated and older trees that were underestimated. To categorize the predicts, aa linear regression was fitted to the reference-prediction data, then the intersect of the fitted line and the 1:1 line was used as the threshold. Trees younger than the intersect reference age were grouped into the overestimation trees, and trees older than the intersect age were grouped as the underestimation trees. The bias for each group in all the modeling zones was calculated using the following formula,

$$ME = \frac{1}{n}\sum_{i=1}^{n}(\hat{y}_i - y_i) \qquad (11)$$

Where $\hat{y}_i$ are the predicted or averaged values, and y_i are the reference age. A positive value indicates a tendency to overestimate, while a negative value indicates a tendency to underestimate.

3.3.3 Tree Age Distribution Assessment

Age Estimation for "All" Trees Across CONUS

From the previous steps, we were able to derive individual tree level age estimations for every FIA tree. To further obtain the population estimates in a certain year from the samples, procedures were adopted and modified from FIA's Population Estimation Guide. FIA uses "evaluation" to describe the process of storing different stratifications, where the plots were assigned to strata that in aggregate can define the population of interest. Different evaluation types were provided to identify the evaluation of interest, including area, growth, volume, number of trees, biomass, mortality, etc. Evaluation groups of the year 2015 for all CONUS states and the evaluations of volume attributes type "EXPVOL" were identified to estimate number of live trees (at least 2.54 cm dbh) on forest land.

Estimation requires linking the plot (PLOT, COND, and TREE tables) to the stratification information (POP_PLOT_STRATUM_ASSGN, POP_STRATUM, and POP_ESTN_UNIT) for the selected evaluation (POP_EVAL, POP_EVAL_GRP, and POP_EVAL_TYP) that defines the sample. See Supplement Table 3-3 for the names and descriptions of each table.

After evaluation selection and the proper table linkage, tree level age estimations were grouped into age classes, then the counts were multiplied by expansion factors to scale up sample data, and the estimations were appropriately aggregated or disaggregated based on the population strata to estimate the total for the population in each age group in 2015.

Quantification of Tree Age Distribution

Based on the tree age data derived above, tree age distribution is quantified in three ways. First tree age histograms are analyzed at the national, sub-national (i.e., eastern vs western US), and ecoregion levels. The level 3 ecoregions are used in this study because the number of ecoregions and the size of the individual ecoregions are deemed more suitable for this analysis than higher or lower level ecoregions. At the ecoregion level, median tree ages are calculated to represent the age of average trees. Ecoregions with low median tree ages are dominated by young trees that have not reached their peak carbon sequestration potential yet, whereas regions having more mature/old growth forests should have higher median tree ages. Finally, the oldest trees in each ecoregion are examined to evaluate how their ages differ by species and ecoregion. In eastern US where much of the original forests were cleared for agricultural uses in the past, the age of the oldest trees is likely determined by past land use history. In western US where at least, some of the original forests had not been cleared in the past by human activities, the age of the oldest trees may serve as an indicator of the longevity of those trees.

From the predicted ages for all the FIA sample trees, we calculated the age of the oldest tree as the median of nine oldest trees for three populations: all living trees in an ecoregion, dominant species in an ecoregion, and selected single species (i.e., Douglas fir, loblolly pine, red maple, white oak, Utah juniper, and ponderosa pine) across ecoregions. The dominant species were identified by sorting the percentage of basal area weighted tree count of each tree species within an ecoregion and selecting the species or groups of species with highest percentage. If the top n tree species had close percentage count against each other, and the total was much higher (>5%) than the (n-1)th species, then the n species formed a co-dominant species group for that ecoregion. Basal area weighted tree count was used instead of simple tree count to balance out

the effect of species with large populations but small in size, or species with lots of larger trees but smaller populations.

3.4 Results

3.4.1 Performance of the Tree Age Model Approach

Improvements from the Zone-Based Modeling Framework

The mapping zones provided a robust framework for modeling relationships between tree age and the predictor variables. Although the RF is capable of modeling complex, nonlinear relationships, age values predicted by a set of models where each model was developed for an individual zone or zone group were substantially more accurate than those predicted by models developed over larger areas (Figure 3-2). At the CONUS level, predictions by the zone-based models had an R^2 of 0.75 and an RMSE of 26.99, while for the predictions by the FIA region-based models, the R^2 was reduced to 0.72 and the RMSE increased to 29.00. Predictions by a single model developed for CONUS had the lowest R^2 of 0.57 and highest RMSE of 36.05. Given these demonstrated advantages of the zone-based modeling framework, all results presented in the remaining sections of this chapter were produced using this modeling framework.

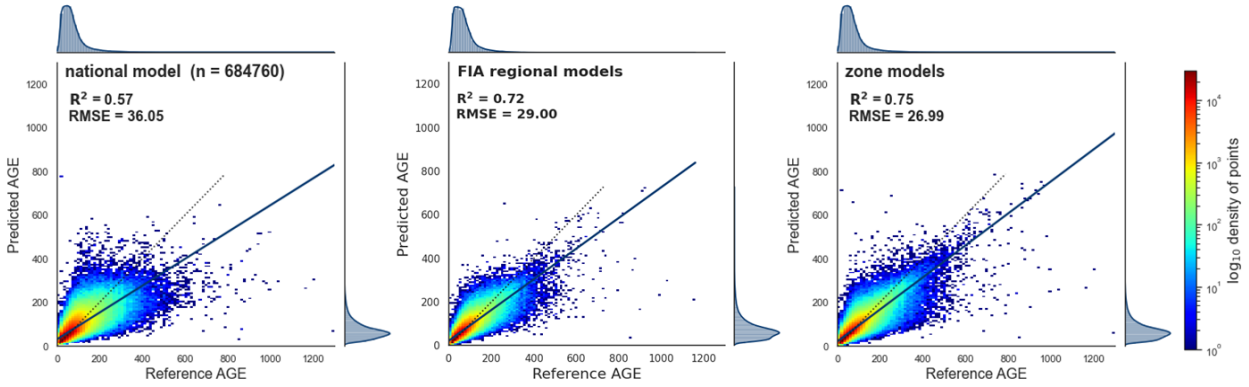

Figure 3-2 Comparison of the validation results of a single national model, individual FIA regional, and zone-based models. Left: cross validation of the single national model using set aside reference plots not used in model calibration; middle: scatterplot of cross validation results pulled from FIA regional models; right: scatterplot of cross validation results pulled from zone-based models. The dashed lines are the 1:1 line. The blue solid line is the fitted line between reference and predicted values.

Complementarity of Different Age Models

The modeling approach consisted of RF models developed using and without using height as predictor variables in order to produce robust age estimates even though height is not populated consistently in the FIA data (Table 3-2). While the models that included height as a predictor variable performed slightly better than those that did not use height as a predictor variable (see Supplement Figure 3-13, Figure 3-14, Figure 3-15, and Figure 3-16) in many zones, the two groups of models had essentially the same accuracies as indicated by their R^2 and RMSE values in other zones, indicating that together, they could produce robust age estimates regardless a tree had a height measurement or not. As expected, the OLS models developed for the zones located in eastern US were less accurate than the RF models. However, the OLS models were only applied to trees with DBH less than 12.7 cm. The age of trees with larger DBH values were predicted using the RF models.

Effectiveness of Bias Correction through Median Adjustment

Models at different scales all show similar tends of biases - slight overestimation on the low end and substantial underestimation for the trees older than 200 years. Bias correction is needed for better estimations. Fig shows examples of the median adjustment approach and results in two zones. Polynomial functions were able to capture some of the relationships between the predicted and reference age (Fig second column). After applying these functions, the bias was eliminated in the corrected values (Fig third column), where the fitted line between corrected values and reference values overlapped with the 1:1 line. After the correction, although a slight increase was seen in RMSE, the overall model performance (evaluated by RMSE in conjunction with R^2) was not largely influenced. However, because the polynomial functions produces negative values, which were forced to 1 in the correction, and also because the polynomial increasing brought the corrected values of high-end values to extremely high levels, which were capped to 85 percentile of ages in the last bin, directly using polynomial functions may lead to different tree age distribution from the reference dataset, see the side histograms in Figure 3-3 third column of zone 1 for an example of such alterations in distribution. Therefore, the average of prediction and bias corrected value was used as the final corrected value (Figure 3-3 fourth column), this way the effectiveness of bias correction was not as evident as the original corrections from the polynomial functions, but the distributions of corrected values were kept consistent with the reference ages.

From the comparison between biases before and after the averaging correction (Figure 3-4), we can see for most zones, the bias after correction is closer to 0 than the initial model predictions. The method was tested effective to reduce the bias in both directions (i.e., underestimation and overestimation).

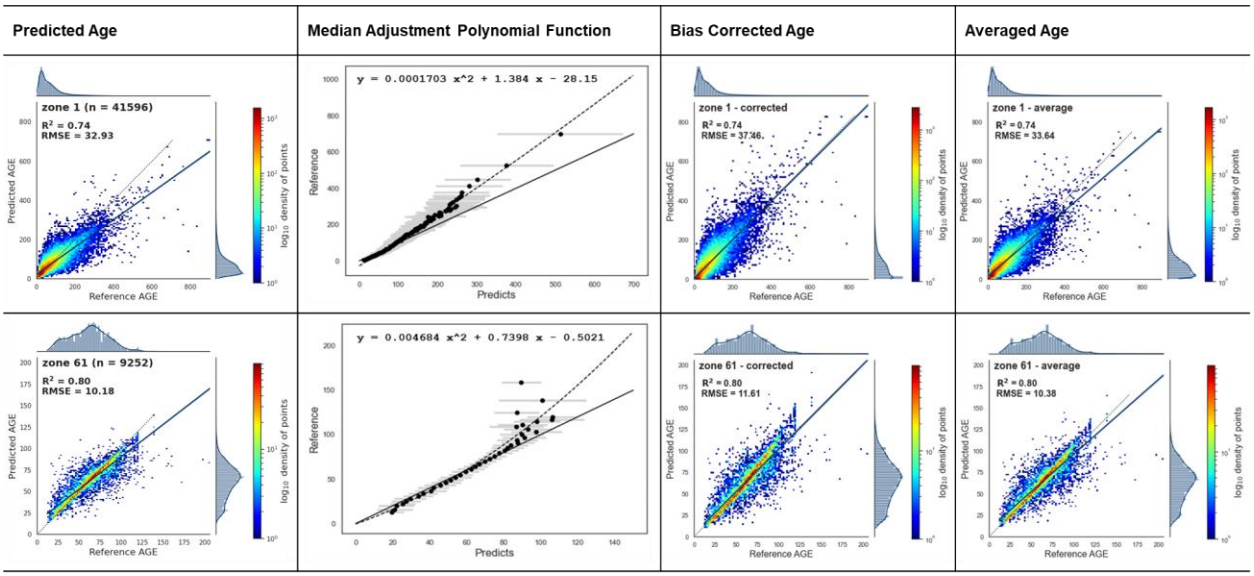

Figure 3-3 Examples of using the median adjustment polynomial functions to correct model prediction bias in mapping zone 1 and 61. First column: original model predictions; second column: the fitted median adjustment polynomial function and curve. The curve was fitted through the medians of 3-year bins; third column: corrected age after applying fitted function to the original predictions. The correction's high end was capped to 85th percentile of the last bin, the negative values on the low end, if any, was forced to 1 year old; fourth column: the average between prediction and corrected age.

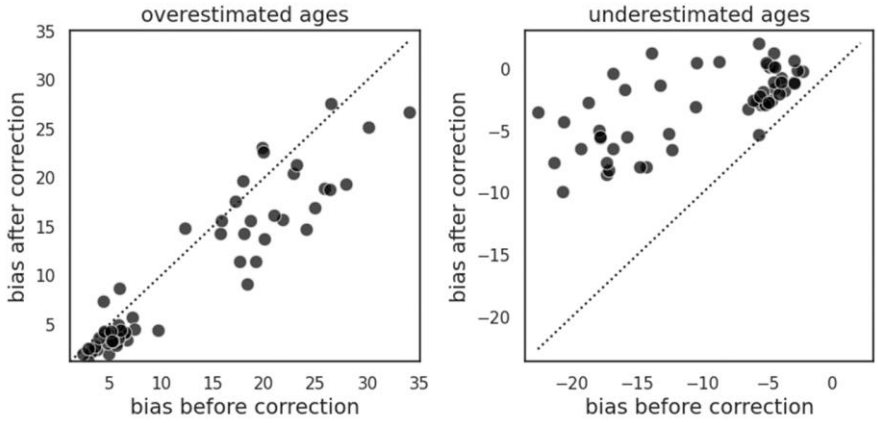

Figure 3-4 Comparison of bias before and after the median adjustment and average process. Each dot represents the bias of one modeling zone. Left: bias comparison for tree ages that were overestimated in the initial model prediction. Right: bias comparison for tree ages that were underestimated in the initial model prediction.

Accuracies of the Final Age Estimates

Figure 3-5 shows the accuracy of final age estimation in each zone. For trees with both diameter and height measurements, the R^2 ranged from 0.51 to 0.87 (Figure 3-5 A-1), and the relative RMSE ranged from 0.14 to 0.49 (Figure 3-5 A-2). The mapping zones in the middle of the country had the lowest R^2s and relatively high rRMSEs. Most of these zones had low forest cover, for example, zone 26 is located near Chihuahuan Deserts, which has only less than 1% of forest cover; zone 29 and 30, located near the central areas of Northwestern Greater Plain, has around 6.33% of forest cover. In addition to these regions, higher rRMSE were also seen in the coastal zones, which was probably due to the wide range of tree ages in those areas. The rRMSE of old trees can be particularly high since it was calculated using the mean as the denominator. Highest R^2 and lowest rRMSE were seen in the eastern zones. Figure 3-5 B-1 and B-2 are the R^2 and rRMSE maps for tree ages estimated with diameter measurements only. The accuracy of these models was similar to models including height as a predictor in the western zones. In eastern zones such as zones 39, and 59, the R^2s of these models were lower than models including height as a predictor, and the rRMSEs were higher. The zone model's performances show that the modeling method can be applied to the whole country and the accuracies were higher or at least comparable to methods in published studies focusing on smaller sites.

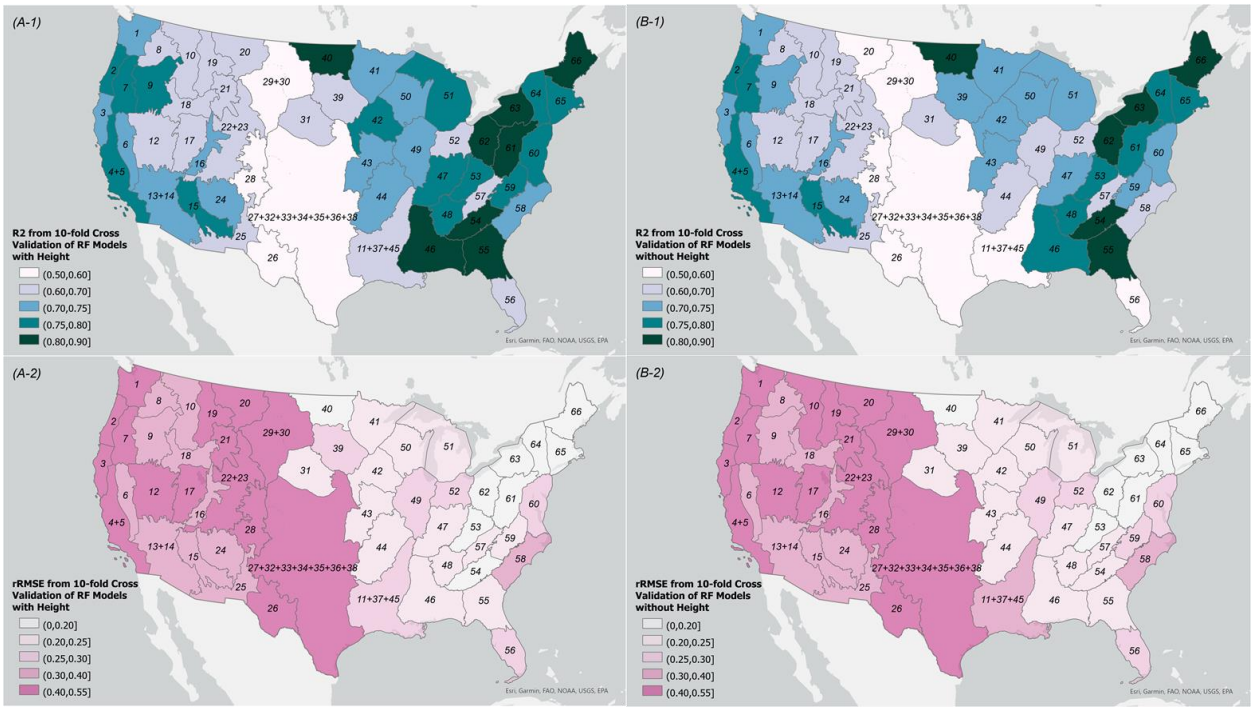

Figure 3-5 Maps of R^2 and relative RMSE for the age models including (A-1, A-2) and not including height as a predictor variable (B-1, B-2).

3.4.2 Tree Age Distribution Assessment

Tree Age Distributions at the National Scales

At the national scale, the age of trees with DBH > 12.7 cm roughly follows a log-normal distribution, with the age group 54-70 having the highest percentage of trees (Figure 3-6). The tree percentage decreases slightly faster along the right tail than along the left tail. This slight asymmetry is likely due to a more obvious asymmetry in the age histogram of trees in eastern US, which also peaks at the 54-70 age group. To the left side of the peak the percentages of tree age groups between 25 and 54 years are also high, but the percentages decrease sharply along the right tail. There are few trees older than 148 years. The age histogram of trees in western US

exhibits a more typical log-normal distribution, with the age groups from 54 to 148 years having the highest percentages. The western forest has substantially more old trees than the east. More than 20 percent of the trees are older than 148 years.

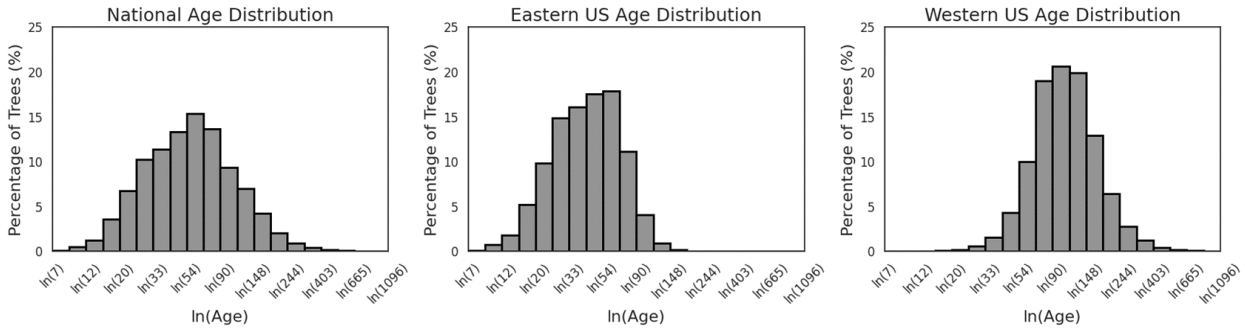

Figure 3-6 Tree age distribution of national, eastern and western forests in 2015. x-axis: natural logarithm of tree age (range: 2-7), labeled by the actual age: 7-1096. y-axis: percentage of tree population in each age group in 2015. Note: seedlings and saplings were not included.

Regional Patterns of Tree Age Structure

At sub-national scales, tree age distribution exhibited substantial regional variations. To reveal the regional patterns of tree age structure, the number of trees binned at a 5-year interval was plotted for each of the level 3 ecoregions in (see supplement Figure 3-17). Figure 3-7shows a few representative age structures of selected ecoregions. The difference in tree age structure is the result of a combination of factors, including climatic conditions, elevation and topography, soil types and quality, disturbance regimes, species adaptations and diversity, and etc.

Many ecoregions in the west have an overall tree age structure similar to that of Cascades or Eastern Cascades Slopes and Foothills, where the age of peak number of trees is after 50 years, then the tree count gradually decreases as age increases. Due to variations in species, disturbance history, and other factors, the distributions could be different. For example, compared to

Cascades, the Willamette Valley has more young trees and less old trees. One possible reason is that the Willamette Valley has seen more intensive land use changes due to agriculture and urban development, which can lead to younger forest ages or more homogeneous age structures. In ecoregions like Willamette Valley, Northern Rockies, Coast Range and Blue Mountains, there are more variations to the number of trees from age group to age group (small peaks and valleys in the dot series), which could be the results of intensive historical disturbance events. For example, for Northern Rockies, there is an obvious smaller number of trees at around 110 years old, compared to other neighboring age groups. That was likely caused by the Great Fire of 1910, which occurred on August 20-21 in 1910 in North Idaho and Western Montana. It burned an area of 12,100 km2, equivalent to the size of Connecticut.

In most ecoregions in the east, the tree age structure is similar to the pattern observed in Blue Ridge and Southwestern Appalachians, where most trees are younger than 80 years, and the number of trees drops suddenly between the ages of 80 to 120 years. These patterns could be shaped by historical events such as the European settlement and the agricultural abandonments. The impact of European settlement on forest age structure in what is now the United States became more pronounced during the 17th, 18th, and particularly in the 19th centuries, as the population grew (Hessburg & Agee, 2003). One of the primary impacts was widespread deforestation to clear land for agriculture and settlements, which resulted in the loss of large areas of old-growth forest and reduced the overall age and size of forested areas. Therefore, there are few trees older than 120 years. Following periods of extensive land clearance, the first major wave of agricultural abandonment in the Eastern U.S. began in the late 19th century and continued into the early 20th century due to industrialization and westward expansion, when land previously used for agricultural purposes is left to revert to its natural state (Williams, 1982,

1992). The agricultural abandonment has led to a significant increase in new forested areas with younger trees, which could explain the sudden increase of trees from older than 120 years to between 80-100 years.

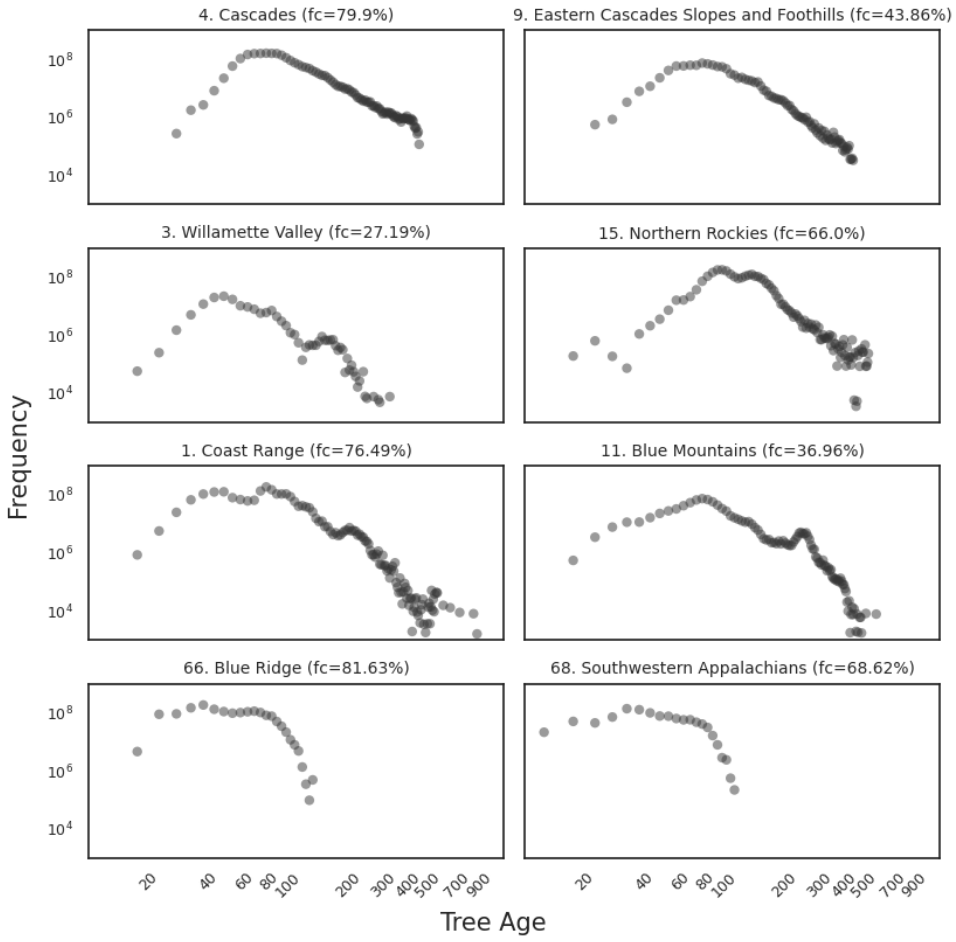

Figure 3-7 Tree age distribution in selected US level 3 ecoregions showing different patterns. Both axes are on logarithm base 10 scale. The title of each plot is showing the ecoregion code, ecoregion name, and the percentage forest cover in that ecoregion calculated from NLCD dataset (Note: seedlings and saplings were not included).

How Old Are the Average Trees?

As with the tree age structure, the age of average trees also exhibited substantial variations among the ecoregions. Figure 3-8 shows that ecoregions with high median tree ages have a

predominantly arid to semi-arid climate, featuring a relatively dry climate with limited precipitation, such as Colorado Plateau and Arizona/New Mexico Plateau. Such environments tend to support slower-growing tree species that are adapted to dry conditions. Idaho Batholith also have high median tree age, partly due to the granitic soils common to see in this area which can affect the tree growth rates, and also due to mountainous terrain. The higher elevations create a range of microclimates including lower temperatures, which contribute to slow growth rate. The mountainous terrain and climate can also be the main reason for high median tree age in the Southern Rockies. In the eastern ecoregions, the median tree ages are mostly 30-40 years. The younger age of eastern forests is a result of the history of land use (discussed above), also because the forest management in the east involved intensive practices like clearcutting and selective logging. Plus, the different dominant species from the western forests.

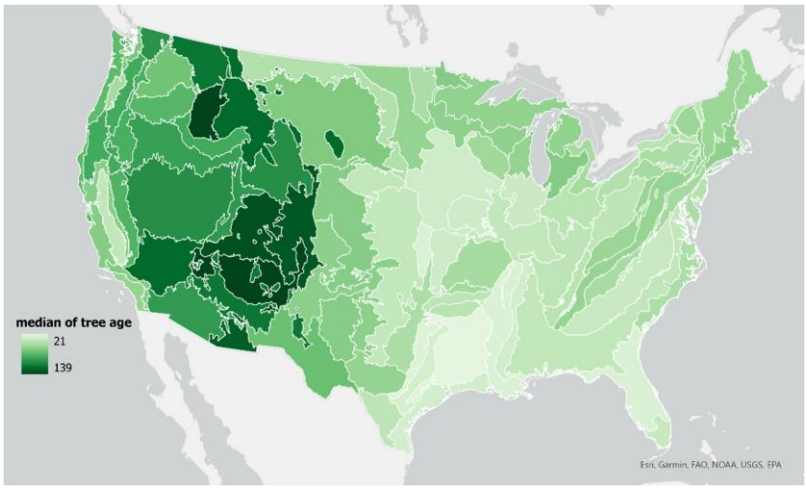

Figure 3-8 Map of median tree age in US level 3 ecoregions. Overall, western forests have higher median ages than eastern forests. High median values are in arid/semi-arid areas, such as Colorado Plateau and Arizona/New Mexico Plateau, and mountainous areas such as Idaho Batholith and Southern Rockies.

The Age of the Oldest Trees

Old trees are integral parts of forest ecosystems. They provide a wide range of ecological functions, many of which could not be provided by younger trees (Lindenmayer & Laurance, 2017). While by definition old trees should be defined by age, practically this is often challenging mainly because it is very difficult to acquired age data for many tree, especially large, old trees. The age data derived through this study provides an opportunity to study the old trees across the US. This chapter will focus on the age of the oldest trees, which may represent the longevity of those trees shaped by past disturbance and/or land use history. The specific questions addressed in this section include: How old are the oldest trees across the country? What are the species types of those oldest trees? And to what extent the age of the oldest trees of the same species vary across the landscape?

Given that the age estimate derived through this study for each individual tree may have unknown uncertainties arising from the modeling approach as well as the uncertainties in the input data, in this analysis the age of the oldest tree within a study domain is defined as the median of the 9 oldest trees in that domain. Here a study domain could include all trees or just the trees of a particular species or species group within an ecoregion. Figure 3-9 shows the age of the oldest trees varies substantially across the ecoregion (Figure 3-9 A-1). In ecoregions in the northwest, such as Coast Range, Cascades and North Cascades, the oldest trees were more than 1000 years by 2015. The species of the oldest trees (Figure 3-9 A-2) in these three ecoregions are redwood, Douglas fir, and western redcedar. Very old trees (>800 years) can also be found in arid/semi-arid regions, the species of which include great basin bristlecone pine, ponderosa pine, and rocky mountain bristlecone pine. They tend to grow slowly and can live for a very long time in these areas where there are less intensive logging and agricultural land use compared to more fertile and accessible regions, allowing many forest areas to mature without significant human-

induced disruption. In the east, the oldest trees in most ecoregions were only between 100 and 200 years old. The common species of these old trees include white oak, bur oak, post oak, red spruce, longleaf pine and so on.

The dominant species (Figure 3-9 B-2), identified as the species with highest diameter weighted tree count, are often not the same as the species of oldest trees. For example, in Coast Range, the oldest trees are redwood, but the dominant species is Douglas fir; in Southeastern Plains, the oldest trees are longleaf pine, but the dominant species is loblolly pine. Other common dominant species include Utah juniper in the Midwest, ponderosa pine, honey mesquite, yellow poplar, etc. The longevity of these dominant species is smaller than the longevity of all living trees, but they have similar spatial patterns across ecoregions. The oldest tree species and the dominant species in a given ecosystem are not necessarily the same and this could be due to a combination of ecological, evolutionary, and environmental factors.

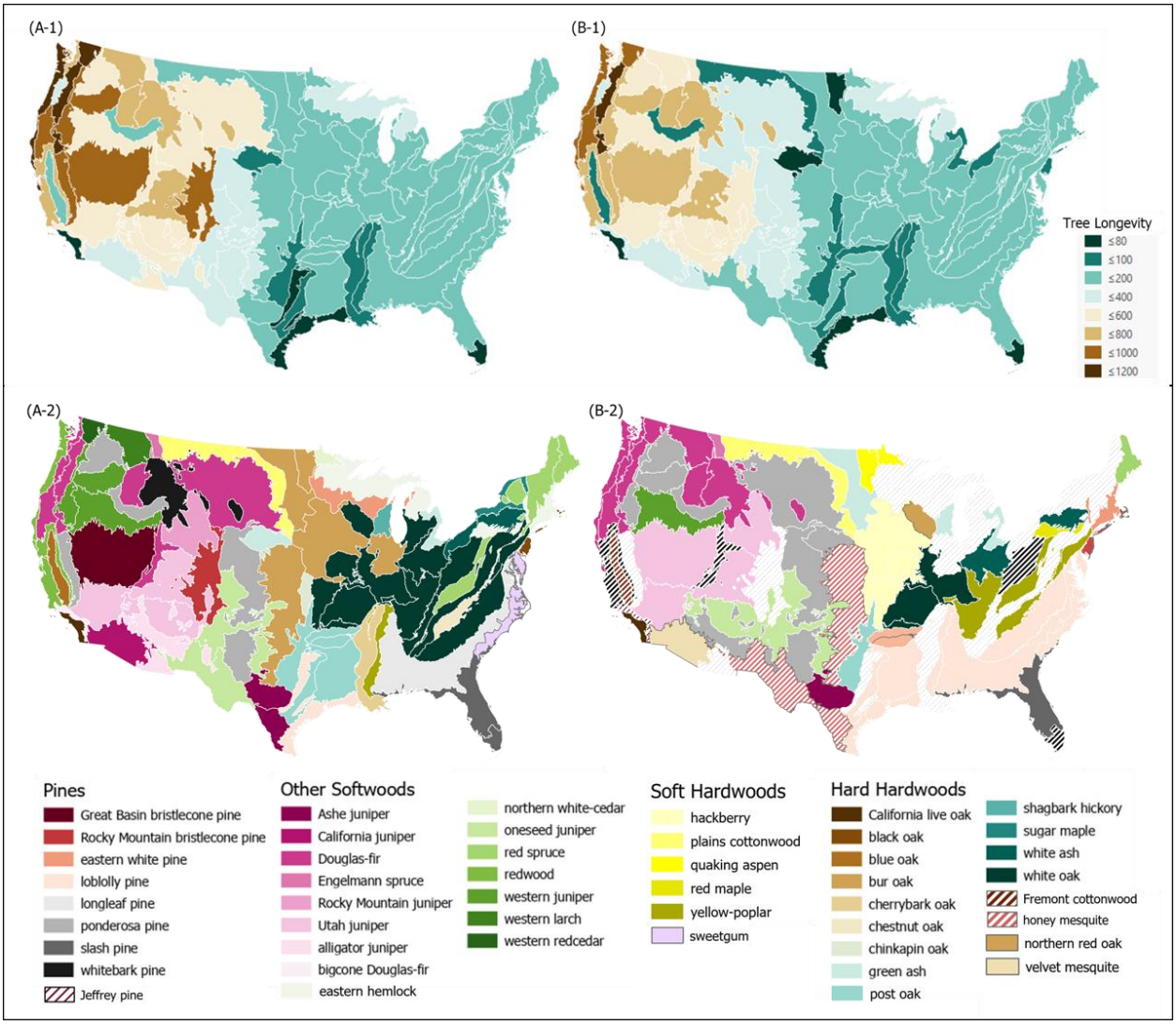

Figure 3-9 Age of the oldest living trees (A-1) and dominant trees (B-1) in US level 3 ecoregions. A-2 shows the species of the oldest living trees, B-2 shows the dominant species in each ecoregion.

And to what extent the age of the oldest trees of the same species vary across the landscape?

The age of the oldest tree of the species could differ substantially among ecoregions. Figure 3-10 shows the age of the oldest trees for selected species (right column) and the weighted abundance of those species (left column) at the ecoregion level. Douglas fir is native to the western regions, with weighted abundance values exceeding 5% in many ecoregions located from the Pacific coast to the Rocky Mountains. While the age of the oldest tree of this species exceeded 1000

years in the Cascades region and 800 years along the Pacific coast, it was substantially shorter (< 600 years) in the Rocky Mountain and several other regions, and was even shorter (<200 years) in Columbia Plateau. Such large variations in the age of the oldest tree can also be found in other tree species native to the western US, such as Utah juniper and ponderosa pine. For species native to the eastern US, such as loblolly pine, the age of the oldest tree also varies, but the variation is much smaller. In Southeastern Plains and South-Central Plains, the oldest loblolly pine trees are over 100 years old, but less than 75 years old in Western Gulf Coastal Plain. Given the fact that most of the original forests in eastern US were cleared for agricultural uses by European settlers and much of the forests that exist today established following agricultural abandonment that occurred over the past century, the age of the oldest trees as calculated by this study likely does not represent the maximum lifespan those trees in this region.

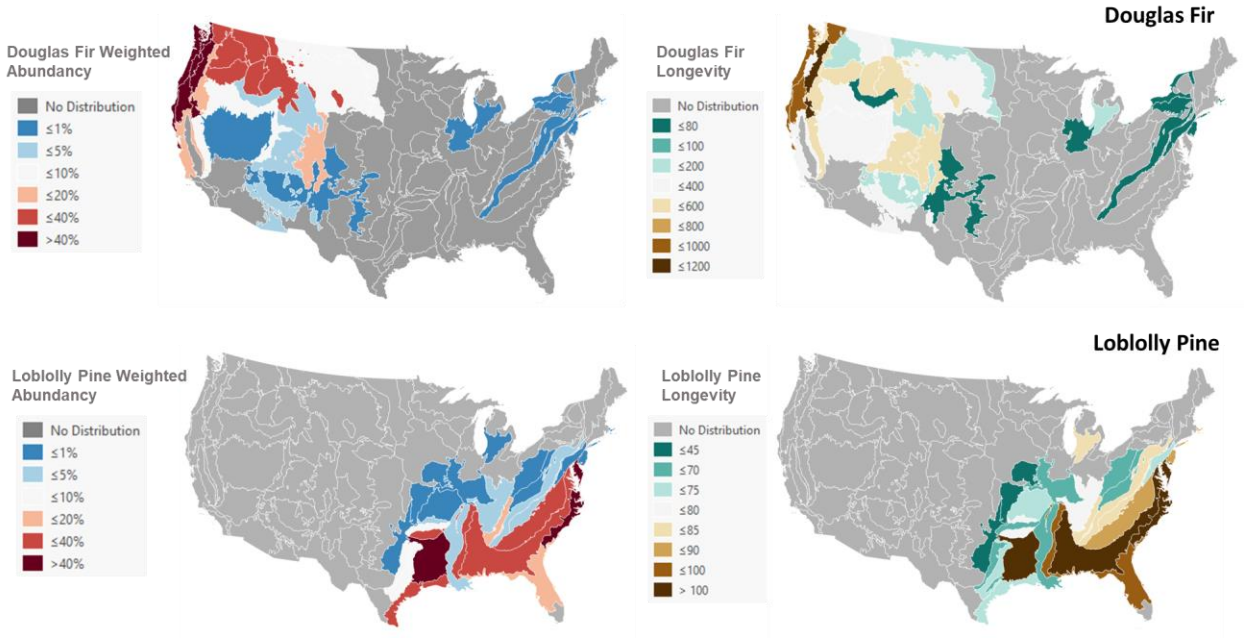

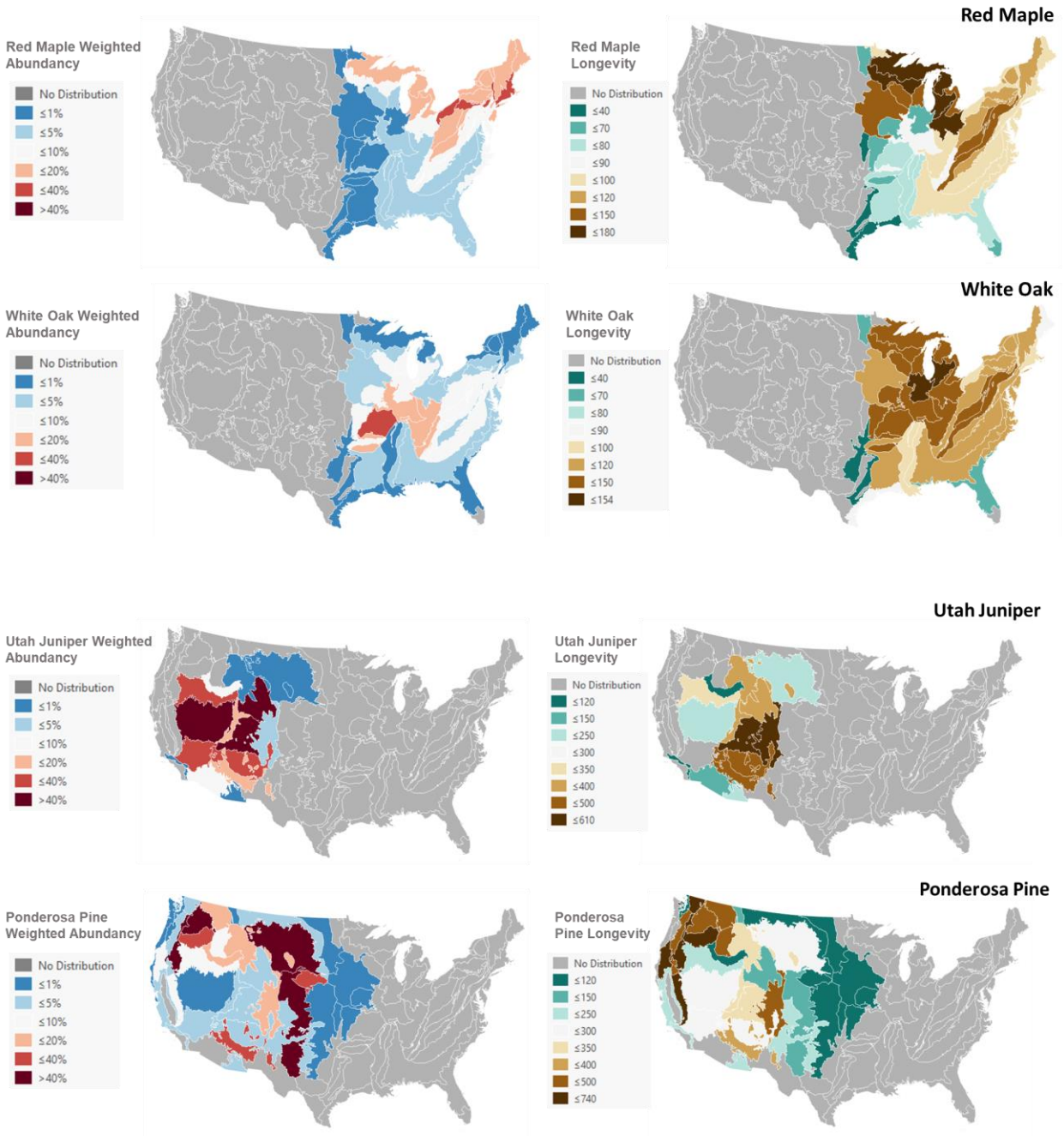

Figure 3-10 Spatial distribution and longevity of selected common species.

3.5 Discussion

Tree age information is a critical component in various fields, from ecology and climate science to forestry management and urban planning. It offers insights into the health, dynamics, and history of both individual trees and forest ecosystems at large. Compared to the classic dendrochronology method, modeling based on the tree age-size relationship can reduce the cost and can be applicable to larger scales,

The tree age dataset presented in this study was derived from models that use tree diameter, height, species, topographic, climate and other environmental variables as predictors. Zone based models have higher accuracies than the regional and national models, which could indicate the relevance of local conditions to tree growth and the importance of tailoring predictive models to these unique factors. While broad models can also capture the general trends, they might miss complex interplay of factors influencing tree growth at a fine scale, which are crucial for accurate predictions. The approach exhibits higher accuracy in its age predictions than existing studies in many areas, and is able to be applied over large areas. However, there are limitations with the derived dataset. Although the FIA database is an invaluable and most comprehensive forest data resource for understanding the status and trends of US forests, the accuracy of predicted age in the east has larger uncertainties due to the data availability in that area. In the eastern states, age was measured only for site trees; there are very limited samples for species that are not often harvested for timber, pulpwood and other products; also, there is no reference data for small trees (< 12.7 cm dbh). Current age sampling method is unable to represent young trees. More sufficient samples that cover more species types and tree sizes will help improve the age estimations.

The derived dataset holds considerable value and has the potential for many practical applications and implications in future research. When the tree age information is combined with tree growth, it is possible to investigate tree growth patterns at different ages. Repeated tree measurements in FIA allow for tracking attribute changes over time, such as the growth rate. For the illustration purpose, we calculated the tree growth rate with the following approach: for selected tree species, in ecoregions where the weighted abundant of target species is no less than 10%, trees that were measured in two or more field visits and not disturbed were identified and their annual AGB growth rate between every two subsequent visits were calculated as

$$GR = (AGB2-AGB1)/nYears \qquad (12)$$

Where GR is the annual growth rate; AGB1 and AGB2 are the AGB of an individual tree from the first and following visit; nYears is the number of years between the two visits. AGB was calculated following FIA's approach (versions prior to the release of The National Scale Volume and Biomass (NSVB) system in Sep 2023) by summing up aboveground biomass from different proportions of the tree, including wood and bark for stump, bole, top, branches, and excluding foliage. Figure 3-11 and Figure 3-12 shows examples of biomass growth rate at different age groups of Douglas fir and loblolly pine in ecoregions where the weighted abundance of the target species is no less than 10%. For both species, the biomass growth rate increases in young age groups, then it becomes stable or begins to decline after a certain age. The turning point from increasing to stabilizing/decreasing is different across ecoregions. For example, for Douglas firs, the biomass growth rate begins to decrease after the 200-300 years age group in Coast Range and Eastern Cascades Slopes and Foothills, but in Cascades, the growth rate continues to increase to

older groups. Douglas fir of the same age can have very different growth rates in different environments. For example, the biomass of a 150-year-old Douglas fir can increase 150 lb. per year in the Coast Range, but only less than 50 lb. per year in the Columbia Plateau. For both species, old trees still have high biomass growth rate, which underscores the substantial carbon sequestration potential of old-growth forests. All these trends and features observed can be valuable for improving the understanding of tree growth. It allows us to investigate the relationships between tree growth with other factors, such as environment (e.g., elevation, climate, etc.). And with such information, it is possible to estimate/predict the biomass growth, furthermore the carbon sequestration potential of US forests.

Other potential usages of the tree age dataset include: the dataset could help identify the old trees that need special protections; with the longevity information, it can provide more insights into the relationship between longevity and growth rate; tree age data also aid the characterization of forest stand age. When only a few trees are sampled in a forest stand, it is hard to use limited samples to produce a stand age estimation that can represent the stand condition. With the availability of tree age of each individual tree in a stand, now it is possible to generate a more reasonable stand age that considers trees of all ages.

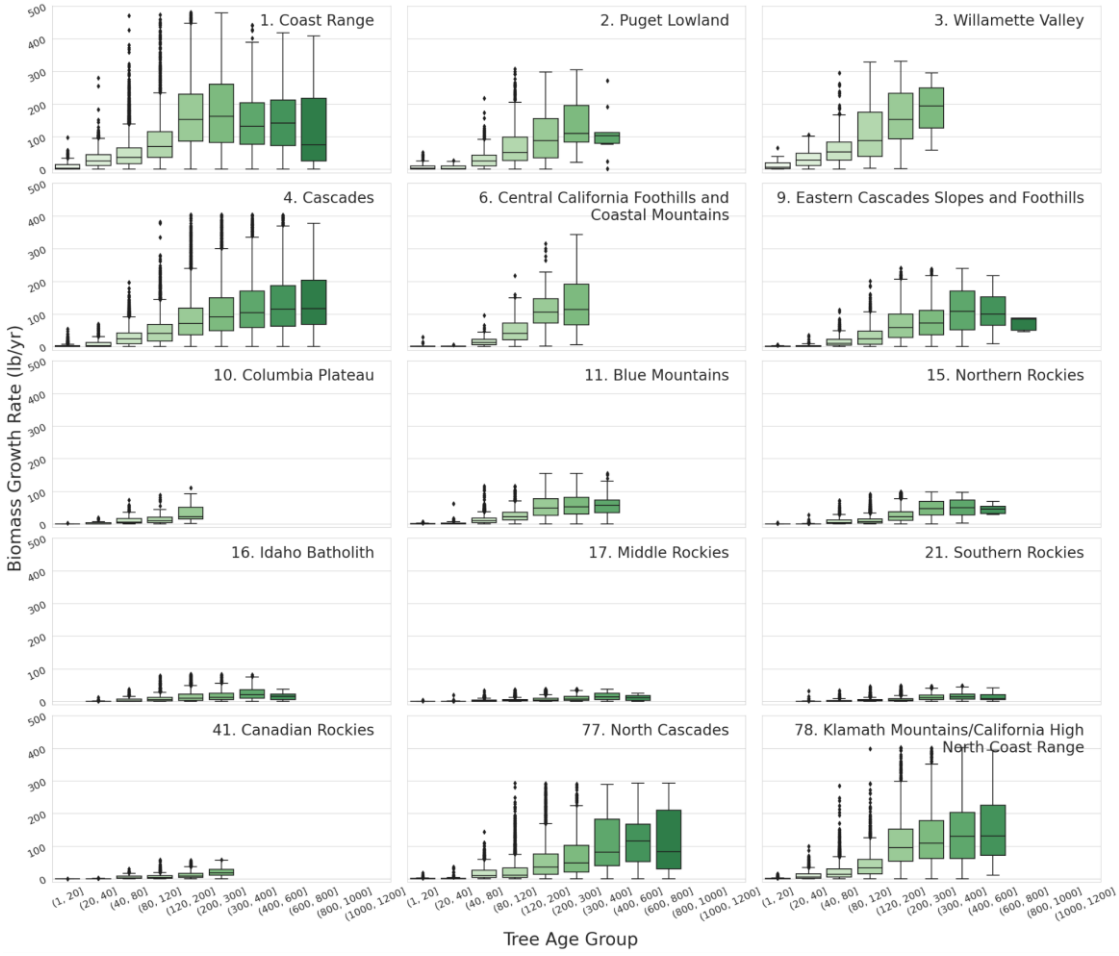

Figure 3-11 The relationship between biomass growth rate and tree age for Douglas fir. Tree growth rate varies across ecoregions and age groups.

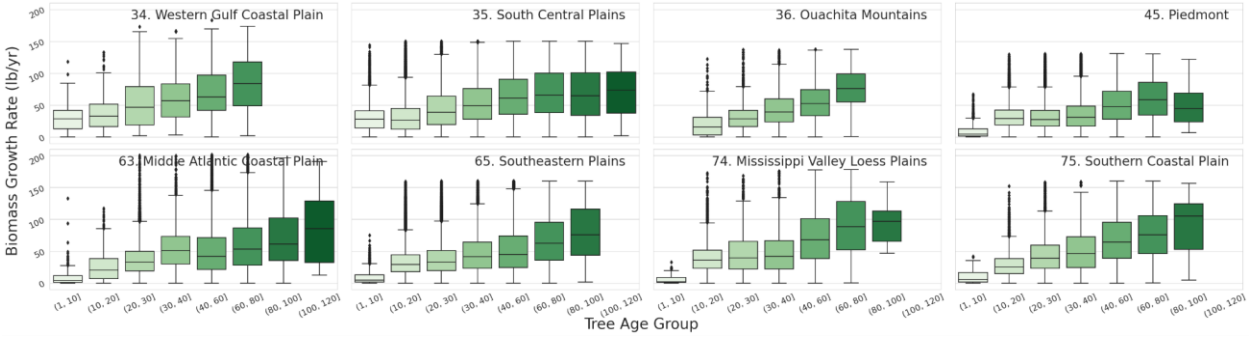

Figure 3-12 The relationship between biomass growth rate and tree age for loblolly pine. Tree growth rate varies across ecoregions and age groups.

3.6 Conclusion

In this study, a modeling framework was developed to estimate tree age which factors in tree size, species and environmental variables. Results indicate that local models are more accurate than national and regional models for age prediction, which underlines the importance of localized data in the modeling of forest variables. 55 zone-based models were built, of which the cross validation indicated the accuracy of our models were higher than existing methods. The modeling framework was able to be transferred to different regions, and with the developed models, age was quantified for every tree in the FIA database (over 10 million trees) across the US, which was previously unavailable. From individual tree age, the population distribution of tree age was estimated for 2015. The tree age distribution was different from western to eastern US, and across ecoregions. The eastern forests feature younger age structures due to historical land use and forest management practices, and the western forests display older age structures influenced by diverse environmental conditions and less intensive human disturbance. Complex pictures were also revealed in the age of the oldest trees, which were shaped by diverse ecological and historical factors. The oldest trees of the same species can have very different ages in different ecoregions. The developed tree age dataset is not only a valuable tool for forest management and conservation efforts but also has the potential to enhance our capacity to accurately estimate carbon sequestration in forests. The age-dependent growth patterns revealed by the study, particularly the sustained biomass accumulation in older trees, hints at the significant carbon sequestration potential of mature and old-growth forests. This emphasized the importance of protecting these ecosystems as part of a broader strategy to mitigate climate change. In the realm of sustainable forestry, the improved understanding of tree age distribution

aids in the development of more effective management practices. By providing a clearer picture of tree dynamics, the research supports more informed decision-making regarding harvesting schedules, reforestation efforts, and overall forest health maintenance.

3.7 Supplementary Materials

Table 3-3 FIA tables used in the population estimation.

Oracle Table Name	Table Name	Description
PLOT	Plot Table	Contains information related to the inventory plots where tree data are collected, including plot identification, establishment and visit Information, fuzzed locations, etc
COND	Condition Table	Complements the plot-level data by offering more granular insights into the forest conditions within each plot, including stand and stocking information, forest type and size class, etc.
TREE	Tree Table	provides tree identification, species, size and other detailed information about individual trees.
POP_PLOT_STRATUM_ASSGN	Population Plot Stratum Assignment Table	Assign plot to a certain stratum record
POP_STRATUM	Population Stratum Table	Provides the expansion factor (i.e., the area the sampled unit represents) and the adjustment factors for macro-, micro- and subplots, which accounts for partially non sampled plots.
POP_ESTN_UNIT	Population Estimation Unit Table	Links population estimation unit record to the evaluation record.
POP_EVAL	Population Evaluation Table	Stores each evaluation used by FIA as a single entry
POP_EVAL_GRP	Population Evaluation Group Table	Stores each evaluation group as a single entry. An evaluation group is the set of evaluations that are included in a typical FIA report for a state.
POP_EVAL_TYP	Population Evaluation Type Table	provides a link between the evaluation groups in POP_EVAL_GRP and the evaluations in POP_EVAL. Can be used to identify a certain evaluation type (e.g., area, growth, volume, number of trees, biomass, mortality, etc)

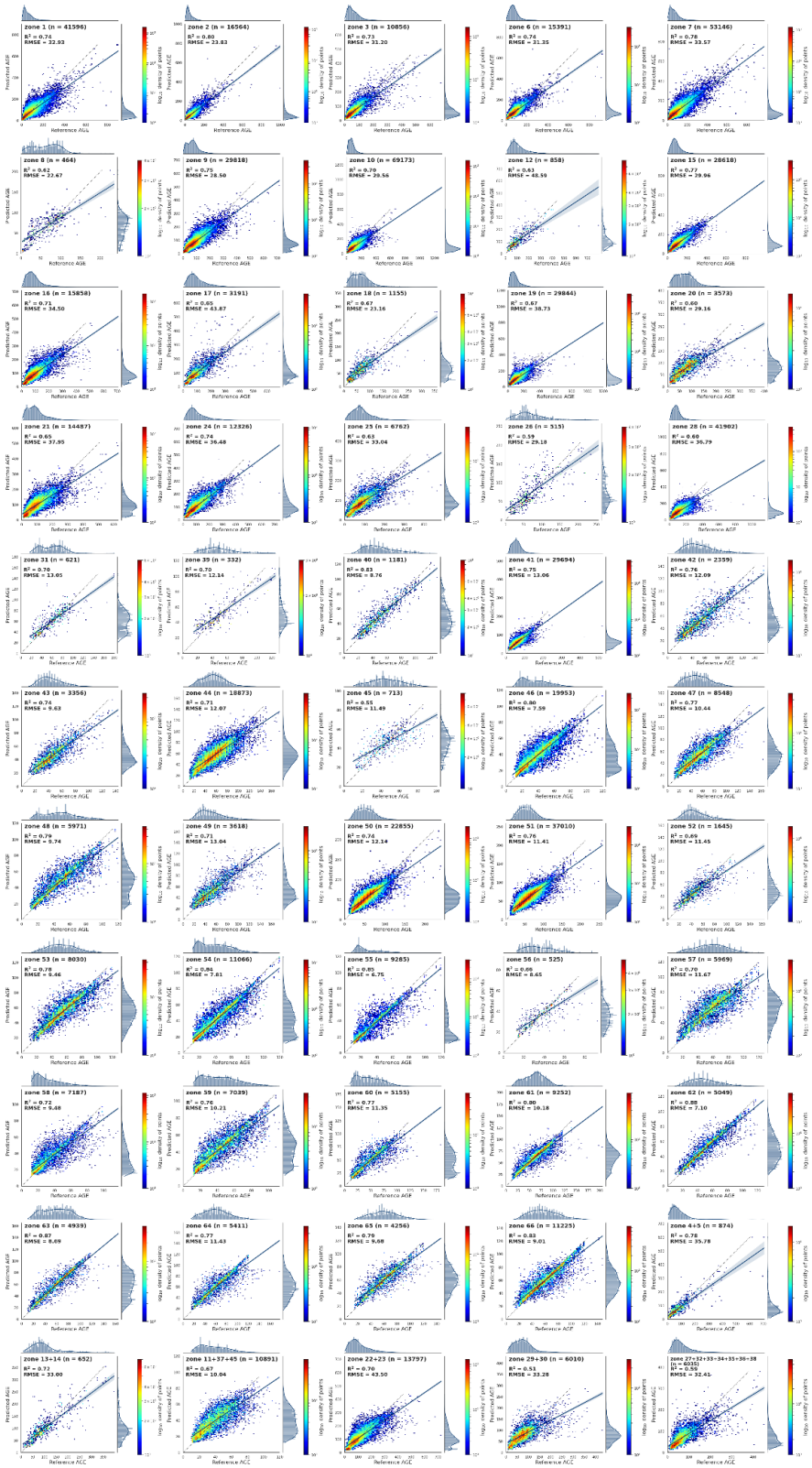

Figure 3-13 Scatterplot of RF models with height for each mapping zone

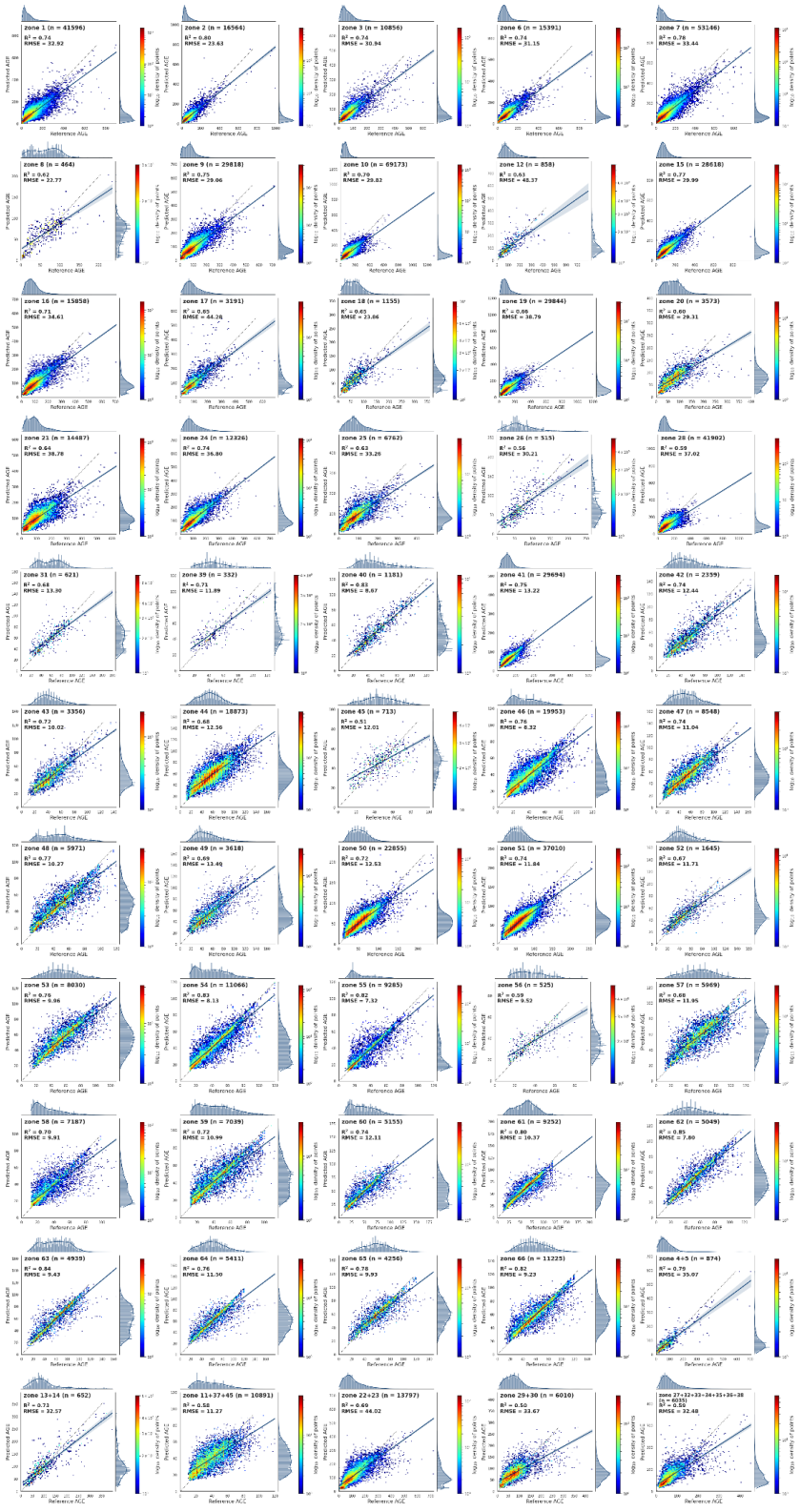

Figure 3-14 Scatterplot of RF models with no height for each mapping zone

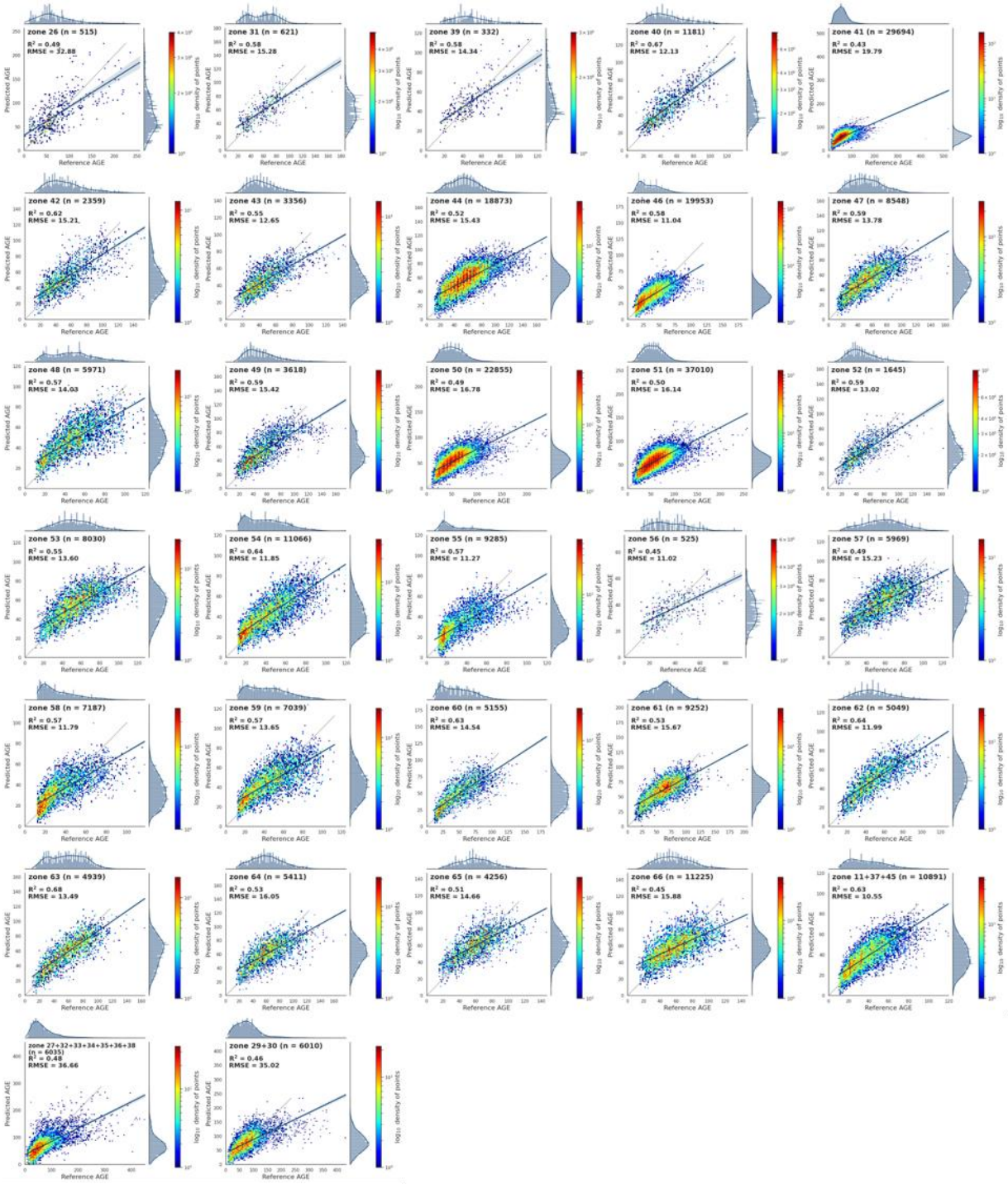

Figure 3-15 Scatterplot of OLS models with height for each mapping zone

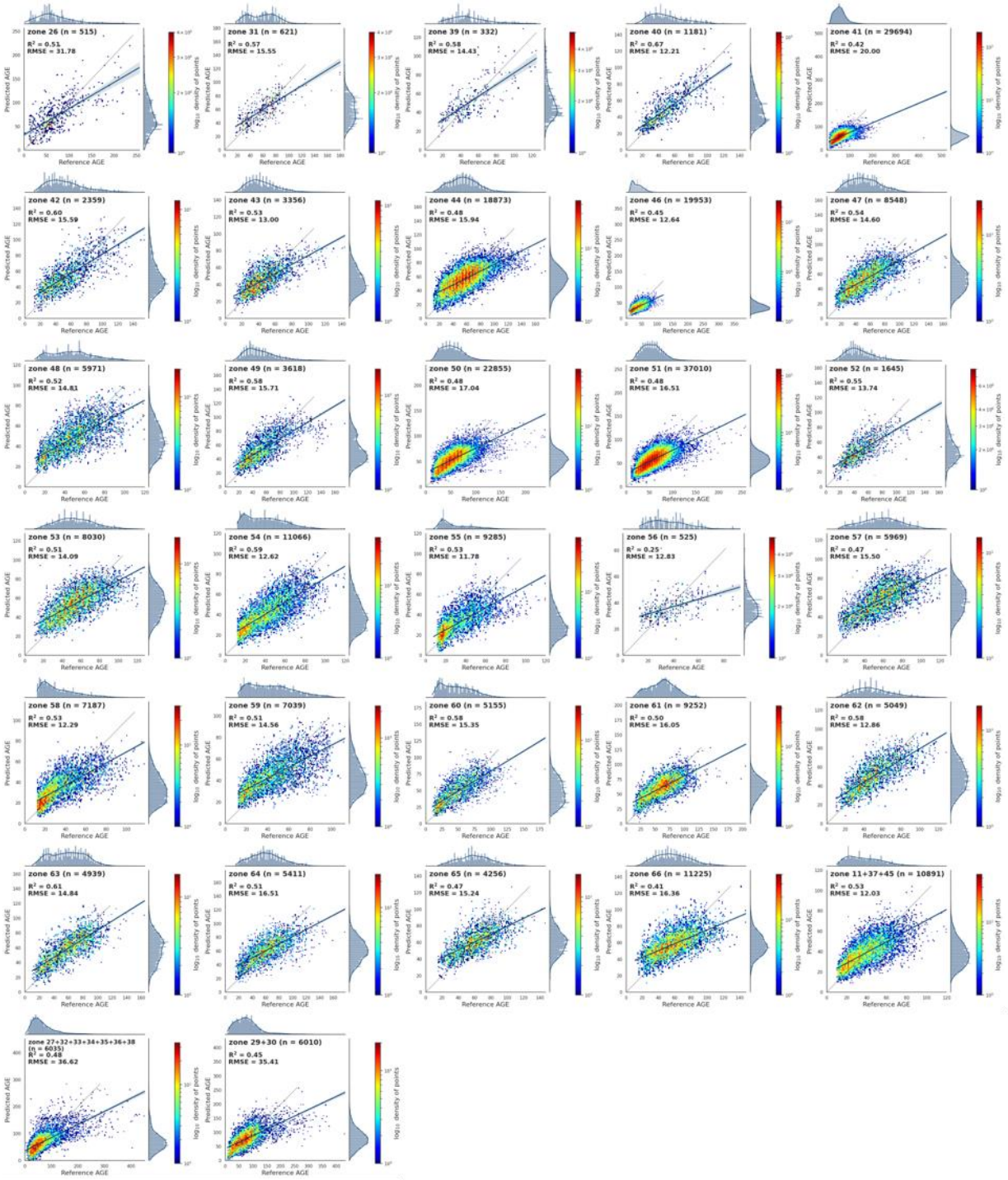

Figure 3-16 Scatterplot of OLS models without height for each mapping zone

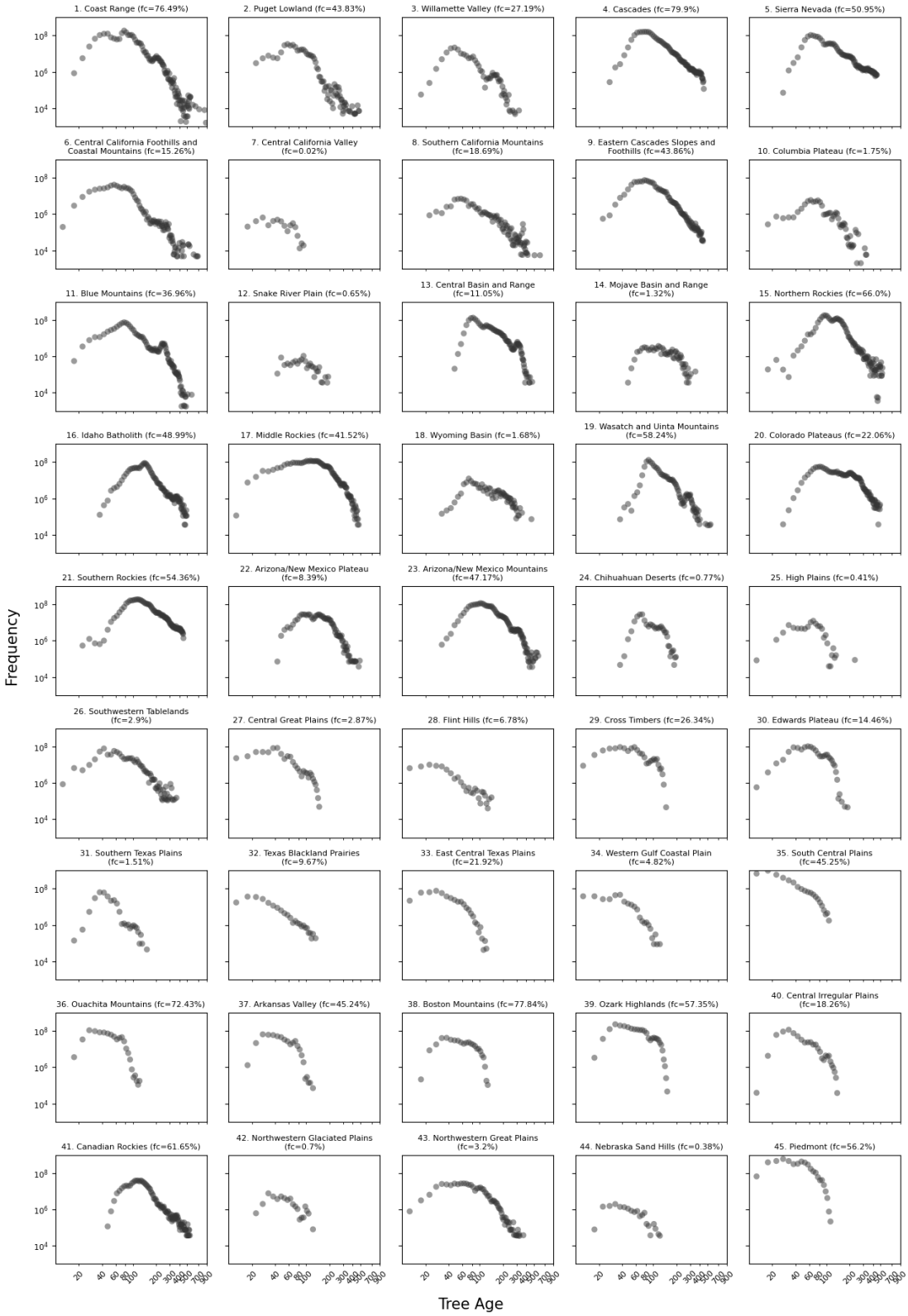
1. Coast Range (fc=76.49%)
2. Puget Lowland (fc=43.83%)
3. Willamette Valley (fc=27.19%)
4. Cascades (fc=79.9%)
5. Sierra Nevada (fc=50.95%)
6. Central California Foothills and Coastal Mountains (fc=15.26%)
7. Central California Valley (fc=0.02%)
8. Southern California Mountains (fc=18.69%)
9. Eastern Cascades Slopes and Foothills (fc=43.86%)
10. Columbia Plateau (fc=1.75%)
11. Blue Mountains (fc=36.96%)
12. Snake River Plain (fc=0.65%)
13. Central Basin and Range (fc=11.05%)
14. Mojave Basin and Range (fc=1.32%)
15. Northern Rockies (fc=66.0%)
16. Idaho Batholith (fc=48.99%)
17. Middle Rockies (fc=41.52%)
18. Wyoming Basin (fc=1.68%)
19. Wasatch and Uinta Mountains (fc=58.24%)
20. Colorado Plateaus (fc=22.06%)
21. Southern Rockies (fc=54.36%)
22. Arizona/New Mexico Plateau (fc=8.39%)
23. Arizona/New Mexico Mountains (fc=47.17%)
24. Chihuahuan Deserts (fc=0.77%)
25. High Plains (fc=0.41%)
26. Southwestern Tablelands (fc=2.9%)
27. Central Great Plains (fc=2.87%)
28. Flint Hills (fc=6.78%)
29. Cross Timbers (fc=26.34%)
30. Edwards Plateau (fc=14.46%)
31. Southern Texas Plains (fc=1.51%)
32. Texas Blackland Prairies (fc=9.67%)
33. East Central Texas Plains (fc=21.92%)
34. Western Gulf Coastal Plain (fc=4.82%)
35. South Central Plains (fc=45.25%)
36. Ouachita Mountains (fc=72.43%)
37. Arkansas Valley (fc=45.24%)
38. Boston Mountains (fc=77.84%)
39. Ozark Highlands (fc=57.35%)
40. Central Irregular Plains (fc=18.26%)
41. Canadian Rockies (fc=61.65%)
42. Northwestern Glaciated Plains (fc=0.7%)
43. Northwestern Great Plains (fc=3.2%)
44. Nebraska Sand Hills (fc=0.38%)
45. Piedmont (fc=56.2%)
Frequency
Tree Age

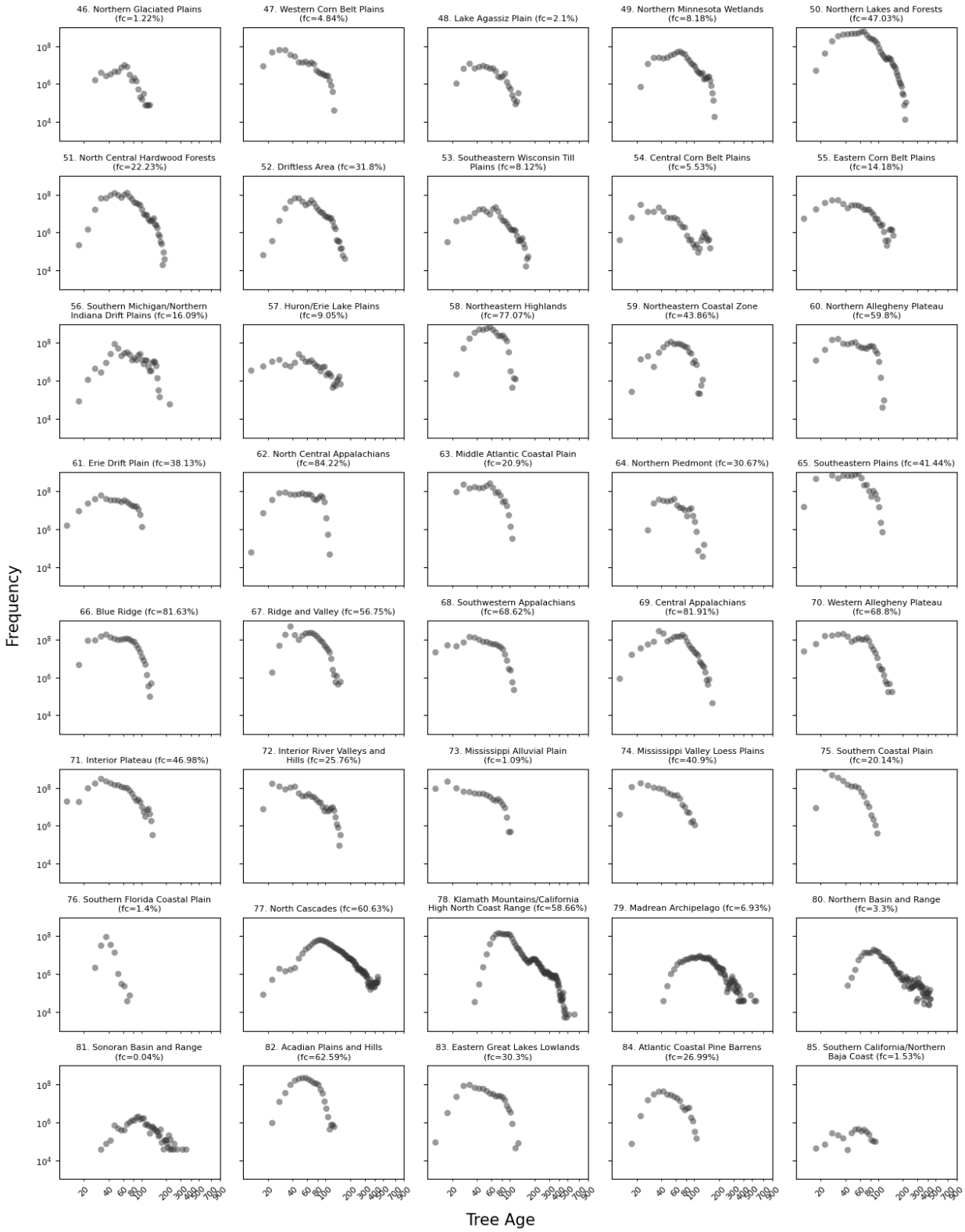

Figure 3-17 Histogram of tree age in level 3 ecoregions

Chapter 4: Mapping Forest Age and Complexity in US Forests

4.1 Abstract

Forest age information is crucial as it influences biodiversity, ecosystem health, carbon sequestration, resilience to disturbances, and informs sustainable forest management practices. Using time since disturbance to approximate age can introduce large bias. Estimating exact forest age at large scale is challenging because of the difficulty to measure ground truth, dilemma in defining a singular age to represent the stand, and the uncertainties in the extent to which spectral reflectance can differentiate forests of different ages. The objective of this study is to develop an approach that considers the historical disturbance intensity, and spectral trajectory of forests, to estimate forest age and complexity for 2015 and 2005. The combination of the two metrics should provide a more comprehensive characterization of the forest stand condition. The reference age was calculated using the age of every tree within a plot, which improved the representation of results compared to age calculated using only a few sample trees. The developed forest age models had higher accuracy than existing studies. The 30-m forest age and complexity mapping products did not exist before this study. They provide valuable information for knowing forest conditions, estimating forest growth and carbon sequestration potential, understanding the relationship between age and other forest attributes, evaluating forest health, and planning sustainable forest management practices.

4.2 Introduction

Similar to individual tree age, forest age information is crucial for assessing biodiversity, estimating the growth rate and capacity of carbon storage in forests, and evaluating the nature and extent of other ecosystem services such as water regulation, soil protection, and recreational opportunities, etc. However, forest age is often considered a highly uncertain variable due to the complexity in determining exact age. Determining the exact age can be challenging for two main reasons. First, in natural forests, trees may be of various ages due to the continuous process of mortality and growth, which creates a mosaic of different age classes rather than a uniform age structure. Therefore, it is challenging to determine a singular age for the uneven-aged stands. In existing studies, definitions of forest stand age include mean age of representative trees (where representative trees can be trees in the uppermost layer, trees of dominant species, trees with largest diameter, most abundant tree-size class, oldest trees, etc.), mean age of all trees in a stand, basal area weighted mean age, age of one representative tree, age of the oldest live tree, etc. See Table 4-1 for the complete summary. National field inventory programs, such as FIA, use a selection of trees in a plot to determine the stand age, under the assumption that the sampled trees are representative of the stand as a whole. But for natural forest stands, the age calculated from a few sample trees may not represent the stand. Second, determining the exact age relies on counting growth rings in a core sample or a stump, which is time-consuming and not always feasible, especially for large-scale assessments. Therefore, it is not practical to produce forest age maps using such field-based methods.

Table 4-1 Definitions of forest age in published studies

Definitions	**Reference**
mean age of representative trees**	Duane et al., 2010; Frate L Carranza ML & G, 2016; Ouyang et al., 2019; Racine et al., 2014; Straub & Koch, 2011; Van Tuyl et al., 2005; C. Zhang et al., 2014
mean age of all trees in a stand	Véga & St-Onge, 2009; Yang et al., 2019
basal area weighted mean age	Jonsson et al., 2020; Maltamo et al., 2020; Sharma et al., 2011
age of one representative tree	Schumacher et al., 2020
Planting years for homogeneous plantations	Diao et al., 2020; Du et al., 2022; Tudge et al., 2023

** *Representative Trees: trees in the uppermost layer; trees that are of dominant species (in the upper layer); trees with largest diameter; oldest 10% of measured trees; trees of the most abundant tree-size class*

Remote sensing provides an opportunity to study forest age at large scales. Different ages and types of vegetation have distinct ways to reflect and absorb light across various wavelengths. These spectral signatures are useful for retrieving forest age, especially for young forests. With the capability to provide tree height information, LiDAR has been used in multiple studies to estimate forest age (Schumacher et al., 2020; Wylie et al., 2019), but this approach is limited by its inability to retrieve historical age information. Landsat imagery holds unique value in its long-term data record, allowing the monitoring of forest growth and disturbances for multiple decades. Landsat-based disturbance history and field inventory data have been combined for age mapping (Diao et al., 2020; Maltman et al., 2023; Pan et al., 2011; Tian et al., 2023). But the derived products are either for small areas, or for large areas but with coarse spatial resolution or low accuracies. In many of these studies, disturbed forests and persisting forests that have never been disturbed (within the Landsat observation period) are often treated differently. For disturbed forests, time since disturbance is used as a proxy to forest stand age, which creates uncertainties since disturbance events vary by their intensity. For example, because partial

disturbances don’t reset the age of the trees that survived those disturbances, the starting age of partially disturbed forests will be higher than 0. For stand clearing disturbances, the time between disturbance and regeneration varies. So, time since disturbance is not equivalent to forest age in many natural cases (Bradford et al., 2008). For persisting forests, spectral indices calculated from surface reflectance of a certain year were used in conjunction with machine learning models or parametric regression models to estimate age for that specific year (Besnard et al., 2021; Diao et al., 2020; C. Zhang et al., 2014). Such methods were tested in small study areas for certain species or plantation forest stands to produce single time maps.

The goal of this chapter is to develop a forest age modeling approach that leverages the disturbance history and forest growth trajectory recorded in the Landsat time series, and the more complete individual tree age dataset produced in the previous chapter, to provide a more comprehensive characterization of forest age dynamics by estimating both forest age and the standard deviation of the age of trees within the forest at higher accuracy.

4.3 Methodology

4.3.1 Data

Tree Age Data

The reference forest age used to train and validate the models was calculated from individual tree age developed in the previous chapter. Tree age was estimated using diameter, height, species, and other environmental variables for every sample tree in the FIA database. The count of sample trees varies in plots, and across FIA regional units. The median count of trees used to

calculate forest age ranges from 4 to 40 per plot. The plots in northeastern and northwestern regions have more sample trees compared to those in other regions (Figure 4-1).

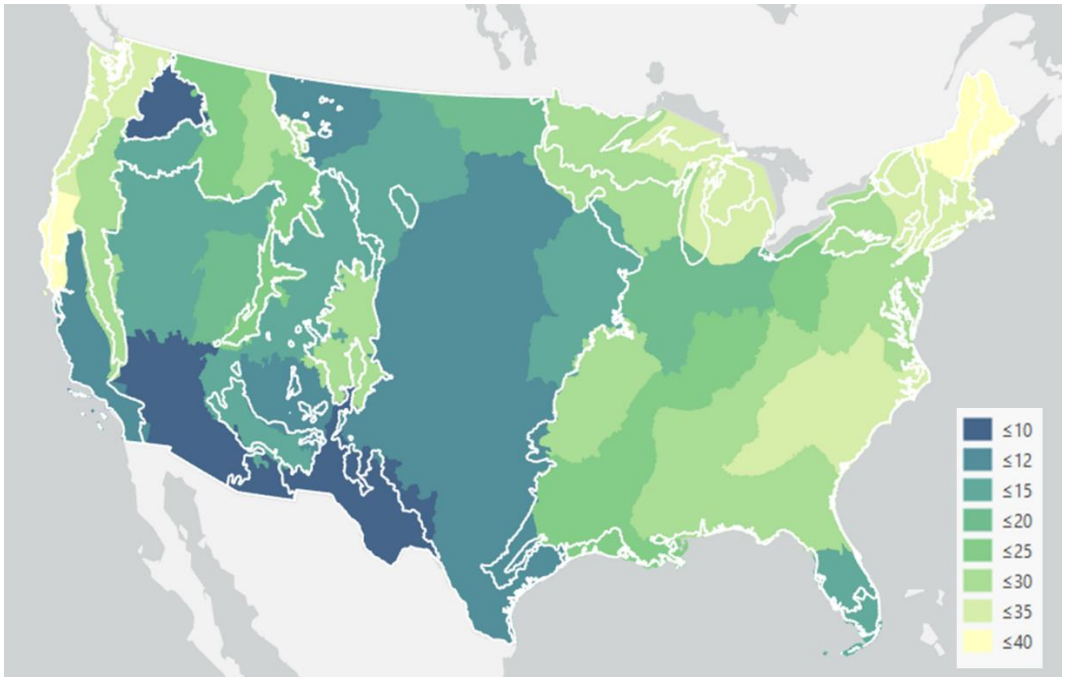

Figure 4-1Map of median number of available FIA sample trees per plot in each NLCD mapping zone. The white lines are the boundaries of the level 1 ecoregions, which serve as the mapping unit in this study.

Landsat Surface Reflectance and Disturbance History

The annual median composite of Landsat surface reflectance was created and downloaded from Google Earth Engine. All available images from the Level 2, Collection 2, Tier 1 of Landsat 4, 5, 7, 8 from the leaf-on season were collected and filtered by the Pixel Quality Assessment Band (QA_PIXEL) and cloud cover property, which were determined by the C Function of Mask (CFMask) algorithm (Foga et al., 2017; Zhu et al., 2015). Images with more than 70% cloud cover were initially filtered out, then pixels flagged as “Dilated Cloud”, “Cirrus”, “Cloud”,

"Cloud Shadow", and "Snow" were masked. Finally, the Radiometric Saturation Quality Assessment (QA_RADSAT) was used to mask and exclude the saturated pixels from median calculation. From the good pixels, the median was calculated for the seven surface reflectance bands, blue, green, red, near infrared, two shortwave infrared bands, and thermal band.

Disturbance location and time was detected by VCT algorithm, same as described in 2.4.2. Disturbance intensity product from chapter 2 was used to determine the intensity of historical disturbance events. The combination of disturbance intensity and surface reflectance from the disturbance year helped determine whether the disturbance was a stand-clearing or partial disturbance event.

Elevation, Slope, Aspect, and Solar Radiation

The Digital Elevation Model (DEM) data used was from the NASA Shuttle Radar Topography Mission (SRTM) Global 1 arc second dataset. The SRTM DEM was a near-global DEM dataset derived based on radar interferometry. The radar data was acquired between 2000-02-11 and 2000-02-21. The spatial resolution of this dataset was 1 arc second (~30 meter). The data was collected in swaths, which are about 225 km wide. To cover CONUS, a total of 1183 swaths/tiles were used (Farr et al., 2007).

From the elevation data, slope, aspect, and annual solar radiation were all calculated with ArcGIS's Python API. Geodesic slope was calculated as the angle formed between the topographic surface and the ellipsoid surface. The aspect identifies the direction the downhill slope faces. To calculate both in a 3D Cartesian coordinate system (Ligas & Banasik, 2011), the coordinates were first converted to 3D Cartesian coordinates, then for each location, a 3 by 3 cell neighborhood plane was fitted around each processing cell to determine the angle and direction.

The annual solar radiation for each location was calculated as the amount of solar radiation energy received per unit area during a year and is measured in kilowatt hours per square meter (kWh/m2). Solar radiation was calculated using a model that accounts for both direct and diffuse sunlight. It factors in the sun's position, terrain variations, and atmospheric conditions (Fu & Rich, 1999).

PRISM

Similar to tree age modeling, the climate variables used were from the PRISM climate dataset developed by the PRISM Climate Group at Oregon State University. The variables used that can affect tree growth include precipitation (ppt), minimum temperature (tmin), maximum temperature (tmax), mean temperature (tmean), mean dew point (tdmean), minimum vapor pressure deficit (vpdmin), and maximum vapor pressure deficit (vpdmax). See section 3.3.1 for more details about this dataset and variable selection.

4.3.2 Stand Clearing vs Partial Disturbance Classification

To differentiate the disturbance events between stand-clearing and partial disturbances, a Random Forest classifier was first trained with the disturbance intensity and the 7 bands of surface reflectance from the disturbance year as predictor variables. 3030 plots that were disturbed were examined by their fuzzy location in Google Earth Imagery and labeled whether the disturbance was stand-clearing. Then the reference data was split into a training (70%) and testing (30%) set. The accuracy of the classification was assessed by the confusion matrix and overall accuracy, calculated by dividing the number of correct predictions by the total number of observations.

4.3.3 Forest Age and Tree Age Standard Deviation Calculation

Defining forest age can be challenging due to the complexity of tree age structure within a forest stand. FIA's stand age considers the sample trees in the dominant class. Here, similar to Lorey's height, we defined forest age as the basal area weighted mean tree (BAWMT) age following the existing studies. For each FIA plot, BAWMT age was obtained by multiplying the age and basal area of each individual sample tree, summing up the age-basal area product of all trees within that plot, and then dividing the sum of the products by the total plot-level basal area. See below for the equation used,

$$\text{BAWMT} = \frac{\sum_{i=1}^{n}(age_i \times BA_i)}{\sum_{i=1}^{n} BA_i} \quad (13)$$

Where age_i is the age of the ith tree, BA_i is the basal area of the ith tree, n is the total number of trees within the current plot.

By weighting tree age using basal area, this definition gives more weight to larger, potentially older trees that represent a significant portion of the forest's biomass, and yet the smaller and median size trees are also considered in the calculation.

The tree age standard deviation within an FIA plot was calculated using the ages of all the sample trees within a plot. A high standard deviation value indicates higher complexity of forest structure with multiple age classes, often reflecting a natural, uneven-aged forest or a forest that has experienced varied disturbances and regrowth patterns. Conversely, a low standard deviation suggests a more uniform age distribution, common in managed forests or those established after a single disturbance event. The tree age standard deviation has implications for assessing the

biodiversity, ecosystem resilience, and stability of a forest stand (Tudge et al., 2023; Yi & Jackson, 2021)

4.3.4 Model Assembly

Four sets of models were developed for each mapping unit. Considering the training data availability, in this chapter, the mapping unit generally follows the US level 1 ecoregion boundaries, dividing the CONUS into 7 mapping units (Figure 4-1). For forests that have been stand-cleared during the Landsat observation period, the BAWMT age was modeled by

Age = f (year since disturbance, disturbance intensity, surface reflectance of the target year, fuzzy location, environmental variables including climate, and elevation/slope/aspect/solar radiation)

The tree age standard deviation within a plot was modeled by

*Tree Age Std Dev = f (year since disturbance, disturbance intensity, standard deviation of surface reflectance within the 3*3 pixel window of the target year, fuzzy location, environmental variables including climate, and elevation/slope/aspect/solar radiation, and standard deviation of environmental variables within the 3*3 pixel window)*

For partially disturbed and persisting forests (not disturbed during the Landsat observation period), forest age was models by

Age = f (10-year time series surface reflectance, fuzzy location, environmental variables including climate, and elevation/slope/aspect/solar radiation)

The tree age standard deviation within the persisting and partial disturbed plot was modeled by

*Tree Age Std Dev = f (time series standard deviation of surface reflectance within the 3*3 pixel window, fuzzy location, environmental variables, standard deviation of environmental variables within the 3*3 pixel window)*

To determine whether the BAWMT age definition allows better modeling of forest age using the above approach than FIA's stand age definition, the two age models described above were also trained for estimating forest stand age as defined by FIA, i.e., the FIA stand age was used as the target age variable in both model training and production. The accuracies of these models as evaluated in the next section were used to determine which age definition allows better modeling of forest age using time series Landsat observations.

4.3.5 Evaluation

Similar to the previous two chapters, the model performance was evaluated by 10-fold cross validation. See section 2.4.4 and section 3.3.2 for the explanation of the cross-validation process. From the cross validation, a set of evaluation metrics were calculated, including R^2 (Eq. 8), RMSE (Eq. 9), relative RMSE (Eq. 13), mean absolute deviation (MAD, Eq. 14), mean deviation (MD, Eq. 15), percentage of predictions within one standard deviation from the reference data (+-SD%). The metrics were used to compare model performance across ecoregions and compare with model accuracy in existing studies.

$$rRMSE = \frac{RMSE}{\bar{y}} \qquad (14)$$

$$MAD = \frac{\sum |y_i - \hat{y}_i|}{n} \qquad (15)$$

$$MD = \frac{\sum (y_i - \hat{y}_i)}{n} \qquad (16)$$

where n is number of samples, y_i is the reference value, $\hat{y}_i$ is the predicted value, $\bar{y}$ is the mean of reference value

The derived 2005 age map is also compared against a 2006 250-m age map (Pan et al., 2011)

to evaluate the map accuracy at national scale. The age from two maps were compared to the BAWMT age calculated from all FIA plots that were measured in year 2005 and 2006. Same plots were used in the evaluation against the two datasets. The reference was calculated from nearly 3 million plots to cover the national area.

4.4 Results

4.4.1 Classification of Forest Disturbances

The overall accuracy of the stand-clearing vs partial disturbance classification is 97.54%. The classifier performed better in classifying partial disturbance compared to stand-clearing disturbance (Table 4-2). Of 878 test samples that were labeled as partial disturbance, 869 (98.97%) were correctly classified. Of 66 test samples that were labeled as stand clearing disturbance, 52 (78.79%) were correctly classified. This is likely due to the small number of training samples of the stand clearing disturbance type.

Table 4-2 Confusion matrix of the stand clearing vs partial disturbance classification.

	Partial (Predicted Label)	Stand-clearing (Predicted Label)
Partial (True Label)	869	9
Stand-clearing (True Label)	14	52

4.4.2 Performance of the Age Estimation Models

In the four-example level 1 ecoregions where we compared the model's accuracy in estimating BAWMT age and FIA's stand age, nearly all the evaluation metrics suggest the model framework can predict BAWMT age at a higher accuracy (Figure 4-2). The largest difference was seen in Mediterranean California, where the R^2 is 0.67 in predicting BAWMT age, but only 0.26 in predicting FIA stand age. In the Great Plains, the R^2 is 0.63 in predicting BAWMT age, but only 0.38 in predicting FIA stand age. In the other two ecoregions, the differences are smaller but still, the models for the BAWMT age yield higher R^2 values, lower RMSE/rRMSE, lower MAD, and lower MD than those for the FIA stand age.

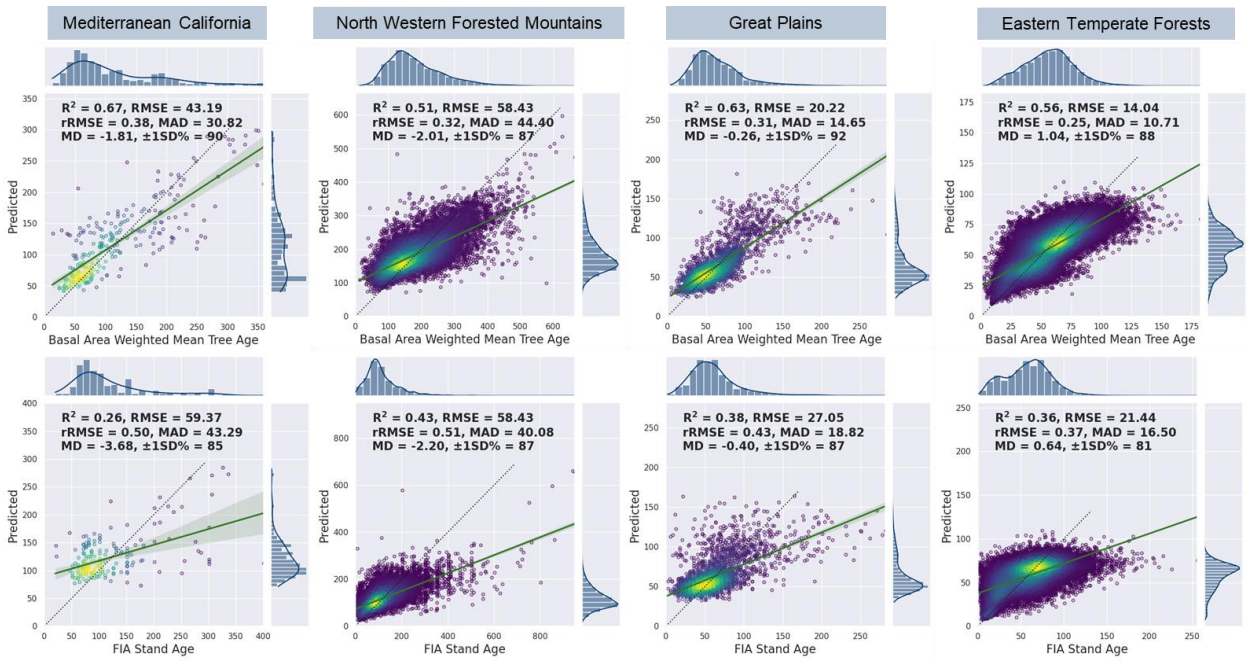

Figure 4-2 Comparison of model performance in estimating BAWMT age (top row) and FIA stand age (bottom row) in four level 1 ecoregions. All evaluation metrics calculated from cross validation suggest the BAWMT age can be predicted at higher accuracy than FIA's stand age.

Based on the comparison results described above, only the BAWMT age models are considered for forest age estimation throughout the rest of this study. Models for estimating BAWMT age (referred to as *forest age* in the rest of the document) and tree age standard deviation (referred to as *stand age complexity* in the rest of the document) were developed and evaluated for all 7 mapping units. The R^2 values in predicting forest age range from less than 0.4 in North American Deserts to 0.67-0.68 in Marine West Coast Forests and Mediterranean California (Figure 4-3 a). The latter two ecoregions with high R^2 values also have the highest relative RMSE values, possibly due to the wide range of forest age in the two regions. For stand age complexity, the model accuracy was lower than the age models in all ecoregions (Figure 4-3 b). The models performed well in Marine West Coast Forest, Mediterranean California, and Northwestern Forested Mountains, but revealed lower R^2 values in the desert area and eastern forests.

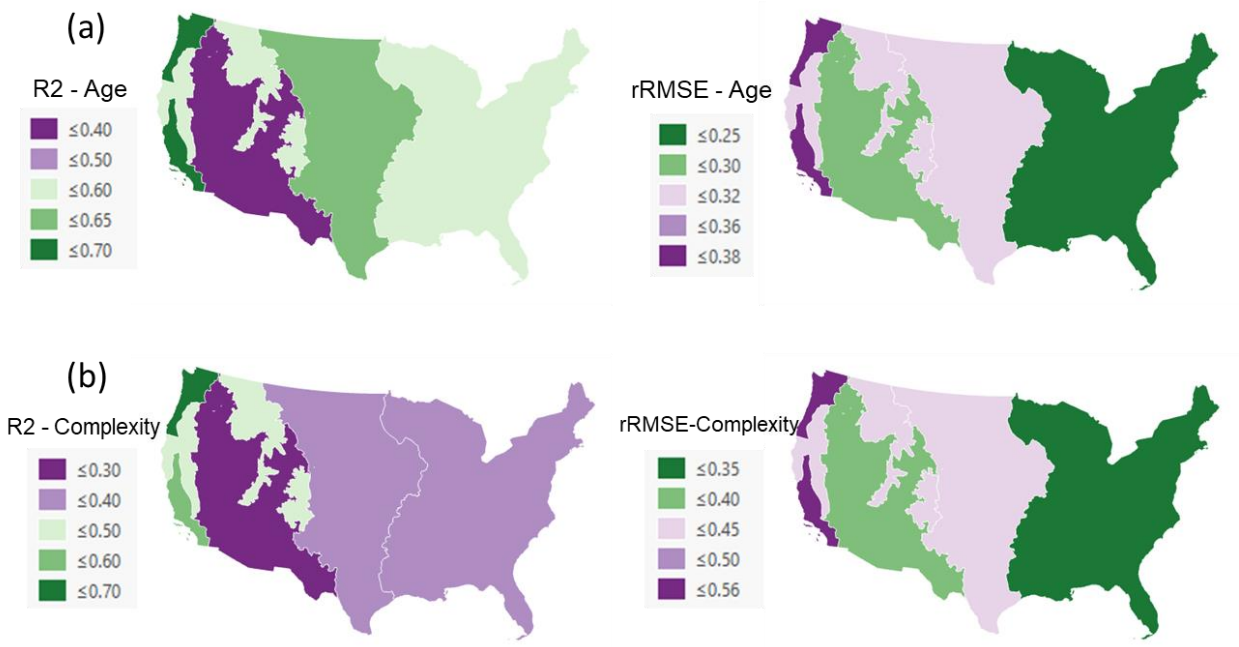

Figure 4-3 Model accuracy in predicting forest age (a) and stand age complexity (b) assessed by cross validation for US level 1 ecoregions.

4.4.3 Evaluation to An Existing Age Map Product

With the developed method, we were able to produce the 30-m forest age maps for the US forests for two years (2015 and 2005). In evaluation again the 2006 250-m age product, the R2, RMSE, and rRMSE indicate the BAWMT age map produced in this study has large improvements over the existing age map (Figure 4-4).

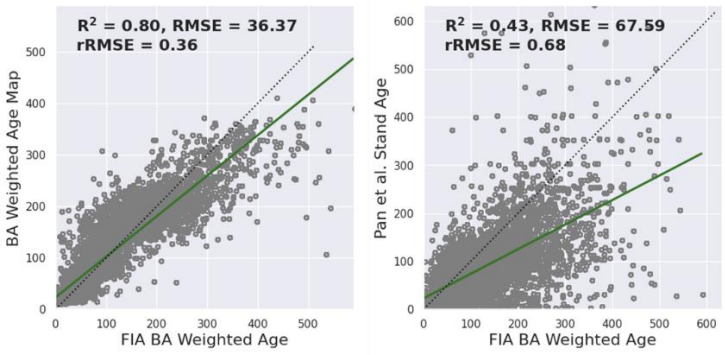

Figure 4-4 The comparison of the 2005 30-m BAWTM age map from this study (left) and the 2006 250-m age map (right) using the same FIA plot derived reference age.

4.4.4 Spatial Patterns of Forest Age and Age Complexity

Forest Age

The spatial distribution pattern of forest age (Figure 4-5) is similar to tree age in the previous chapter. The oldest forests are in Cascades, Sierra Nevada, Klamath Mountains/California High North Coast Range, Southern and Middle Rockies. Eastern forests are much younger. In national parks and forests that have unique management practices of long rotation and low-frequency logging, forests can be older than 200 years. The Redwood State and National Park has some of the oldest forests in the US due to the long lifespan of redwood (Figure 4-5 A). Forests in white River National Forests are old due to the mountainous terrain and climate (Figure 4-5 B). In managed private forests that expect frequent harvesting, the forests are younger, usually less than

80 years old in the eastern forests (Figure 4-5 C). The difference in forest age distribution can also be seen in the histogram (Figure 4-6), which suggests in 2015, the dominant age group in eastern forests is 51-70 years old, while for western forests it is 151-170 years old. The comparison between the forest age maps produced for 2015 and 2005 suggest there is no obvious change in forest age distribution (Figure 4-6). In 2015, the national median forest age was 60. The median age of eastern forests is 54, and for western forests the median is 153. Across US forested ecosystems, 4.72% of forested areas are older than 200 years. The forest younger than 20 years accounted for 6.35% of all the forests. In 2005, the national median forest age was 59. The median age of eastern forests is 52, and for western forests the median is 153. 5.07% of forested areas are older than 200 years. The forest younger than 20 years accounted for 3.73% of all the forests. During the 10 years, the maps suggest there is a slight decrease in old forest areas, and an increase in the area of young forests.

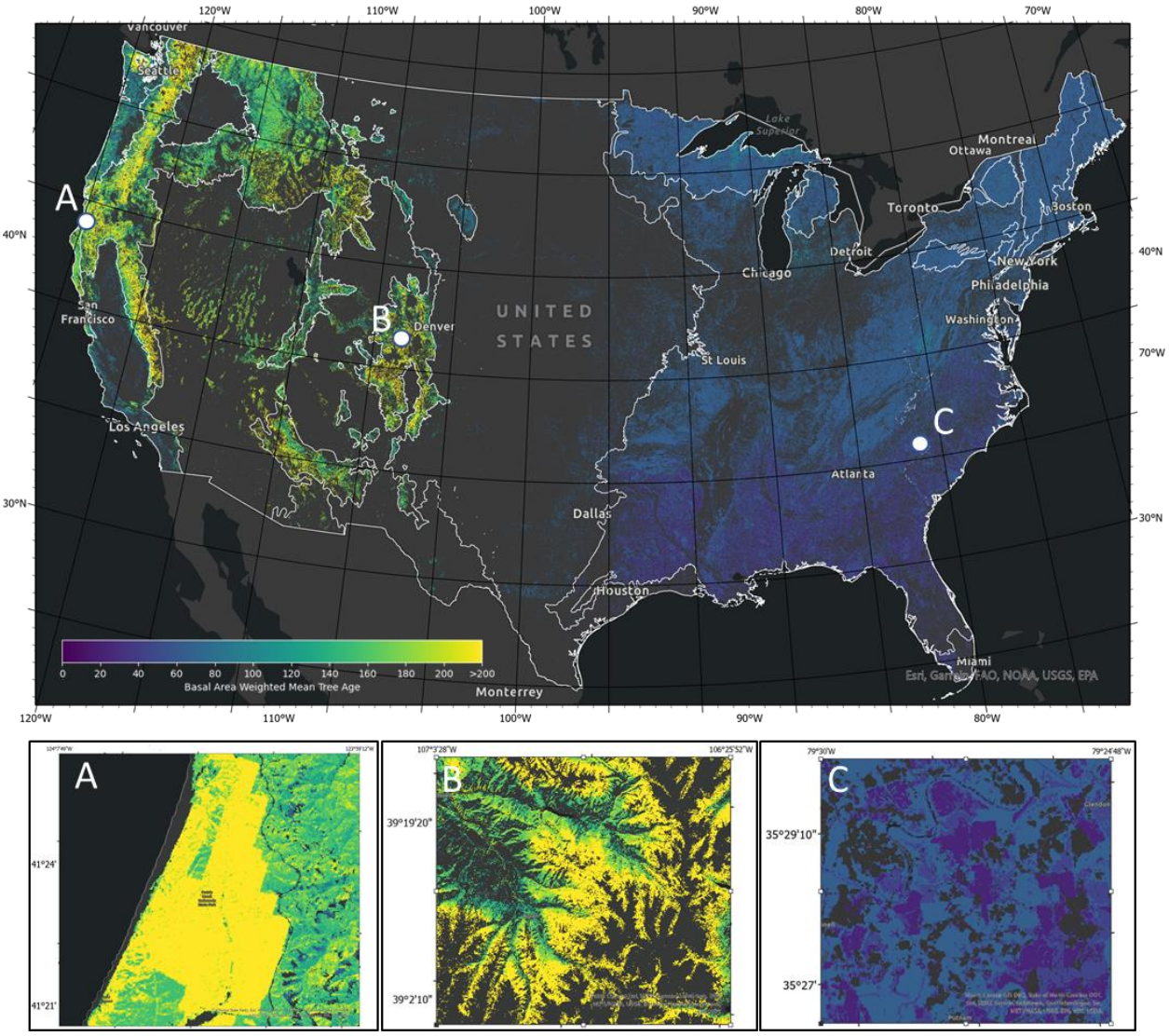

Figure 4-5 Estimated age of US forests in 2015 and site examples in Redwoods State and National Park (A), mountainous area of the White River National Forests in Colorado (B), and private ownership forests in North Carolina (C) revealing distinct patterns of forest age distribution.

Figure 4-7 illustrates the effect of disturbance events on forest age, and provides additional validation of the developed two-year age maps. Large scale forest fires caused tree mortality and decreased the forest age, but not all forest stands saw large decreases in forest age since large and old trees are more likely to survive from fires due to factors like thick bark and higher branches, reducing vulnerability to ground fires. Therefore, forest patches of different ages were created

from the fire events. In forest harvesting areas, stand-clearing removal is more often seen, where forest age can suddenly decrease from around 80 years to near zero (Figure 4-7)

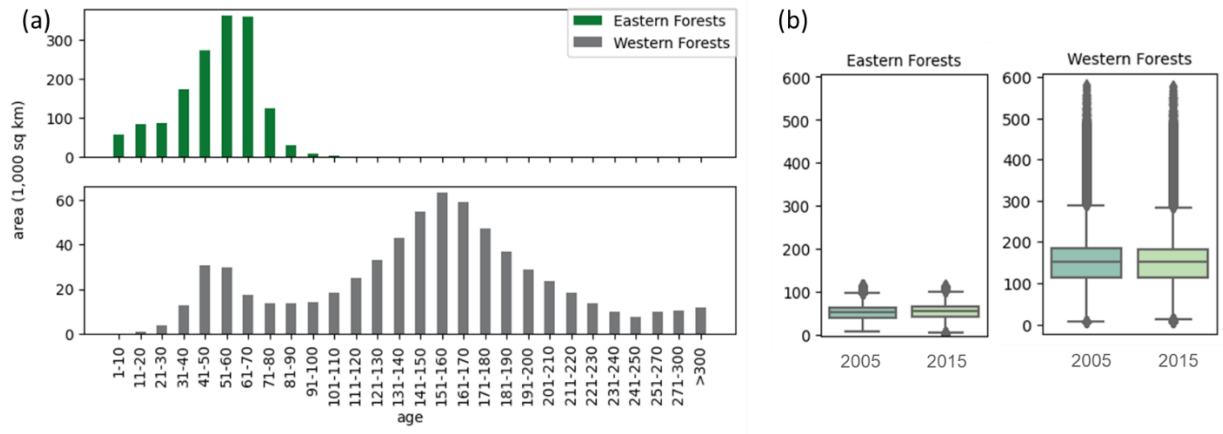

Figure 4-6 (a) Histogram of forest age in eastern and western forests in 2015. (b) boxplot showing the distribution of forest age is similar between the years 2005 and 2015.

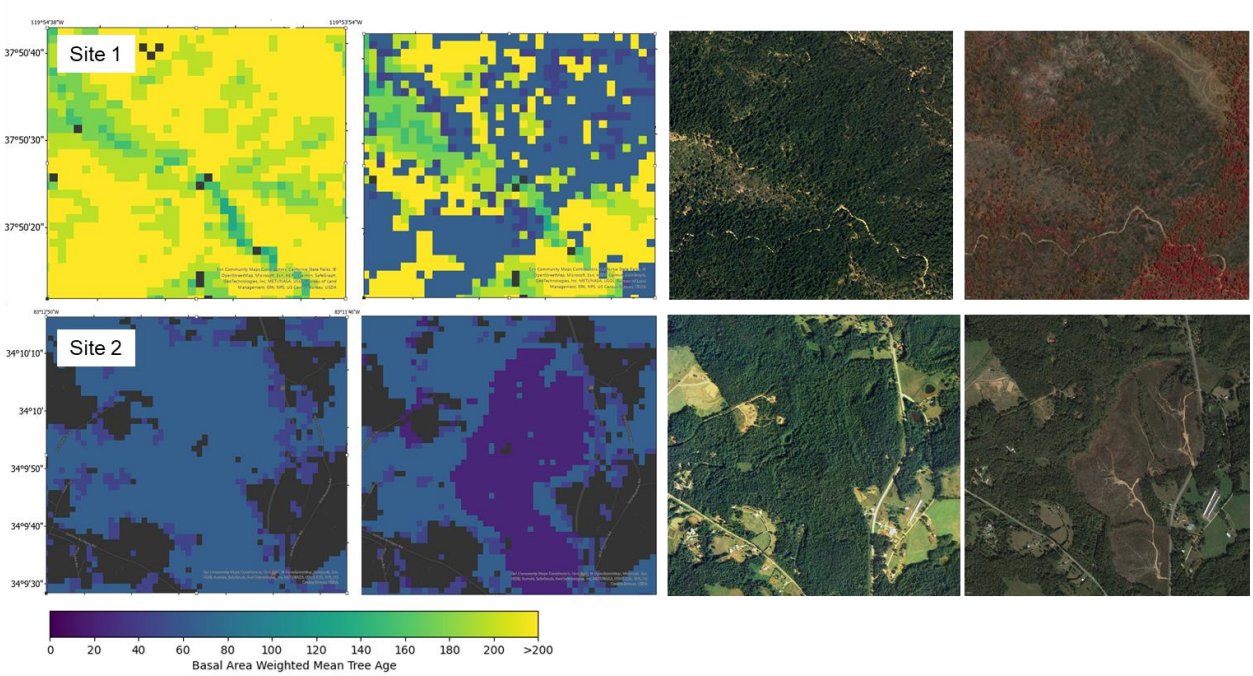

Figure 4-7 Site examples of forest age change in stands experiencing disturbances. The first column is the age map in 2005, the second column is the age map in 2015, the third column is the pre-disturbance forest condition, and the fourth column is the post-disturbance forest condition. The latter two are high-resolution images from Google Earth. Site 1 is in Mather California, which experienced

Rim Fire in 2013. Site 2 is a private ownership forest stand that experienced stand-clearing removal in 2015.

Stand Age Complexity

The spatial distribution pattern of forest age complexity (calculated as the standard deviation of tree age within a forest stand) is similar to forest age (Figure 4-8 -A). High complexity values are found in the old forests in Cascades, Sierra Nevada, Klamath Mountains/California High North Coast Range, Southern and Middle Rockies. The young forests in the east also show low complexity. Some of the smallest complexity values can be found in the southeastern forests. Figure 4-7 B-D show examples of forest age complexities in forests of different ownerships. Public forests around Olympic National Park have high complexity (Figure 4-8-B). Clear boundaries of complexity values were observed between forests of different ownerships (Figure 4-8 C), with state owned forests on the side of high complexity, and private owned forests on the side of low complexity.

In 2015, the national median forest age complexity was 19. Similar to the age distribution, eastern and western forests show very different distributions (Figure 4-9). The median age complexity of eastern forests is 18, and for western forests the median is 45. Across US forested ecosystems, 8.03% of forested areas have complexity values less than 10. The forest with complexity values higher than 80 accounted for 2.38% of all the forests.

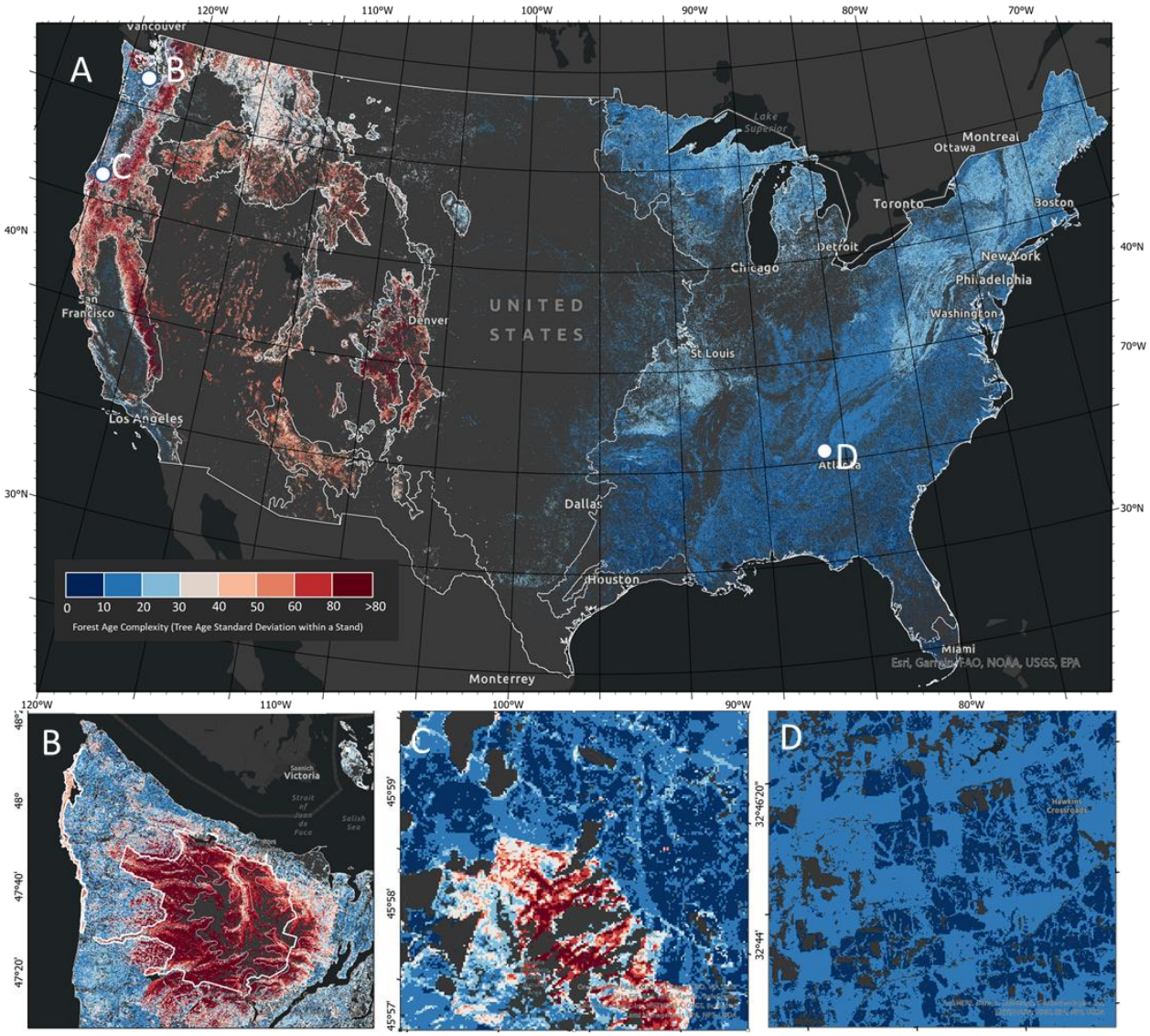

Figure 4-8 Estimated age complexity calculated as tree age standard deviation within forest stands for US forests in 2015 (A) and site examples in Olympic National Park (B), border between Saddle Mountain State Natural Areas and surrounding corporate lands in Oregon (C), and family/Corporate ownership forests in Georgia (D) revealing distinct patterns of forest age complexity distribution.

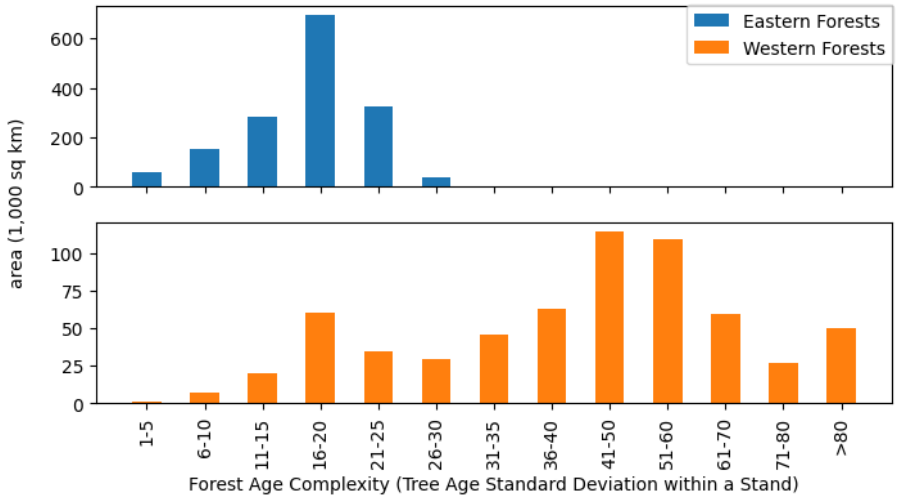

Figure 4-9 Histogram of forest age complexity in eastern and western forests in 2015.

4.5 Discussion

Forest age information is crucial as it influences biodiversity, ecosystem health, carbon sequestration, resilience to disturbances, and informs sustainable forest management practices. Using time since disturbance to approximate age can introduce large bias. Estimating exact forest age at large scale is challenging because of the difficulty to measure ground truth, dilemma in definition of forest age, and the uncertainties in the extent to which spectral reflectance can differentiate forests of different ages. In this study, we developed a modeling framework to estimate forest age and stand age complexity from disturbance intensity, time series surface reflectance (representing growth trajectory), and environmental variables. Forest age was calculated as the BAWMT (basal area weighted mean tree) age, and the stand age complexity was calculated as the standard deviation of all the trees within a forest plot. Cross validations indicate the forest age models have higher accuracy than existing large-scale studies. BAWMT age calculated using age of every tree within the plot provides a more reliable estimate. In the

predicted forest age, more weight was given to larger, potentially older trees that represent a significant portion of the forest's biomass, thus providing a reasonable estimate that can be linked to carbon stock and sequestration potential research. However, the ways to calculate forest age are not definitive, which can vary depending on the research focus. The stand age complexity models have lower accuracy in several ecoregions, but the derived maps are innovative products that can quantify the age structure complexity of a forest stand, which were not seen in existing studies.

Challenges exist in modeling forest age for very old forest stands (> 200 years old) and forests in arid/semi-arid regions. In old forests that have dense canopies, optical signals tend to saturate because the dense canopy absorbs and scatters a significant portion of the light, making it difficult for the sensors to detect variations in reflectance. ALS data may provide the opportunity to increase prediction accuracy by differentiating the vertical structural heterogeneity of the old forests. Accurately modeling forest attributes in arid or semi-arid areas is challenging due to sparse vegetation, high variability in species, and the unique growth pattern of forests in those areas. To improve the modeling of forest age in these areas, future studies may consider using a combination of high-resolution and multispectral remote sensing data, and adapt models to account for the unique species and ecological characteristics of these regions.

There are many potential usages of the produced datasets. In carbon cycle studies, forest age has been incorporated in many terrestrial biosphere models to understand the role of forests in carbon sequestration and climate change mitigation. For example, the ED (Ecosystem Demography) model (Hurtt et al., 1998; Moorcroft et al., 2001) uses age and size to approximate forest patch dynamics. Landscape Succession Models (LANDIS and LANDIS II) (Scheller et al., 2007) use

age classes to simulate vegetation changes and carbon dynamics; 3-PG (Physiological Principles in Predicting Growth) and CABALA (Carbon Balance Model) Models (Battaglia et al., 2004; Landsberg & Waring, 1997) integrate forest age to estimate forest productivity and carbon allocation in different parts of the tree and soil. A large-scale wall-to-wall forest age map for multiple years can aid such models to generate more accurate predictions of future forest ecosystem and carbon dynamics.

The stand age complexity map provides a way to quantify the heterogeneity of tree age and age structural complexity. Stand complexity can affect the forest ecosystem stability, adaptability and resilience to future disturbance events and climate changes, as well as biodiversity and productivity. While LiDAR data can be used to retrieve the vertical structural complexity of a forest stand, the developed approach can provide another unique view and can be applied to historical datasets for characterizing stand complexity.

4.6 Conclusion

In this chapter, we produced 30-m forest age and complexity maps for US forest in 2015 and 2005 considering historical disturbance intensity, time series spectral trajectory, and environmental variables. The model accuracy varies across ecoregions, with R^2 values in predicting forest age ranging from less than 0.4 in North American Deserts to 0.67-0.68 in Marine West Coast Forests and Mediterranean California. In general, these accuracies are better than those reported in previous studies, especially in large scale studies. Given the inherent difficulty to represent forest age accurately using a single age value, especially for un-even aged stands, this study demonstrated that the basal area weighted mean tree (BAWMT) age can be

better estimated based on time series Landsat observations than the stand age value provided by FIA.

The stand age complexity models are less accurate than the forest age models in general. However, they performed well in Marine West Coast Forest, Mediterranean California, and Northwestern Forested Mountains. But such dataset has not been produced in any previous studies for CONUS before. In 2015, the national median forest age was 60. The median age of eastern forests is 54, and for western forests the median is 153. Across US forested ecosystems, 4.72% of forested areas are older than 200 years. The forest younger than 20 years accounted for 6.35% of all the forests. The comparison between the 2015 and 2005 forest age maps did not show obvious change in the age distribution between the two years. The approach developed in this study is portable to be applied to other regions and time periods. The 30-m age and complexity maps of US forests did not exist before this study. They provide valuable information for knowing forest conditions, estimating forest growth and carbon sequestration potential, understanding the relationship between age and other forest attributes, evaluating forest health, and planning sustainable forest management practices.

Chapter 5: Conclusion

5.1 Major Findings

This dissertation introduces a new framework for the enhanced monitoring of critical forest attributes, integrating the interconnectedness of these attributes, such as the diameter-age relationship, to ensure consistent retrieval while simultaneously enhancing the accuracy of individual attributes. The dissertation first provided a more complete characterization of forest disturbance by quantifying the intensity of forest disturbances, then demonstrated the use of the integrated approach to produce more accurate estimations of tree age and forest age distribution in US forests.

Chapter 2 presents the first set of annual forest disturbance intensity map products quantifying the percentage of basal area removal (PBAR) at the 30-m resolution for the conterminous United States from 1986 to 2015 by integrating field plot measurements collected by the FIA program and time series Landsat observations. Disturbance intensity is an important variable for accurate characterization of the impact of disturbance events and for assessing post-disturbance recovery processes. While significant progress has been made to map forest disturbances, mapping forest disturbance intensity remains a research frontier. The derived map products are the first set of 30-m, CONUS-wide forest disturbance intensity maps spanning over three decades. They complement the Landsat-based annual forest disturbance naps derived through previous studies for CONUS (Zhao et al., 2018). These disturbance intensity maps revealed that during the 30-year study period, the annual average PBAR values of all disturbed pixels across CONUS ranged from 66% to 70%, and the proportion of those pixels having stand-clearing disturbances ranged

from 40% to 58%. High disturbance intensity values were concentrated in the Southeastern states and along the Pacific coast and the Cascades in the West. At the national scale, the annual mean disturbance intensity values appeared to follow 2nd order trajectories starting with increasing trends at the beginning and decreasing trends towards the end, along with turning points around 2003. The temporal trends of disturbance intensity differed substantially among many states and ecoregions. Compared to other published disturbance products, the maps derived through this study can provide the unique thematic (intensity) information on forest disturbances, precise details critical for understanding forest dynamics across CONUS over multiple decades. The temporal dynamics of disturbance intensity revealed by these map products may shed light on different practices and processes causing basal area loss across different regions. The chapter was published in peer-reviewed journal Remote Sensing of Environment. The map product is available from Oak Ridge National Laboratory Distribution Active Archive Center (ORNL-DAAC): https://doi.org/10.3334/ORNLDAAC/2059.

In Chapter 3, a modeling approach was developed to estimate tree age, incorporating factors such as tree size, species, and environmental conditions. The results indicate that field measurements of diameter and other structural variables such as height can be used to derive age estimates with relatively high accuracies for individual trees. Given that in forest inventory programs such as the FIA program, typically all large trees (e.g., diameter > 12.7 cm) within selected plots are populated with diameter measurements but only a small fraction of those trees has age values, this chapter demonstrates a practical approach for greatly increase the number of sample trees that have age data. The experiments conducted in this chapter show that locally tailored models outperform broader national and regional models in age prediction, highlighting the significance of localized data for forest variable modeling. A total of 55 zone-based models were constructed,

with cross-validation reflecting superior accuracy compared to existing methodologies. The transferable modeling framework enabled the quantification of the age for over 10 million trees that did not have age information in the original FIA database. This increased the number of sample trees with age information by almost 22 times. By deriving individual tree ages, the study provided an accurate depiction of the U.S. forest tree age distribution, making it possible to derive statistically more representative estimates of both the median age and the age of the oldest trees at different geographical scales. The curated tree age dataset emerges as a crucial resource for forest management and conservation, enhancing our ability to estimate forest carbon sequestration accurately. In sustainable forestry, this granular understanding of tree age distribution contributes to the development of more effective management practices, informing decisions about harvesting, reforestation, and the maintenance of overall forest health.

Building on the historical disturbance intensity mapped in Chapter 2 and the extensive tree age data generated in Chapter 3, Chapter 4 presents the first set of 30-meter resolution forest age and complexity maps for U.S. forests in 2015 and 2005. The approach outperformed existing large-scale studies in accuracy. Given the inherent difficulty to represent forest age accurately using a single age value, especially for un-even aged forest stands, this study demonstrated that the basal area weighted mean tree (BAWMT) age can be better estimated based on time series Landsat observations than the stand age value provided by FIA. While the models for forest age complexity show slightly less precision than those for forest age, they exhibit robust performance in the Marine West Coast Forest, Mediterranean California, and Northwestern Forested Mountains. To my knowledge, this study is the first effort to map tree age standard deviation as a measure of forest age complexity at the 30 m spatial resolution over a study area as large as the CONUS. The derived forest age and age complexity maps can serve as a valuable asset for

assessing forest conditions, forecasting forest growth and carbon sequestration capabilities, elucidating the relationship between age and other forest attributes, evaluating forest health, and strategizing sustainable forest management practices.

5.2 Future Research

Forest attributes, including basal area, age, and biomass, play a pivotal role in driving the dynamics of forest ecosystems, particularly with regard to processes such as recruitment, growth, and mortality, as well as in the quantification of carbon sequestration both in vegetation and soil substrates. In this dissertation, tree age was selected as a prototype attribute to evaluate the viability and effectiveness of the newly developed integrated modeling framework. This methodology demonstrated its robustness in consolidating various data sources and analytical techniques to enhance the precision and consistency of forest attribute estimations. The potential applications of this integrated approach are extensive and can be adapted to measure other vital forest attributes such as canopy height, biomass, and tree density with greater accuracy. By applying this framework to these additional attributes, it becomes possible to gain a more detailed and multifaceted understanding of forest structure. Such detailed characterization is indispensable for creating a holistic picture of forest ecosystems, which in turn informs a myriad of ecological studies and management practices. Moreover, the accurate estimations of these attributes are crucial for modeling forest dynamics, assessing habitat quality, and predicting responses to environmental changes and management interventions. For instance, tree height is an important indicator of habitat complexity and biodiversity, biomass estimates are central to carbon cycle and climate change models, and tree density impacts competition for resources among forest inhabitants. The comprehensive application of this integrated modeling framework

to a broader set of attributes promises to significantly advance our ability to monitor, manage, and conserve forest ecosystems in an era where understanding the impacts of global change on forested landscapes is more important than ever.

The disturbance intensity maps produced in this dissertation represent a significant advancement in our ability to differentiate and quantify partial and stand-clearing disturbances within forested landscapes. This level of detail is critical as it enables a nuanced understanding of the varying impacts that different types of disturbances have on forest ecosystems. By distinguishing the severity and extent of these events, these maps provide essential data that can be integrated into ecosystem models, thereby enhancing the models' capacity to simulate post-disturbance forest recovery processes and successional patterns with greater fidelity.

Future research could also focus on unraveling the intricate relationship between historical disturbances and the resulting age structure of forests. By leveraging the tree age distribution estimated in this study, now we have a unique opportunity to trace back the legacies of past events such as fires, storms, or human activities that have left an indelible mark on forest demographics. Investigating the spatial and temporal patterns of these disturbances and their corresponding influence on age distribution will shed light on forest resilience and succession processes. Such insights are crucial for predicting future forest dynamics and informing conservation efforts aimed at maintaining forest health and biodiversity in the face of climate change and anthropogenic pressures.

The tree age dataset can be used for exploration of the relationship between tree and forest age and AGB growth. Utilizing the tree age product, studies can quantify how age demographics influence biomass accumulation rates, crucial for understanding carbon sequestration trends. The

integration of age-related growth patterns into carbon and ecosystem models will enhance their predictive power, providing more accurate forecasts of carbon dynamics across various forest types. This integration is key to refining global carbon budgets and can inform effective forest management practices, contributing to climate change mitigation efforts and the conservation of ecosystem services provided by forested landscapes.

The datasets developed in this dissertation can be used to examine other ecological issues. For example, there are studies observing, increasing stem density and basal area and decreasing canopy height, biomass and species richness as elevation increases. Such changes could be caused by tree growth change or mortality rate change. It will be interesting to examine the factors contributing to changes in forest attributes with elevation gradient.

Bibliography

Abatzoglou, J. T., & Kolden, C. A. (2011). Climate change in western US deserts: potential for increased wildfire and invasive annual grasses. *Rangeland Ecology & Management*, *64*(5), 471–478.

Abatzoglou, J. T., & Williams, A. P. (2016). Impact of anthropogenic climate change on wildfire across western US forests. *Proceedings of the National Academy of Sciences*, *113*(42), 11770–11775.

Ahmed, O. S., Franklin, S. E., Wulder, M. A., & White, J. C. (2015). Characterizing stand-level forest canopy cover and height using Landsat time series, samples of airborne LiDAR, and the Random Forest algorithm. *ISPRS Journal of Photogrammetry and Remote Sensing*, *101*, 89–101.

Akselsson, C., Westling, O., Sverdrup, H., Holmqvist, J., Thelin, G., Uggla, E., & Malm, G. (2007). Impact of harvest intensity on long-term base cation budgets in Swedish forest soils. In *Acid Rain-Deposition to Recovery* (pp. 201–210). Springer.

Allen, C. D., Macalady, A. K., Chenchouni, H., Bachelet, D., McDowell, N., Vennetier, M., Kitzberger, T., Rigling, A., Breshears, D. D., Hogg, E. H. (Ted), Gonzalez, P., Fensham, R., Zhang, Z., Castro, J., Demidova, N., Lim, J. H., Allard, G., Running, S. W., Semerci, A., & Cobb, N. (2010). A global overview of drought and heat-induced tree mortality reveals emerging climate change risks for forests. *Forest Ecology and Management*, *259*(4), 660–684. https://doi.org/10.1016/j.foreco.2009.09.001

Asner, G. P. (2001). Cloud cover in Landsat observations of the Brazilian Amazon. *International Journal of Remote Sensing*, *22*(18), 3855–3862.

Aubry-Kientz, M., Dutrieux, R., Ferraz, A., Saatchi, S., Hamraz, H., Williams, J., Coomes, D., Piboule, A., & Vincent, G. (2019). A comparative assessment of the performance of individual tree crowns delineation algorithms from ALS data in tropical forests. *Remote Sensing*, *11*(9), 1086.

Avitabile, V., Baccini, A., Friedl, M. A., & Schmullius, C. (2012). Capabilities and limitations of Landsat and land cover data for aboveground woody biomass estimation of Uganda. *Remote Sensing of Environment*, *117*, 366–380. https://doi.org/10.1016/j.rse.2011.10.012

Baker, P. J. (2003). Tree age estimation for the tropics: a test from the southern Appalachians. *Ecological Applications*, *13*(6), 1718–1732.

Banks, S. C., Cary, G. J., Smith, A. L., Davies, I. D., Driscoll, D. A., Gill, A. M., Lindenmayer, D. B., & Peakall, R. (2013). How does ecological disturbance influence genetic diversity? *Trends in Ecology & Evolution*, *28*(11), 670–679.

Bar-On, Y. M., Phillips, R., & Milo, R. (2018). The biomass distribution on Earth. *Proceedings of the National Academy of Sciences*, *115*(25), 6506–6511.

Battaglia, M., Sands, P., White, D., & Mummery, D. (2004). CABALA: a linked carbon, water and nitrogen model of forest growth for silvicultural decision support. *Forest Ecology and Management*, *193*(1), 251–282. https://doi.org/https://doi.org/10.1016/j.foreco.2004.01.033

Beaudoin, A., Bernier, P. Y., Villemaire, P., Guindon, L., & Guo, X. J. (2018). Tracking forest attributes across Canada between 2001 and 2011 using ak nearest neighbors mapping approach applied to MODIS imagery. *Canadian Journal of Forest Research*, *48*(1), 85–93.

Bechtold, W. A., & Patterson, P. L. (2005). The enhanced forest inventory and analysis program-national sampling design and estimation procedures. *Gen. Tech. Rep. SRS-80. Asheville, NC: US Department of Agriculture, Forest Service, Southern Research Station. 85 p., 80*.

Belgiu, M., & Drăguţ, L. (2016). Random forest in remote sensing: A review of applications and future directions. *ISPRS Journal of Photogrammetry and Remote Sensing*, *114*, 24–31.

Ben-Asher, J., Alpert, P., & Ben-Zvi, A. (2010). Dew is a major factor affecting vegetation water use efficiency rather than a source of water in the eastern Mediterranean area. *Water Resources Research*, *46*(10). https://doi.org/https://doi.org/10.1029/2008WR007484

Besnard, S., Koirala, S., Santoro, M., Weber, U., Nelson, J., Gütter, J., Herault, B., Kassi, J., N'Guessan, A., Neigh, C., Poulter, B., Zhang, T., & Carvalhais, N. (2021). Mapping global forest age from forest inventories, biomass and climate data. *Earth System Science Data*, *13*(10), 4881–4896. https://doi.org/10.5194/essd-13-4881-2021

Birdsey, R. A., & Lewis, G. M. (2003). *Current and historical trends in use, management, and disturbance of US forestlands*. CRC Press, New York.

Bouvet, A., Mermoz, S., Ballère, M., Koleck, T., & Le Toan, T. (2018). Use of the SAR shadowing effect for deforestation detection with Sentinel-1 time series. *Remote Sensing*, *10*(8), 1250.

Bradford, J. B., Birdsey, R. A., Joyce, L. A., & Ryan, M. G. (2008). Tree age, disturbance history, and carbon stocks and fluxes in subalpine Rocky Mountain forests. *Global Change Biology. 14: 2882-2897.* , *14*. https://www.fs.usda.gov/treesearch/pubs/31448

Bradford, J. B., Weishampel, P., Smith, M.-L., Kolka, R., Birdsey, R. A., Ollinger, S. V, & Ryan, M. G. (2010). Carbon pools and fluxes in small temperate forest landscapes: variability and implications for sampling design. *Forest Ecology and Management*, *259*(7), 1245–1254.

Brand, G. J., Nelson, M. D., Wendt, D. G., & Nimerfro, K. K. (1981). The hexagon/panel system for selecting FIA plots under an annual inventory. *USFS FIA Research Publications*.

Breiman, L. (2001). Random forests. *Machine Learning*, *45*(1), 5–32.

Broadbent, E. N., Asner, G. P., Keller, M., Knapp, D. E., Oliveira, P. J. C., & Silva, J. N. (2008). Forest fragmentation and edge effects from deforestation and selective logging in the Brazilian Amazon. *Biological Conservation*, *141*(7), 1745–1757. https://doi.org/10.1016/j.biocon.2008.04.024

Buma, B., & Schultz, C. (2020). Disturbances as opportunities: Learning from disturbance-response parallels in social and ecological systems to better adapt to climate change. *Journal of Applied Ecology*, *57*(6), 1113–1123.

Burrill, Ea, Christensen, Ga, Conkling, BL, DiTommaso, Am, Lepine, Perry, CJ, Pugh, Sa, Turner, Ja, Walker, Williams, & Ma. (2023). *FIA Database Description and User Guide for Phase 2 (version: 9.1) The Forest Inventory and Analysis Database: Database Description and User Guide for Phase 2 (version 9.1) Contents Preface User Guide Updates Changes from the Previous Database Version*.

Caswell, H., & Salguero-Gómez, R. (2013). Age, stage and senescence in plants. *Journal of Ecology*, *101*(3), 585–595.

Chambers, J. Q., Fisher, J. I., Zeng, H., Chapman, E. L., Baker, D. B., & Hurtt, G. C. (2007). Hurricane Katrina's carbon footprint on US Gulf Coast forests. *Science*, *318*(5853), 1107.

Chen, D., Loboda, T. V, Krylov, A., & Potapov, P. V. (2016). Mapping stand age dynamics of the Siberian larch forests from recent Landsat observations. *Remote Sensing of Environment*, *187*, 320–331.

Chrysafis, I., Mallinis, G., Gitas, I., & Tsakiri-Strati, M. (2017). Estimating Mediterranean forest parameters using multi seasonal Landsat 8 OLI imagery and an ensemble learning method. *Remote Sensing of Environment*, *199*, 154–166. https://doi.org/10.1016/j.rse.2017.07.018

Cohen, W. B., & Goward, S. N. (2004). Landsat's role in ecological applications of remote sensing. *Bioscience*, *54*(6), 535–545.

Cohen, W. B., Maierspergers, T. K., Spies, T. A., & Oetter, D. R. (2001). Modelling forest cover attributes as continuous variables in a regional context with Thermatic Mapper data. *International Journal of Remote Sensing*, *22*(12), 2279–2310. https://doi.org/10.1080/01431160121472

Cohen, W. B., Yang, Z., Stehman, S. V., Schroeder, T. A., Bell, D. M., Masek, J. G., Huang, C., & Meigs, G. W. (2016). Forest disturbance across the conterminous United States from 1985-2012: The emerging dominance of forest decline. *Forest Ecology and Management*, *360*, 242–252. https://doi.org/10.1016/j.foreco.2015.10.042

Coops, N. C., Tompalski, P., Goodbody, T. R. H., Queinnec, M., Luther, J. E., Bolton, D. K., White, J. C., Wulder, M. A., van Lier, O. R., & Hermosilla, T. (2021). Modelling lidar-derived estimates of forest attributes over space and time: A review of approaches and future trends. *Remote Sensing of Environment*, *260*, 112477.

Dale, V. H., Joyce, L. A., McNulty, S., Neilson, R. P., Ayres, M. P., Flannigan, M. D., Hanson, P. J., Irland, L. C., Lugo, A. E., Peterson, C. J., Simberloff, D., Swanson, F. J., Stocks, B. J., & Michael Wotton, B. (2001). Climate Change and Forest Disturbances. *BioScience*, *51*(9), 723. https://doi.org/10.1641/0006-3568(2001)051[0723:ccafd]2.0.co;2

Daly, C., Taylor, G. H., Gibson, W. P., Parzybok, T. W., Johnson, G. L., & Pasteris, P. A. (2000). High-quality spatial climate data sets for the United States and beyond. *Transactions of the ASAE*, *43*(6), 1957–1962.

DeFries, R. (2008). Terrestrial Vegetation in the Coupled Human-Earth System: Contributions of Remote Sensing. *Annual Review of Environment and Resources*, *33*(1), 369–390. https://doi.org/10.1146/annurev.environ.33.020107.113339

DeVries, B., Verbesselt, J., Kooistra, L., & Herold, M. (2015). Robust monitoring of small-scale forest disturbances in a tropical montane forest using Landsat time series. *Remote Sensing of Environment*, *161*, 107–121. https://doi.org/10.1016/j.rse.2015.02.012

Diallo, A., Agbangba, E. C., Ndiaye, O., & Guisse, A. (2013). *Ecological structure and prediction equations for estimating tree age, and dendometric parameters of acacia senegal in the senegalese semi-arid zone—ferlo*.

Diao, J., Feng, T., Li, M., Zhu, Z., Liu, J., Biging, G., Zheng, G., Shen, W., Wang, H., & Wang, J. (2020). Use of vegetation change tracker, spatial analysis, and random forest regression to assess the evolution of plantation stand age in Southeast China. *Annals of Forest Science*, *77*(2), 1–16.

Diffenbaugh, N. S., Swain, D. L., & Touma, D. (2015). Anthropogenic warming has increased drought risk in California. *Proceedings of the National Academy of Sciences*, *112*(13), 3931–3936.

Duane, M. V., Cohen, W. B., Campbell, J. L., Hudiburg, T., & Turner, D. P. (2010). *Implications of Alternative Field-Sampling Designs on Landsat-Based Mapping of Stand Age and Carbon Stocks in Oregon Forests*. https://watermark.silverchair.com/forestscience0405.pdf?token=AQECAHi208BE49Ooan9kkhW_Ercy7Dm3ZL_9Cf3qfKAc485ysgAAAn0wggJ5BgkqhkiG9w0BBwagggJqMIICZgIBADCCAl8GCSqGSIb3DQEHATAeBglghkgBZQMEAS4wEQQMJN4TiD9y7KDSuwIdAgEQgIICMK6xE-UGy6om8q9l2lkWACQtw6cLl6E-2F_2Y

Dubayah, R., Blair, J. B., Goetz, S., Fatoyinbo, L., Hansen, M., Healey, S., Hofton, M., Hurtt, G., Kellner, J., & Luthcke, S. (2020). The Global Ecosystem Dynamics Investigation: High-resolution laser ranging of the Earth's forests and topography. *Science of Remote Sensing*, *1*, 100002.

Dube, T., & Mutanga, O. (2015). Evaluating the utility of the medium-spatial resolution Landsat 8 multispectral sensor in quantifying aboveground biomass in uMgeni catchment, South Africa. *ISPRS Journal of Photogrammetry and Remote Sensing*, *101*, 36–46.

Duncanson, L. I., Niemann, K. O., & Wulder, M. A. (2010). Integration of GLAS and Landsat TM data for aboveground biomass estimation. *Canadian Journal of Remote Sensing*, *36*(2), 129–141.

Egnell, G. (2017). A review of Nordic trials studying effects of biomass harvest intensity on subsequent forest production. *Forest Ecology and Management*, *383*, 27–36.

Ellison, D., Morris, C. E., Locatelli, B., Sheil, D., Cohen, J., Murdiyarso, D., Gutierrez, V., Van Noordwijk, M., Creed, I. F., & Pokorny, J. (2017). Trees, forests and water: Cool insights for a hot world. *Global Environmental Change*, *43*, 51–61.

Englhart, S., Keuck, V., & Siegert, F. (2011). Aboveground biomass retrieval in tropical forests - The potential of combined X- and L-band SAR data use. *Remote Sensing of Environment*, *115*(5), 1260–1271. https://doi.org/10.1016/j.rse.2011.01.008

FAO. (2018). *The States of the World's Forests*. https://doi.org/10.1016/b0-12-145160-7/00156-3

Farr, T. G., Rosen, P. A., Caro, E., Crippen, R., Duren, R., Hensley, S., Kobrick, M., Paller, M., Rodriguez, E., Roth, L., Seal, D., Shaffer, S., Shimada, J., Umland, J., Werner, M., Oskin, M., Burbank, D., & Alsdorf, D. (2007). The Shuttle Radar Topography Mission. *Reviews of Geophysics*, *45*(2). https://doi.org/https://doi.org/10.1029/2005RG000183

Fassnacht, F. E., White, J. C., Wulder, M. A., & Næsset, E. (2023). Remote sensing in forestry: current challenges, considerations and directions. *Forestry: An International Journal of Forest Research*, cpad024.

Foga, S., Scaramuzza, P. L., Guo, S., Zhu, Z., Dilley, R. D., Beckmann, T., Schmidt, G. L., Dwyer, J. L., Joseph Hughes, M., & Laue, B. (2017). Cloud detection algorithm comparison and validation for operational Landsat data products. *Remote Sensing of Environment*, *194*, 379–390. https://doi.org/https://doi.org/10.1016/j.rse.2017.03.026

Forest Service Forest Inventory. (2023). *Forest Inventory and Analysis National Core Field Guide, Volume I: Field Data Collection Procedures for Phase 2 Plots (Version 9.2)*.

Frate L Carranza ML, G. V. F. M. D. T. D. M. M. O. M. S. G., & G, C. (2016). Spatially explicit estimation of forest age by integrating remotely sensed data and inverse yield modeling techniques. *IForest - Biogeosciences and Forestry*, *1*, 63–71. https://doi.org/10.3832/ifor1529-008

Frazer, G. W., Magnussen, S., Wulder, M. A., & Niemann, K. O. (2011). Simulated impact of sample plot size and co-registration error on the accuracy and uncertainty of LiDAR-derived estimates of forest stand biomass. *Remote Sensing of Environment*, *115*(2), 636–649. https://doi.org/10.1016/j.rse.2010.10.008

Frazier, R. J., Coops, N. C., Wulder, M. A., & Kennedy, R. (2014). Characterization of aboveground biomass in an unmanaged boreal forest using Landsat temporal segmentation metrics. *ISPRS Journal of Photogrammetry and Remote Sensing*, *92*, 137–146.

Fridman, J., Holm, S., Nilsson, M., Nilsson, P., Ringvall, A. H., & Ståhl, G. (2014). Adapting National Forest Inventories to changing requirements–the case of the Swedish National Forest Inventory at the turn of the 20th century. *Silva Fennica*, *48*(3), 1–29.

Fu, P., & Rich, P. M. (1999). *Design and Implementation of the Solar Analyst: an ArcView Extension for Modeling Solar Radiation at Landscape Scales*.

Gatsuk, L. E., Smirnova, O. V, Vorontzova, L. I., Zaugolnova, L. B., & Zhukova, L. A. (1980). Age states of plants of various growth forms: a review. *The Journal of Ecology*, 675–696.

Gelfand, A. E., Ghosh, S., & Clark, J. S. (2013). Scaling integral projection models for analyzing size demography. *Statistical Science*, *28*(4), 641–658.

Giam, X. (2017). Global biodiversity loss from tropical deforestation. *Proceedings of the National Academy of Sciences*, *114*(23), 5775–5777.

Gibson, L., Lee, T. M., Koh, L. P., Brook, B. W., Gardner, T. A., Barlow, J., Peres, C. A., Bradshaw, C. J. A., Laurance, W. F., Lovejoy, T. E., & Sodhi, N. S. (2011). Primary forests are irreplaceable for sustaining tropical biodiversity. *Nature*, *478*(7369), 378–381. https://doi.org/10.1038/nature10425

Gilhen-Baker, M., Roviello, V., Beresford-Kroeger, D., & Roviello, G. N. (2022). Old growth forests and large old trees as critical organisms connecting ecosystems and human health. A review. *Environmental Chemistry Letters*, *20*(2), 1529–1538.

Gillespie, A. J. R. (1999). Rationale for a national annual forest inventory program. *Journal of Forestry*, *97*(12), 16–20.

Grossiord, C., Buckley, T. N., Cernusak, L. A., Novick, K. A., Poulter, B., Siegwolf, R. T. W., Sperry, J. S., & McDowell, N. G. (2020). Plant responses to rising vapor pressure deficit. *New Phytologist*, *226*(6), 1550–1566. https://doi.org/https://doi.org/10.1111/nph.16485

Haddad, N. M., Brudvig, L. A., Clobert, J., Davies, K. F., Gonzalez, A., Holt, R. D., Lovejoy, T. E., Sexton, J. O., Austin, M. P., Collins, C. D., Cook, W. M., Damschen, E. I., Ewers, R. M., Foster, B. L., Jenkins, C. N., King, A. J., Laurance, W. F., Levey, D. J., Margules, C. R., … Townshend, J. R. (2015). Habitat fragmentation and its lasting impact on Earth's ecosystems. *Science Advances*, *1*(2), 1–9. https://doi.org/10.1126/sciadv.1500052

Hall, R. J., Skakun, R. S., Arsenault, E. J., & Case, B. S. (2006). Modeling forest stand structure attributes using Landsat ETM+ data: Application to mapping of aboveground biomass and stand volume. *Forest Ecology and Management*, *225*(1–3), 378–390. https://doi.org/10.1016/j.foreco.2006.01.014

Hansen, M. C., & Loveland, T. R. (2012). A review of large area monitoring of land cover change using Landsat data. *Remote Sensing of Environment*, *122*, 66–74.

Hansen, M. C., Potapov, P. V, Goetz, S. J., Turubanova, S., Tyukavina, A., Krylov, A., Kommareddy, A., & Egorov, A. (2016). Mapping tree height distributions in Sub-Saharan Africa using Landsat 7 and 8 data. *Remote Sensing of Environment*, *185*, 221–232.

Hansen, M. C., Potapov, P. V, Moore, R., Hancher, M., Turubanova, S. a, Tyukavina, A., Thau, D., Stehman, S. V, Goetz, S. J., Loveland, T. R., Kommareddy, A., Egorov, A., Chini, L., Justice, C. O., & Townshend, J. R. G. (2013). High-resolution global maps of 21st-century forest cover change. *Science (New York, N.Y.)*, *342*(2013), 850–853. https://doi.org/10.1126/science.1244693

Hanson, J. J., & Lorimer, C. G. (2007). Forest structure and light regimes following moderate wind storms: Implications for multi-cohort management. *Ecological Applications*, *17*(5), 1325–1340.

Harris, R. M. B., Beaumont, L. J., Vance, T. R., Tozer, C. R., Remenyi, T. A., Perkins-Kirkpatrick, S. E., Mitchell, P. J., Nicotra, A. B., McGregor, S., & Andrew, N. R. (2018). Biological responses to the press and pulse of climate trends and extreme events. *Nature Climate Change*, *8*(7), 579–587.

Healey, S. P., Yang, Z., Cohen, W. B., & Pierce, D. J. (2006). Application of two regression-based methods to estimate the effects of partial harvest on forest structure using Landsat data. *Remote Sensing of Environment*, *101*(1), 115–126. https://doi.org/10.1016/j.rse.2005.12.006

He, L., Chen, J. M., Zhang, S., Gomez, G., Pan, Y., McCullough, K., Birdsey, R., & Masek, J. G. (2011). Normalized algorithm for mapping and dating forest disturbances and regrowth for the United States. *International Journal of Applied Earth Observation and Geoinformation*, *13*(2), 236–245.

Hermosilla, T., Wulder, M. A., White, J. C., Coops, N. C., & Hobart, G. W. (2015). An integrated Landsat time series protocol for change detection and generation of annual gap-free surface reflectance composites. *Remote Sensing of Environment*, *158*, 220–234. https://doi.org/10.1016/j.rse.2014.11.005

Hessburg, P. F., & Agee, J. K. (2003). An environmental narrative of Inland Northwest United States forests, 1800–2000. *Forest Ecology and Management*, *178*(1), 23–59. https://doi.org/https://doi.org/10.1016/S0378-1127(03)00052-5

Hill, T. C., Ryan, C. M., & Williams, M. (2015). A framework for estimating forest disturbance intensity from successive remotely sensed biomass maps: moving beyond average biomass loss estimates. *Carbon Balance and Management*, *10*(1), 27. https://doi.org/10.1186/s13021-015-0039-0

Hirschmugl, M., Deutscher, J., Sobe, C., Bouvet, A., Mermoz, S., & Schardt, M. (2020). Use of SAR and optical time series for tropical forest disturbance mapping. *Remote Sensing*, *12*(4), 727.

Homer, C., Dewitz, J., Jin, S., Xian, G., Costello, C., Danielson, P., Gass, L., Funk, M., Wickham, J., & Stehman, S. (2020). Conterminous United States land cover change patterns 2001–2016 from the 2016 national land cover database. *ISPRS Journal of Photogrammetry and Remote Sensing*, *162*, 184–199.

Hoogwijk, M., Faaij, A., Eickhout, B., de Vries, B., & Turkenburg, W. (2005). Potential of biomass energy out to 2100, for four IPCC SRES land-use scenarios. *Biomass and Bioenergy*, *29*(4), 225–257.

Hoppus, M., Riemann, R., & Lister, A. (2000). Remote sensing strategies for Forest Inventory and Analysis utilizing the FIA plot database. *Proceedings of RS*.

Houghton, R. A. (2005). Aboveground forest biomass and the global carbon balance. *Global Change Biology*, *11*(6), 945–958. https://doi.org/10.1111/j.1365-2486.2005.00955.x

Huang, C., Goward, S. N., Masek, J. G., Gao, F., Vermote, E. F., Thomas, N., Schleeweis, K., Kennedy, R. E., Zhu, Z., Eidenshink, J. C., & Townshend, J. R. G. (2009). Development of time series stacks of landsat images for reconstructing forest disturbance history. *International Journal of Digital Earth*, *2*(3), 195–218. https://doi.org/10.1080/17538940902801614

Huang, C., Goward, S. N., Masek, J. G., Thomas, N., Zhu, Z., & Vogelmann, J. E. (2010). An automated approach for reconstructing recent forest disturbance history using dense Landsat time series stacks. *Remote Sensing of Environment*, *114*(1), 183–198. https://doi.org/10.1016/j.rse.2009.08.017

Huang, C., Peng, Y., Lang, M., Yeo, I. Y., & McCarty, G. (2014). Wetland inundation mapping and change monitoring using Landsat and airborne LiDAR data. *Remote Sensing of Environment*, *141*, 231–242. https://doi.org/10.1016/j.rse.2013.10.020

Hudak, A. T., Lefsky, M. A., Cohen, W. B., & Berterretche, M. (2002). Integration of lidar and Landsat ETM+ data for estimating and mapping forest canopy height. *Remote Sensing of Environment*, *82*(2–3), 397–416.

Hurtt, G. C., Chini, L. P., Frolking, S., Betts, R. A., Feddema, J., Fischer, G., Fisk, J. P., Hibbard, K., Houghton, R. A., & Janetos, A. (2011). Harmonization of land-use scenarios for the period 1500–2100: 600 years of global gridded annual land-use transitions, wood harvest, and resulting secondary lands. *Climatic Change*, *109*(1–2), 117.

Hurtt, G. C., Moorcroft, PauL. R., And, S. W. P., & Levin, S. A. (1998). Terrestrial models and global change: challenges for the future. *Global Change Biology*, *4*(5), 581–590. https://doi.org/https://doi.org/10.1046/j.1365-2486.1998.t01-1-00203.x

IPCC. (2014). Climate Change 2013 - The Physical Science Basis. *Climate Change 2014: Synthesis Report*, 151. https://doi.org/10.1017/CBO9781107415324

Johnstone, J. F., Allen, C. D., Franklin, J. F., Frelich, L. E., Harvey, B. J., Higuera, P. E., Mack, M. C., Meentemeyer, R. K., Metz, M. R., Perry, G. L., Schoennagel, T., & Turner, M. G. (2016). Changing disturbance regimes, ecological memory, and forest resilience. *Frontiers in Ecology and the Environment*, *14*(7), 369–378. https://doi.org/10.1002/fee.1311

Jonsson, M., Bengtsson, J., Moen, J., Gamfeldt, L., & Snäll, T. (2020). Stand age and climate influence forest ecosystem service delivery and multifunctionality. *Environmental Research Letters*, *15*(9), 0940a8. https://doi.org/10.1088/1748-9326/abaf1c

Ju, J., & Roy, D. P. (2008). The availability of cloud-free Landsat ETM+ data over the conterminous United States and globally. *Remote Sensing of Environment*, *112*(3), 1196–1211.

Kalliovirta, J., & Tokola, T. (2005). Functions for estimating stem diameter and tree age using tree height, crown width and existing stand database information. *Silva Fennica*, *39*(2), 227–248.

Kautz, M., Meddens, A. J. H., Hall, R. J., & Arneth, A. (2017). Biotic disturbances in Northern Hemisphere forests–a synthesis of recent data, uncertainties and implications for forest monitoring and modelling. *Global Ecology and Biogeography*, *26*(5), 533–552.

King, D. A. (2011). Size-related changes in tree proportions and their potential influence on the course of height growth. In *Size-and age-related changes in tree structure and function* (pp. 165–191). Springer.

Köhl, M., Neupane, P. R., & Lotfiomran, N. (2017). The impact of tree age on biomass growth and carbon accumulation capacity: A retrospective analysis using tree ring data of three tropical tree species grown in natural forests of Suriname. *Plos One*, *12*(8), e0181187.

Kreuzwieser, J., & Gessler, A. (2010). Global climate change and tree nutrition: influence of water availability. *Tree Physiology*, *30*(9), 1221–1234. https://doi.org/10.1093/treephys/tpq055

Landsberg, J. J., & Waring, R. H. (1997). A generalised model of forest productivity using simplified concepts of radiation-use efficiency, carbon balance and partitioning. *Forest Ecology and Management*, *95*(3), 209–228. https://doi.org/https://doi.org/10.1016/S0378-1127(97)00026-1

Lefsky, M. A. (2010). A global forest canopy height map from the Moderate Resolution Imaging Spectroradiometer and the Geoscience Laser Altimeter System. *Geophysical Research Letters*, *37*(15), n/a-n/a. https://doi.org/10.1029/2010GL043622

Lefsky, M. A., Cohen, W. B., Parker, G. G., & Harding, D. J. (2002). Lidar remote sensing for ecosystem studies: Lidar, an emerging remote sensing technology that directly measures the three-dimensional distribution of plant canopies, can accurately estimate vegetation structural attributes and should be of particular inte. *BioScience*, *52*(1), 19–30.

Lefsky, M. A., Turner, D. P., Guzy, M., & Cohen, W. B. (2005). Combining lidar estimates of aboveground biomass and Landsat estimates of stand age for spatially extensive validation of modeled forest productivity. *Remote Sensing of Environment*, *95*(4), 549–558. https://doi.org/10.1016/j.rse.2004.12.022

Legaard, K. R., Sader, S. A., & Simons-Legaard, E. M. (2015). Evaluating the impact of abrupt changes in forest policy and management practices on landscape dynamics: analysis of a Landsat image time series in the Atlantic Northern Forest. *PloS One*, *10*(6), e0130428.

Leverkus, A. B., Lindenmayer, D. B., Thorn, S., & Gustafsson, L. (2018). Salvage logging in the world's forests: Interactions between natural disturbance and logging need recognition. *Global Ecology and Biogeography*, *27*(10), 1140–1154. https://doi.org/10.1111/geb.12772

Li, A., Huang, C., Sun, G., Shi, H., Toney, C., Zhu, Z., Rollins, M. G., Goward, S. N., & Masek, J. G. (2011). Modeling the height of young forests regenerating from recent disturbances in Mississippi using Landsat and ICESat data. *Remote Sensing of Environment*, *115*(8), 1837–1849.

Ligas, M., & Banasik, P. (2011). Conversion between Cartesian and geodetic coordinates on a rotational ellipsoid by solving a system of nonlinear equations. In *GEODESY AND CARTOGRAPHY c Polish Academy of Sciences* (Vol. 60, Issue 2).

Lindenmayer, D. B., Burton, P. J., & Franklin, J. F. (2012). *Salvage logging and its ecological consequences*. Island Press.

Lindenmayer, D. B., & Laurance, W. F. (2017). The ecology, distribution, conservation and management of large old trees. *Biological Reviews*, *92*(3), 1434–1458.

Lister, A., Scott, C., King, S., Hoppus, M., Butler, B., & Griffith, D. (2005). Strategies for preserving owner privacy in the national information management system of the USDA Forest Service's Forest Inventory and Analysis unit. *UNITED STATES DEPARTMENT OF AGRICULTURE FOREST SERVICE GENERAL TECHNICAL REPORT NC*, *352*, 163.

Lu, D. (2006). The potential and challenge of remote sensing-based biomass estimation. *International Journal of Remote Sensing*, *27*(7), 1297–1328. https://doi.org/10.1080/01431160500486732

Lu, D., Chen, Q., Wang, G., Liu, L., Li, G., & Moran, E. (2016). A survey of remote sensing-based aboveground biomass estimation methods in forest ecosystems. *International Journal of Digital Earth*, *9*(1), 63–105. https://doi.org/10.1080/17538947.2014.990526

Luisa, B. G. (2012). *The ecology of natural disturbance and patch dynamics*. Academic press.

Maltamo, M., Kinnunen, H., Kangas, A., & Korhonen, L. (2020). Predicting stand age in managed forests using National Forest Inventory field data and airborne laser scanning. *Forest Ecosystems*, *7*(1), 44. https://doi.org/10.1186/s40663-020-00254-z

Maltman, J. C., Hermosilla, T., Wulder, M. A., Coops, N. C., & White, J. C. (2023). Estimating and mapping forest age across Canada's forested ecosystems. *Remote Sensing of Environment*, *290*, 113529. https://doi.org/https://doi.org/10.1016/j.rse.2023.113529

Masek, J. G., Vermote, E. F., Saleous, N. E., Wolfe, R., Hall, F. G., Huemmrich, K. F., Gao, F., Kutler, J., & Lim, T.-K. (2006). A Landsat surface reflectance dataset for North America, 1990-2000. *IEEE Geoscience and Remote Sensing Letters*, *3*(1), 68–72.

Matasci, G., Hermosilla, T., Wulder, M. A., White, J. C., Coops, N. C., Hobart, G. W., & Zald, H. S. J. (2018). Large-area mapping of Canadian boreal forest cover, height, biomass and other structural attributes using Landsat composites and lidar plots. *Remote Sensing of Environment*, *209*(June 2017), 90–106. https://doi.org/10.1016/j.rse.2017.12.020

McRoberts, R. E., Bechtold, W. A., Patterson, P. L., Scott, C. T., & Reams, G. A. (2005). The enhanced Forest Inventory and Analysis program of the USDA Forest Service: Historical perspective and announcement of statistical documentation. *Journal of Forestry*, *103*(6), 304–308.

McRoberts, R. E., Cohen, W. B., Naesset, E., Stehman, S. V, & Tomppo, E. O. (2010). Using remotely sensed data to construct and assess forest attribute maps and related spatial products. *Scandinavian Journal of Forest Research*, *25*(4), 340–367.

McRoberts, R. E., & Tomppo, E. O. (2007). Remote sensing support for national forest inventories. *Remote Sensing of Environment*, *110*(4), 412–419.

Meigs, G. W., Kennedy, R. E., Gray, A. N., & Gregory, M. J. (2015). Spatiotemporal dynamics of recent mountain pine beetle and western spruce budworm outbreaks across the Pacific Northwest Region, USA. *Forest Ecology and Management*, *339*, 71–86.

Mikoláš, M., Svitok, M., Tejkal, M., Leitão, P. J., Morrissey, R. C., Svoboda, M., Seedre, M., & Fontaine, J. B. (2015). Evaluating forest management intensity on an umbrella species: Capercaillie persistence in central Europe. *Forest Ecology and Management*, *354*, 26–34.

Millar, C. I., & Stephenson, N. L. (2015). Temperate forest health in an era of emerging megadisturbance. *Science*, *349*(6250), 823–826. https://doi.org/10.1126/science.aaa9933

Moorcroft, P. R., Hurtt, G. C., & Pacala, S. W. (2001). A METHOD FOR SCALING VEGETATION DYNAMICS: THE ECOSYSTEM DEMOGRAPHY MODEL (ED). *Ecological Monographs*, *71*(4), 557–586. https://doi.org/https://doi.org/10.1890/0012-9615(2001)071[0557:AMFSVD]2.0.CO;2

Mushinski, R. M., Gentry, T. J., Dorosky, R. J., & Boutton, T. W. (2017). Forest harvest intensity and soil depth alter inorganic nitrogen pool sizes and ammonia oxidizer community composition. *Soil Biology and Biochemistry*, *112*, 216–227.

Nakajima, T., Shiraishi, N., Kanomata, H., & Matsumoto, M. (2017). A method to maximise forest profitability through optimal rotation period selection under various economic, site and silvicultural conditions. *New Zealand Journal of Forestry Science*, *47*, 1–13.

Nelson, M. D., Healey, S. P., Moser, W. K., & Hansen, M. H. (2009). Combining satellite imagery with forest inventory data to assess damage severity following a major blowdown event in northern Minnesota, USA. *International Journal of Remote Sensing*, *30*(19), 5089–5108.

Neuenschwander, A., & Pitts, K. (2019). The ATL08 land and vegetation product for the ICESat-2 Mission. *Remote Sensing of Environment*, *221*, 247–259.

Niklas, K. J. (1995). Size-dependent allometry of tree height, diameter and trunk-taper. *Annals of Botany*, *75*(3), 217–227.

North, M. P., Kane, J. T., Kane, V. R., Asner, G. P., Berigan, W., Churchill, D. J., Conway, S., Gutiérrez, R. J., Jeronimo, S., & Keane, J. (2017). Cover of tall trees best predicts California spotted owl habitat. *Forest Ecology and Management*, *405*, 166–178.

Olofsson, P., Foody, G. M., Herold, M., Stehman, S. V, Woodcock, C. E., & Wulder, M. A. (2014). Good practices for estimating area and assessing accuracy of land change. *Remote Sensing of Environment*, *148*, 42–57.

Olsson, B. A., Bengtsson, J., & Lundkvist, H. (1996). Effects of different forest harvest intensities on the pools of exchangeable cations in coniferous forest soils. *Forest Ecology and Management*, *84*(1–3), 135–147.

Omernik, J. M. (1987). Ecoregions of the Conterminous United States. *Annals of the Association of American Geographers*, *77*(1), 118–125. https://doi.org/10.1111/j.1467-8306.1987.tb00149.x

Ouyang, S., Xiang, W., Wang, X., Xiao, W., Chen, L., Li, S., Sun, H., Deng, X., Forrester, D. I., Zeng, L., Lei, P., Lei, X., Gou, M., & Peng, C. (2019). Effects of stand age, richness and density on productivity in subtropical forests in China. *Journal of Ecology*, *107*(5), 2266–2277. https://doi.org/https://doi.org/10.1111/1365-2745.13194

Panfil, S. N., & Gullison, R. E. (1998). Short term impacts of experimental timber harvest intensity on forest structure and composition in the Chimanes Forest, Bolivia. *Forest Ecology and Management*, *102*(2–3), 235–243.

Pan, Y., Chen, J. M., Birdsey, R., McCullough, K., He, L., & Deng, F. (2011). Age structure and disturbance legacy of North American forests. *Biogeosciences. 8: 715-732.*, *8*, 715–732.

Paritsis, J., & Veblen, T. T. (2011). Dendroecological analysis of defoliator outbreaks on Nothofagus pumilio and their relation to climate variability in the Patagonian Andes. *Global Change Biology*, *17*(1), 239–253.

Parrotta, J. A., Francis, J. K., & Knowles, O. H. (2002). Harvesting intensity affects forest structure and composition in an upland Amazonian forest. *Forest Ecology and Management*, *169*(3), 243–255.

Peng, C. (2000). Growth and yield models for uneven-aged stands: past, present and future. *Forest Ecology and Management*, *132*(2–3), 259–279.

Peterson, D. L. (2014). *Climate Change and United States Forests* (D. L. Peterson, J. M. Vose, & T. Patel-Weynand, Eds.; Vol. 57). Springer Netherlands. https://doi.org/10.1007/978-94-007-7515-2

Pflugmacher, D., Cohen, W. B., & Kennedy, R. E. (2012). Using Landsat-derived disturbance history (1972-2010) to predict current forest structure. *Remote Sensing of Environment*, *122*, 146–165. https://doi.org/10.1016/j.rse.2011.09.025

Phipps, R. L. (1985). *Collecting, preparing, crossdating, and measuring tree increment cores* (Issues 85–4148). US Department of the Interior, Geological Survey.

Piovesan, G., & Biondi, F. (2021). On tree longevity. *New Phytologist*, *231*(4), 1318–1337.

Potapov, P., Li, X., Hernandez-Serna, A., Tyukavina, A., Hansen, M. C., Kommareddy, A., Pickens, A., Turubanova, S., Tang, H., & Silva, C. E. (2021). Mapping global forest canopy height through integration of GEDI and Landsat data. *Remote Sensing of Environment*, *253*, 112165.

Powell, S. L., Cohen, W. B., Healey, S. P., Kennedy, R. E., Moisen, G. G., Pierce, K. B., & Ohmann, J. L. (2010). Quantification of live aboveground forest biomass dynamics with Landsat time-series and field inventory data: A comparison of empirical modeling approaches. *Remote Sensing of Environment*, *114*(5), 1053–1068. https://doi.org/10.1016/j.rse.2009.12.018

Qi, W., & Dubayah, R. O. (2016). Combining Tandem-X InSAR and simulated GEDI lidar observations for forest structure mapping. *Remote Sensing of Environment*, *187*(2016), 253–266. https://doi.org/10.1016/j.rse.2016.10.018

Racine, E. B., Coops, N. C., St-Onge, B., & Bégin, J. (2014). Estimating Forest Stand Age from LiDAR-Derived Predictors and Nearest Neighbor Imputation. *Forest Science*, *60*(1), 128–136. https://doi.org/10.5849/forsci.12-088

Reid, D. J., Quinn, J. M., & Wright-Stow, A. E. (2010). Responses of stream macroinvertebrate communities to progressive forest harvesting: influences of harvest intensity, stream size and riparian buffers. *Forest Ecology and Management*, *260*(10), 1804–1815.

Repo, A., Rajala, T., Henttonen, H. M., Lehtonen, A., Peltoniemi, M., & Heikkinen, J. (2021). Age-dependence of stand biomass in managed boreal forests based on the Finnish National Forest Inventory data. *Forest Ecology and Management*, *498*, 119507.

Rishmawi, K., Huang, C., & Zhan, X. (2021). Monitoring key forest structure attributes across the conterminous United States by integrating GEDI LiDAR measurements and VIIRS data. *Remote Sensing*, *13*(3), 442.

Rohner, B., Bugmann, H., & Bigler, C. (2013). Towards non-destructive estimation of tree age. *Forest Ecology and Management*, *304*, 286–295.

Rosen, P. A., Hensley, S., Shaffer, S., Veilleux, L., Chakraborty, M., Misra, T., Bhan, R., Sagi, V. R., & Satish, R. (2015). The NASA-ISRO SAR mission-An international space partnership for science and societal benefit. *2015 IEEE Radar Conference (RadarCon)*, 1610–1613.

Rozas, V. (2003). Tree age estimates in Fagus sylvatica and Quercus robur: testing previous and improved methods. *Plant Ecology*, *167*, 193–212.

Rüetschi, M., Small, D., & Waser, L. T. (2019). Rapid detection of windthrows using Sentinel-1 C-band SAR data. *Remote Sensing*, *11*(2), 115.

Saatchi, S. S., Harris, N. L., Brown, S., Lefsky, M., Mitchard, E. T. A., Salas, W., Zutta, B. R., Buermann, W., Lewis, S. L., Hagen, S., Petrova, S., White, L., Silman, M., & Morel, A. (2011). Benchmark map of forest carbon stocks in tropical regions across three continents. *Proceedings of the National Academy of Sciences of the United States of America*, *108*(24), 9899–9904. https://doi.org/10.1073/pnas.1019576108

Schall, P., Gossner, M. M., Heinrichs, S., Fischer, M., Boch, S., Prati, D., Jung, K., Baumgartner, V., Blaser, S., Böhm, S., Buscot, F., Daniel, R., Goldmann, K., Kaiser, K., Kahl, T., Lange, M., Müller, J., Overmann, J., Renner, S. C., … Ammer, C. (2018). The impact of even-aged and uneven-aged forest management on regional biodiversity of multiple taxa in European beech forests. *Journal of Applied Ecology*, *55*(1), 267–278. https://doi.org/10.1111/1365-2664.12950

Scheller, R. M., Domingo, J. B., Sturtevant, B. R., Williams, J. S., Rudy, A., Gustafson, E. J., & Mladenoff, D. J. (2007). Design, development, and application of LANDIS-II, a spatial landscape simulation model with flexible temporal and spatial resolution. *Ecological Modelling*, *201*(3), 409–419. https://doi.org/https://doi.org/10.1016/j.ecolmodel.2006.10.009

Scheller, R. M., Hua, D., Bolstad, P. V, Birdsey, R. A., & Mladenoff, D. J. (2011). The effects of forest harvest intensity in combination with wind disturbance on carbon dynamics in Lake States Mesic Forests. *Ecological Modelling*, *222*(1), 144–153.

Schleeweis, K. G., Moisen, G. G., Schroeder, T. A., Toney, C., Freeman, E. A., Goward, S. N., Huang, C., & Dungan, J. L. (2020). US National Maps Attributing Forest Change: 1986–2010. *Forests*, *11*(6), 653.

Schleeweis, K., Goward, S. N., Huang, C., Dwyer, J. L., Dungan, J. L., Lindsey, M. A., Michaelis, A., Rishmawi, K., & Masek, J. G. (2016). Selection and quality assessment of Landsat data for the North American forest dynamics forest history maps of the US. *International Journal of Digital Earth*, *9*(10), 963–980.

Schumacher, J., Hauglin, M., Astrup, R., & Breidenbach, J. (2020). Mapping forest age using National Forest Inventory, airborne laser scanning, and Sentinel-2 data. *Forest Ecosystems*, *7*(1), 60. https://doi.org/10.1186/s40663-020-00274-9

Seidl, R., Schelhass, M., & Lexer, M. J. (2011). Unraveling the drivers of intensifying forest disturbance regimes in Europe. *Global Change Biology*, *17*(9), 2842–2852. https://doi.org/10.1111/j.1365-2486.2011.02452.x

Seidl, R., Thom, D., Kautz, M., Martin-Benito, D., Peltoniemi, M., Vacchiano, G., Wild, J., Ascoli, D., Petr, M., Honkaniemi, J., Lexer, M. J., Trotsiuk, V., Mairota, P., Svoboda, M., Fabrika, M., Nagel, T. A., & Reyer, C. P. O. (2017). Forest disturbances under climate change. In *Nature Climate Change* (Vol. 7, Issue 6, pp. 395–402). Nature Publishing Group. https://doi.org/10.1038/nclimate3303

Senf, C., & Seidl, R. (2021). Mapping the forest disturbance regimes of Europe. *Nature Sustainability*, *4*(1), 63–70.

Sharma, R. P., Brunner, A., Eid, T., & Øyen, B.-H. (2011). Modelling dominant height growth from national forest inventory individual tree data with short time series and large age errors. *Forest Ecology and Management*, *262*(12), 2162–2175. https://doi.org/https://doi.org/10.1016/j.foreco.2011.07.037

Sheffield, R. M. (1992). *Hurricane Hugo: effects on South Carolina's forest resource* (Vol. 284). Southeastern Forest Experiment Station.

Sieg, C. H., Linn, R. R., Pimont, F., Hoffman, C. M., McMillin, J. D., Winterkamp, J., & Baggett, L. S. (2017). Fires following bark beetles: Factors controlling severity and disturbance interactions in ponderosa pine. *Fire Ecology*, *13*(3), 1–23. https://doi.org/10.4996/fireecology.130300123

Silva, L. B., Teixeira, A., Alves, M., Elias, R. B., & Silva, L. (2017). Tree age determination in the widespread woody plant invader Pittosporum undulatum. *Forest Ecology and Management*, *400*, 457–467.

Singleton, M. P., Thode, A. E., Meador, A. J. S., & Iniguez, J. M. (2019). Increasing trends in high-severity fire in the southwestern USA from 1984 to 2015. *Forest Ecology and Management*, *433*, 709–719.

Siry, J. P. (2002). Intensive timber management practices. *Southern Forest Resource Assessment*, *14*, 327–340.

Smith, W. B. (2002). Forest inventory and analysis: a national inventory and monitoring program. *Environmental Pollution*, *116*, S233–S242.

Smith, W. B., & Darr, D. R. (2004). *US forest resource facts and historical trends*.

Sousa, W. P. (1980). The responses of a community to disturbance: the importance of successional age and species' life histories. *Oecologia*, *45*, 72–81.

Soutiere, E. C. (1979). Effects of timber harvesting on marten in Maine. *The Journal of Wildlife Management*, 850–860.

SRS Field Guide. (2022). *FOREST INVENTORY AND ANALYSIS NATIONAL CORE FIELD GUIDE VOLUME I: FIELD DATA COLLECTION PROCEDURES FOR PHASE 2 PLOTS*.

Storey, J., Choate, M., & Lee, K. (2014). Landsat 8 operational land imager on-orbit geometric calibration and performance. *Remote Sensing*, *6*(11), 11127–11152.

Storey, J., Roy, D. P., Masek, J., Gascon, F., Dwyer, J., & Choate, M. (2016). A note on the temporary misregistration of Landsat-8 Operational Land Imager (OLI) and Sentinel-2 Multi Spectral Instrument (MSI) imagery. *Remote Sensing of Environment*, *186*, 121–122.

Straub, C., & Koch, B. (2011). Enhancement of bioenergy estimations within forests using airborne laser scanning and multispectral line scanner data. *Biomass and Bioenergy*, *35*(8), 3561–3574. https://doi.org/https://doi.org/10.1016/j.biombioe.2011.05.017

Sugarbaker, L., Constance, E. W., Heidemann, H. K., Jason, A. L., Lucas, V., Saghy, D., & Stoker, J. M. (2014). *The 3D Elevation Program initiative: a call for action*. US Geological Survey.

Tao, X., Huang, C., Zhao, F., Schleeweis, K., Masek, J., & Liang, S. (2019). Mapping forest disturbance intensity in North and South Carolina using annual Landsat observations and field inventory data. *Remote Sensing of Environment*, *221*(November 2018), 351–362. https://doi.org/10.1016/j.rse.2018.11.029

Thom, D., & Seidl, R. (2016). Natural disturbance impacts on ecosystem services and biodiversity in temperate and boreal forests. *Biological Reviews*, *91*(3), 760–781. https://doi.org/10.1111/brv.12193

Tian, L., Liao, L., Tao, Y., Wu, X., & Li, M. (2023). Forest Age Mapping Using Landsat Time-Series Stacks Data Based on Forest Disturbance and Empirical Relationships between Age and Height. *Remote Sensing*, *15*(11). https://doi.org/10.3390/rs15112862

Tinkham, W. T., Mahoney, P. R., Hudak, A. T., Domke, G. M., Falkowski, M. J., Woodall, C. W., & Smith, A. M. S. (2018). Applications of the United States Forest Inventory and Analysis dataset: a review and future directions. *Canadian Journal of Forest Research*, *48*(11), 1251–1268.

Tomppo, E., Olsson, H., Ståhl, G., Nilsson, M., Hagner, O., & Katila, M. (2008). Combining national forest inventory field plots and remote sensing data for forest databases. *Remote Sensing of Environment*, *112*(5), 1982–1999.

Torres, R., Snoeij, P., Geudtner, D., Bibby, D., Davidson, M., Attema, E., Potin, P., Rommen, B., Floury, N., & Brown, M. (2012). GMES Sentinel-1 mission. *Remote Sensing of Environment*, *120*, 9–24.

Treuhaft, R. N., Law, B. E., & Asner, G. P. (2004). Forest attributes from radar interferometric structure and its fusion with optical remote sensing. *BioScience*, *54*(6), 561–571.

Trotsiuk, V., Hobi, M. L., & Commarmot, B. (2012). Age structure and disturbance dynamics of the relic virgin beech forest Uholka (Ukrainian Carpathians). *Forest Ecology and Management*, *265*, 181–190.

Tudge, S. J., Harris, Z. M., Murphy, R. J., Purvis, A., & De Palma, A. (2023). Global trends in biodiversity with tree plantation age. *Global Ecology and Conservation*, *48*, e02751. https://doi.org/https://doi.org/10.1016/j.gecco.2023.e02751

Tullus, T., Lutter, R., Randlane, T., Saag, A., Tullus, A., Oja, E., Degtjarenko, P., Pärtel, M., & Tullus, H. (2022). The effect of stand age on biodiversity in a 130-year chronosequence of Populus tremula stands. *Forest Ecology and Management*, *504*, 119833.

Turner, I. M. (1996). Species Loss in Fragments of Tropical Rain Forest: A Review of the Evidence. *The Journal of Applied Ecology*, *33*(2), 200. https://doi.org/10.2307/2404743

Turner, M. G. (2010). Disturbance and landscape dynamics in a changing world. *Ecology*, *91*(10), 2833–2849. https://doi.org/10.1890/10-0097.1

U.S. Environmental Protection Agency. (2010). *Level III Ecoregions of the Continental United States (revision of Omernik, 1987)*. Map.

Van der Werf, G. R., Morton, D. C., DeFries, R. S., Olivier, J. G. J., Kasibhatla, P. S., Jackson, R. B., Collatz, G. J., & Randerson, J. T. (2009). CO 2 emissions from forest loss. *Nature Geoscience*, *2*(11), 737–738.

Van Tuyl, S., Law, B. E., Turner, D. P., & Gitelman, A. I. (2005). Variability in net primary production and carbon storage in biomass across Oregon forests—an assessment integrating data from forest inventories, intensive sites, and remote sensing. *Forest Ecology and Management*, *209*(3), 273–291. https://doi.org/https://doi.org/10.1016/j.foreco.2005.02.002

Véga, C., & St-Onge, B. (2009). Mapping site index and age by linking a time series of canopy height models with growth curves. *Forest Ecology and Management*, *257*(3), 951–959. https://doi.org/https://doi.org/10.1016/j.foreco.2008.10.029

Venter, O., Sanderson, E. W., Magrach, A., Allan, J. R., Beher, J., Jones, K. R., Possingham, H. P., Laurance, W. F., Wood, P., Fekete, B. M., Levy, M. A., & Watson, J. E. M. (2016). *ARTICLE Sixteen*

years of change in the global terrestrial human footprint and implications for biodiversity conservation. https://doi.org/10.1038/ncomms12558

Vitousek, P. M., Mooney, H. A., Lubchenco, J., & Melillo, J. M. (1997). Human domination of Earth's ecosystems. *Science*, *277*(5325), 494–499.

Vlam, M., van der Sleen, P., Groenendijk, P., & Zuidema, P. A. (2017). Tree age distributions reveal large-scale disturbance-recovery cycles in three tropical forests. *Frontiers in Plant Science*, *7*, 1984.

Westerling, A. L., Hidalgo, H. G., Cayan, D. R., & Swetnam, T. W. (2006). Warming and earlier spring increase western US forest wildfire activity. *Science*, *313*(5789), 940–943.

Whitney, G. G., & Foster, D. R. (1988). Overstorey composition and age as determinants of the understorey flora of woods of central New England. *The Journal of Ecology*, 867–876.

Williams, M. (1982). Clearing the United States forests: pivotal years 1810-1860. *Journal of Historical Geography*, *8*(1). https://doi.org/10.1016/0305-7488(82)90242-0

Williams, M. (1992). *Americans and Their Forests: A Historical Geography*. Cambridge University Press. https://books.google.com/books?id=HupJE8k4SnUC

Woodall, C. W., & Leutscher, B. (2005). Extending and intensifying the FIA inventory of down forest fuels: Boundary Waters Canoe Area and Pictured Rocks National Lakeshore. *In: Proceedings of the Fifth Annual Forest Inventory and Analysis Symposium; 2003 November 18-20; New Orleans, LA. Gen. Tech. Rep. WO-69. Washington, DC: US Department of Agriculture Forest Service. 222p., 69.*

Woodcock, C. E., Allen, R., Anderson, M., Belward, A., Bindschadler, R., Cohen, W., Gao, F., Goward, S. N., Helder, D., & Helmer, E. (2008). Free access to Landsat imagery. *Science*, *320*(5879), 1011.

Wuebbles, D. J., Fahey, D. W., Hibbard, K. A., Arnold, J. R., DeAngelo, B., Doherty, S., Easterling, D. R., Edmonds, J., Edmonds, T., & Hall, T. (2017). *Climate science special report: Fourth national climate assessment (NCA4), Volume I*.

Wulder, M. A., Loveland, T. R., Roy, D. P., Crawford, C. J., Masek, J. G., Woodcock, C. E., Allen, R. G., Anderson, M. C., Belward, A. S., & Cohen, W. B. (2019). Current status of Landsat program, science, and applications. *Remote Sensing of Environment*, *225*, 127–147.

Wulder, M. A., White, J. C., Nelson, R. F., Næsset, E., Ørka, H. O., Coops, N. C., Hilker, T., Bater, C. W., & Gobakken, T. (2012). Lidar sampling for large-area forest characterization: A review. *Remote Sensing of Environment*, *121*, 196–209.

Wylie, R. R. M., Woods, M. E., & Dech, J. P. (2019). Estimating Stand Age from Airborne Laser Scanning Data to Improve Models of Black Spruce Wood Density in the Boreal Forest of Ontario. *Remote Sensing*, *11*(17). https://doi.org/10.3390/rs11172022

Yamori, W., Hikosaka, K., & Way, D. A. (2014). Temperature response of photosynthesis in C3, C4, and CAM plants: temperature acclimation and temperature adaptation. *Photosynthesis Research*, *119*(1), 101–117. https://doi.org/10.1007/s11120-013-9874-6

Yanai, R. D., Currie, W. S., & Goodale, C. L. (2003). Soil carbon dynamics after forest harvest: an ecosystem paradigm reconsidered. *Ecosystems*, 197–212.

Yang, B., Xue, W., Yu, S., Zhou, J., & Zhang, W. (2019). Effects of Stand Age on Biomass Allocation and Allometry of Quercus Acutissima in the Central Loess Plateau of China. *Forests*, *10*(1). https://doi.org/10.3390/f10010041

Yi, C., & Jackson, N. (2021). A review of measuring ecosystem resilience to disturbance. *Environmental Research Letters*, *16*(5), 053008. https://doi.org/10.1088/1748-9326/abdf09

Zald, H. S. J., Wulder, M. A., White, J. C., Hilker, T., Hermosilla, T., Hobart, G. W., & Coops, N. C. (2016). Integrating Landsat pixel composites and change metrics with lidar plots to predictively map forest structure and aboveground biomass in Saskatchewan, Canada. *Remote Sensing of Environment*, *176*, 188–201. https://doi.org/10.1016/j.rse.2016.01.015

Zhang, C., Ju, W., Chen, J. M., Li, D., Wang, X., Fan, W., Li, M., & Zan, M. (2014). Mapping forest stand age in China using remotely sensed forest height and observation data. *Journal of Geophysical Research: Biogeosciences*, *119*(6), 1163–1179. https://doi.org/https://doi.org/10.1002/2013JG002515

Zhang, C., Zhou, Y., & Qiu, F. (2015). Individual tree segmentation from LiDAR point clouds for urban forest inventory. *Remote Sensing*, *7*(6), 7892–7913.

Zhang, Y., Li, H., Zhang, X., Lei, Y., Huang, J., & Liu, X. (2022). An Approach to Estimate Individual Tree Ages Based on Time Series Diameter Data—A Test Case for Three Subtropical Tree Species in China. *Forests*, *13*(4), 614.

Zhao, F., Huang, C., Goward, S. N., Schleeweis, K., Rishmawi, K., Lindsey, M. A., Denning, E., Keddell, L., Cohen, W. B., Yang, Z., Dungan, J. L., & Michaelis, A. (2018). Development of Landsat-based annual US forest disturbance history maps (1986–2010) in support of the North American Carbon Program (NACP). *Remote Sensing of Environment*, *209*, 312–326. https://doi.org/10.1016/j.rse.2018.02.035

Zhao, P., Lu, D., Wang, G., Wu, C., Huang, Y., & Yu, S. (2016). Examining spectral reflectance saturation in landsat imagery and corresponding solutions to improve forest aboveground biomass estimation. *Remote Sensing*, *8*(6). https://doi.org/10.3390/rs8060469

Zhu, Z., Bergamaschi, B., Bernknopf, R., Clow, D., Dye, D., Faulkner, S., Forney, W., Gleason, R., Hawbaker, T., & Liu, J. (2010). A method for assessing carbon stocks, carbon sequestration, and greenhouse-gas fluxes in ecosystems of the United States under present conditions and future scenarios. *Scientific Investigations Report 2010-5233. Reston, VA: US Geological Survey. 188 p.*

Zhu, Z., Wang, S., & Woodcock, C. E. (2015). Improvement and expansion of the Fmask algorithm: cloud, cloud shadow, and snow detection for Landsats 4–7, 8, and Sentinel 2 images. *Remote Sensing of Environment*, *159*, 269–277. https://doi.org/https://doi.org/10.1016/j.rse.2014.12.014

Zhu, Z., Wulder, M. A., Roy, D. P., Woodcock, C. E., Hansen, M. C., Radeloff, V. C., Healey, S. P., Schaaf, C., Hostert, P., & Strobl, P. (2019). Benefits of the free and open Landsat data policy. *Remote Sensing of Environment*, *224*, 382–385.

Zhu, Z., Zhang, J., Yang, Z., Aljaddani, A. H., Cohen, W. B., Qiu, S., & Zhou, C. (2019). Continuous monitoring of land disturbance based on Landsat time series. *Remote Sensing of Environment*, *238*(November 2018), 111116. https://doi.org/10.1016/j.rse.2019.03.009